FORCE RECOVERY TECHNIQUE FOR MULTI COMPONENT BALANCES UNDER IMPULSIVE LOADING IN HIGH SPEED FLOW EXPERIMENTS

A thesis

Submitted in Partial Fulfillment of the Requirements for
the Award of the Degree of

DOCTOR OF PHILOSOPHY

By

Soumya Ranjan Nanda

DEPARTMENT OF MECHANICAL ENGINEERING
INDIAN INSTITUTE OF TECHNOLOGY GUWAHATI

AUGUST 2018

Dedicated to my Parents

DECLARATION

I hereby certify that the work compiled in this dissertation is the outcome of the research work, performed by myself, else stated, under the guidance of **Prof. Niranjan Sahoo** and **Dr. Vinayak Kulkarni.**

Any part of this work has not been submitted for the award of any degree, diploma, associate-fellowship, fellowship or its equivalent to any university or institution.

Soumya Ranjan Nanda

Registration No. 136103040
Department of Mechanical Engineering
Indian Institute of Technology Guwahati

Department of Mechanical Engineering
Indian Institute of Technology Guwahati
Guwahati-781039, India

CERTIFICATE

It is certified that the work contained in the thesis entitled **“Force Recovery Technique for Multi Component Balances Under Impulsive Loading in High Speed Flow Experiments”** by **Mr. Soumya Ranjan Nanda**, a student, in the Department of Mechanical Engineering, Indian Institute of Technology Guwahati, India, for the award of the degree of the Doctor of Philosophy, has been carried out under our supervision and, that this work has not been submitted elsewhere for the degree.

Date:

Dr. Niranjan Sahoo
Professor
Department of Mechanical Engineering
Indian Institute of Technology Guwahati
Guwahati-781039, Assam, India

Dr. Vinayak Kulkarni
Associate Professor
Department of Mechanical Engineering
Indian Institute of Technology Guwahati
Guwahati-781039, Assam, India

ACKNOWLEDGEMENTS

At first, I would like to express my heartfelt gratitude to my supervisor, **Prof. Niranjan Sahoo** and **Dr. Vinayak Kulkarni**, who have relentlessly supported me during the course of my research work with their motivation, encouragement and colossal knowledge. Their guidance has shaped my basic understanding in this domain up to a greater extent. Without their keen interest and help, I would not have been able to put forth the best foot forward during the current research work. I would also convey my deepest regard to **Dr. Ganesh** Natarajan for guiding and giving me his expert opinion towards my research work. I am also deeply obligated to the Director of Indian Institute of Technology Guwahati for providing such pleasing circumstances for the inception of my research career.

Besides my supervisor, I would like to acknowledge the doctoral committee members, **Prof. Santosha K. Dwivedy**, **Late. Dr. A. N. Reddy** and **Dr. Amit Shelke**, for their valuable recommendations and insightful remarks throughout the course of research activities, which has constantly engaged me towards undertaking a meaningful thesis work. I am extremely gratified to all the faculty and staff members of the Mechanical Department and **Dr. Amit Shelke** from Department of Civil Engineering for endowing their whole-hearted support during the entire course of my stay. Further, special appreciation for the senior technician and support staff of the Department of Mechanical Engineering for their valuable help namely, **Mr. Nip Borah**, **Mr. Rituraj Saikia**, **Mr. Monuranjan Dowarh**, **Mr. Saiffuddin Ahmed**, **Mr. Sanjib Sarma**, **Mr. N.K Das**, **Mr. Dilip Chetri**, **Mr. Nabajyoti Dutta** and **Mr. Raju Talukdar**.

I would deeply thank all my fellow lab-mates in Aerodynamic Laboratory: **Dr. P Ramesh Babu**, **Dr. Shrutidhara Sarma**, **Dr. Sumit Agarwal, Mr. Saibal Kanchan Barik**, **Mr. Anil Kumar Rout**, **Mr. Santosh Kumar Hotta**, **Mrs. Rameswari Sadangi, Miss Priyanka Dash**, **Mrs. DVN Lakshmi, Mr. Shuvayan Brahmachary, Mr. Siddesh Desai, Mr. Abhishek Kamal, Mr. Anand Verma, Mr. Nikki Rajaura, Mr. Sashank Kulkarni, Mr. Menelik Walle**, **Mr. Himansu Sahoo, Mr. Deepak Yadav, Mr. Shobhit Kumar Singh, Mr. Adil, Mr. Anurag Shrivastav, Mr. Ranveer Negi, Mr. Manish Sonkar and Mr. Gagan** for all the enriching and valuable discussions and sleepless nights we had to work together. Without this group, my journey perhaps would have been of less fun.

I also owe thanks to my seniors, fellow mates and Utkalika family members namely, **Mr. Rasmi Ranjan Behera**, **Mr. Anupam Alok**, **Mr. Kelli Durgaprasad**, **Miss Sangjukta Devi**, **Mr. Rajeev Anupoju**, **Mr. Parag Kamal Talukdar**, **Mr. Devarshi Kashyap, Mr. Shahnawaz Ahmed, Mr. Manish Dubey,Mr. Sunil Kumar Singh, Mr. Debabrta Gayen, Mr. Kamal basumatary, Mr. Dipankar Das, Mr. Dipendra Roy, Mr. Sibananda Mohanty, Mr. Sujit Das, Mr. Ramesh Kumar, Mrs. Jayashree Das, Mr. Abinash Mahapatro, Mr. Mirzaul Hussain, Mr. Uttam Tarai, Mr. Shranish Kar, Mr. Saurav Dutta, Mr. Ankan Mishra, Dr. Kajwal Patra, Mr. Pratap Behera, Mr. Priyabrata Nath, Mr. Sunil Biswal, Mr. Sangram Jena, Mr. Rupak Dalai, Mr. Swagat Dwivedy, Mr. Bidhu Bhusan Mukut, Mr. Sanjeev Mishra, Mr. Ojing Siram, Mr. Buddhadeb Maity, Mr. Pyarimohan Dehury, Mr. Dudul Das, Mr. Samar Das, Mr. Mrutunjaya Maharana, Mr. Mr. Gautam, Mr. Sibabrata Sahoo, Mr. Bibhuti, Mr. Sritam Swapnadarshi Sahu, Mr. Anand Nayak, Mr. Biswa, Mr. Umesh, Mr. Manoj, Mr. Manmath, Mr. Tushar, Mr. Dillip, Mr. Subas, Mr. Niranjan, Mr. Subhasish, Miss Tapaswini, Mr. Prince, Mr. Bikas, Mr. Juba, Mr. Shailendra, Dr. Santosh Behera, Dr. Hari, Dr. Manoj, Mr. Sandeep Sahoo, Mr. Abhhishek, Mr. Swaroop, Mr. Lalatendu, Miss Shrestha, Mr. Bighna, Mr. Sai, Dr. Gyana, Dr. Ramesh Mishra, Dr. Asish Chaudhary, Mr. Achyut, Mr. Vighnesh, Mrs. Firdausa.**

My sincere obligations to **Prof. Viren Menzes** for offering me an opportunity to visit Shock Tunnel Laboratory, Indian Institute of Technology Bombay for conducting valuable experiments and providing essential insights for the research work. A special mention of **Dr. Kiran Joy Irimpan, Mr. Alex, Mr. Ashok** and **Mr. Amol** is indeed for helping in every possible aspect during the visit.

Last but not the least; I owe my profound gratitude towards my parents **Mr. Santosh Kumar Nanda Mrs. Suprava Nanda**, my sister **Miss Sasmita Nanda, Mr. Suresh Chandra Dash**, **Mrs. Charulata Dash**, **Mr. Nihar Ranjan Dash** and **Miss Priyanka Dash** for being the constant guiding, and supporting force throughout.

Soumya Ranjan Nanda
Indian Institute of Technology Guwahati
August 2018

LIST OF PUBLICATIONS

Journals:

1. **Nanda SR**, Kulkarni V and Sahoo N (2016) Design of artificial neuro-fuzzy based methodology for six component force balance. *Procedia Engineering*, 144, 528-536.

2. **Nanda SR**, Agarwal S, Kulkarni V and Sahoo N (2017) Shock tube as an impulsive application device, *International Journal of Aerospace Engineering*, 2010476. [doi: https://doi.org/10.1155/2017/2010476]

3. **Nanda SR**, Kulkarni V and Sahoo N (2017) Apt strain measurement technique for impulsive loading applications, *Measurement Science and Technology*, 28(3), 037001.

4. **Nanda SR**, Kulkarni V, Sahoo N and Menezes V (2019) An innovative approach for prediction of aerodynamic coefficients in shock tunnel testing with soft computing techniques, *Measurement*, 134, pp. 773-780.

5. **Nanda SR**, Desai S, Kulkarni V and Sahoo N (2018) Piezofilm as a potential sensor for force measurement in short duration impulse test facilities, *Shock Waves*. (Under Review).

6. **Nanda SR**, Kulkarni V, Sahoo N and Menezes V (2018) Multi component piezofilm balance: An alternative low cost measurement in impulse facilities, *Journal of Aerospace Engineering: Part-G* (Under Review).

7. **Nanda SR**, Kulkarni V, Sahoo N and Menezes V (2018) Assessment of Three Component Accelerometer Force Balance and ANFIS Based Force Recovery Technique for Prediction of Aerodynamic Coefficients, Aerospace Science and Technology (Under Review).

Conferences:

1. **Nanda SR**, SR, Barik SK, Sahoo N and Kulkarni V, Drag measurement in shock tube using stress wave force balance, *Proceedings of 4th National Symposium on Shock Waves (NSSW)*, Karunya University, February 25-26, 2016.

2. **Nanda SR**, Kulkarni V, Sahoo N and Menezes V, New calibration technique for three component accelerometer based force balance for hypersonic application, *Proceedings of 5th National Symposium on Shock Waves (NSSW)*, TBRL, Chandigarh, February 28-March 2, 2018.

ABSTRACT

Accurate force measurement is a major concern in the design phase of any high speed vehicle in order to assess its stability and to estimate the fuel requirement. Evolution of new strategy for force prediction has to be authenticated by implementing the same in various impulse facilities like shock tube, shock tunnel, expansion tunnel etc. Force measurement experiments in such facilities are necessarily sophisticated due to the short duration. Further, inclusion of the whole system dynamics during force measurement studies is also a challenging task. Since stiffness based balance represents the system more accurately, present investigations mainly focus on the stiffness based force balances.

To monitor the strain variation, usually strain gauge and pizofilm are opted as dynamic sensors in case of stress wave balance systems. Present study has been initiated to explore the types of configurations by which strain gauge can be connected in a Wheatstone bridge circuit. During dynamic calibration of the instrumented model and stress bar assembly, strain responses are captured and analyzed in temporal as well as frequency domain. This investigation reveals that half bridge circuit is more suitable for application in impulsive facilities. Further, piezofilm is also mounted on the model assembly and in order to assess the capabilities of both the sensors, the model is subjected to low supersonic flow environment in shock tube to measure the drag force. Drag force acting on the model during the experiment is predicted through de-convolution technique and Adaptive Neuro-Fuzzy Inference System (ANFIS) using the system response function derived from the dynamic calibration responses. Keeping in view of the good agreement between force obtained though experiments and numerical method, it is further planned to extend the application of ANFIS to multi component systems.

Usually during evaluation of system response function for multi component systems, single point dynamic calibration is performed. This seems to be the prime factor for deviation in force magnitude estimation, since recovery of aerodynamic coefficients depends upon the choice of calibration point. In this regard, a new multi-point calibration method is proposed for accurate measurement of aerodynamic coefficients. This methodology is developed using genetic algorithm, with an intention to calculate the responses upon application of forces in orthogonal directions. Thereafter, this methodology in conjunction with ANFIS is assessed through comparative analysis of the force recovery method reported in the literature. Internal accelerometer and piezofilm based force balance systems have been developed and employed for the verification of the proposed strategy. In this regard, a blunt bi-cone shaped model is employed to test in the IITB-Shock Tunnel at two angles of inclination. Encouraging match has been observed between theory and ANFIS based prediction methodology, at all angle of attack conditions, for both accelerometer and piezofilm balances. Thereafter, this method has been extended for drag reduction studies using hemispherical and sharp spikes where sensitivity of force measurement and prediction techniques has been monitored.

CONTENTS

Nomenclature and Abbreviations

Nomenclature

a_1	Speed of sound in the driver section of the shock tube (m/s)
a_4	Speed of sound in the driven section of the shock tube (m/s)
A_{ref}	Reference area of the model (m^2, mm^2)
b_c	Breadth of piezofilm (m)
$C(t)$	Axial force (N)
C_i	Mass concentration of species 'i' (kg/m^3)
Cp_i	Specific heat of species 'i' at constant pressure (J/kmol K)
C_d, C_l, C_m	Coefficients of Drag force, Lift force and Pitching moment
CF	Feedback Capacitance (nF)
d_{31}, d_{32}	Piezo-strain Constant (pC/N)
E	Total energy (J/kg); $E = e + \frac{1}{2}(u^2 + v^2)$
E	Internal energy (J/kg); $e = \sum_{i=1}^{N} e_I \frac{C_i}{\rho MW_i}$
e_I	Internal energy of species 'I' (J/mol); $e_I = h_{f_i}^0 + \int_{T_R}^{T} C_{pi} dT - R_u T$
F	Flux vectors in x direction
F_i	Applied force at ith location (N)
G	Flux vectors in y direction
$g(t)$	Impulse response function of the system
$h_{f_i}^0$	Heat of formation of species 'i' (J/mol)
I	Moment of Inertia of the model (mm^4, m^4)
K_1, K_2, K_3	Spring constant (N/m)
Lc	Length of piezofilm (m)
m	Mass of the model (kg)
$M_{s,e}$	Experimentally obtained incident shock Mach number

$M_{s,t}$	Theoretical shock Mach number
M_∞	Free stream Mach number
MW_i	Molecular weight of species 'i'
N	No. of species
$N(t)$	Normal force (N)
p_4, p_1	Pressure in the driver and driven section of the shock tube (N/m^2, bar)
p_2	Pressure across incident shock wave (N/m^2, bar)
p_5	Pressure in the driven section of the shock tube after the shock reflection (N/m^2, bar)
p_∞	Freestream pressure (N/m^2, bar)
P_{02}	Stagnation / Total pressure (N/m^2, bar)
q_∞	Freestream dynamic pressure (N/m^2, bar)
Re_∞	Freestream Reynolds number
Ru	Universal gas constant (J/kmol K)
S	Source term vector
SI	Inviscid axi-symmetric source term
Si	Mass production rate of species 'i' (kg/m^{3}s)
T_1, T_4	Temperature of the driven and driver section of shock tube (K, °C)
T_2	Temperature across incident shock wave (K, °C)
T_5	Temperature in the driven section of the shock tube after the shock reflection (K, °C)
T_∞	Freestream temperature (K, °C)
TR	Reference temperature for thermodynamic properties (K)
u	Velocity in x direction (m/s)
U	Conserved variable vector
v	Velocity in y direction (m/s)

V_{out}	Voltage output from the circuit (V)
γ_1, γ_4	Specific heat ratio in the driver and driven section of the shock tube
θ	Angle of incidence
ξ_1, ξ_2, ξ_3	Axial, Front lift and Aft lift accelerations of the model (m/s^2)
ε	Output Strain
C_d, C_l, C_m	Coefficients of Drag force, Lift force and Pitching moment
μ_∞	Freestream dynamic viscosity (Pa-s)
ρ	Density (kg/m^3)
υ	Poisson's Ratio
α_i	Weights corresponding to location 'i'

Abbreviations

2-D	Two-Dimensional
AF	Amplification Factor
AFB	Accelerometer Force Balance
ANFIS	Adaptive Neuro Fuzzy Inference System
AOA	Angle of Attack
AUSM	Advection Upstream Splitting Method
C-D	Converging Diverging
CFD	Computational Fluid Dynamics
CG	Center of Gravity
DAS	Data Acquisition System
FE	Finite Element
FEA	Finite Element Analysis
FFT	Fast Fourier Transform
FL	Fuzzy Logic
GA	Genetic Algorithm
GF	Gauge Factor
IITB-ST	Indian Institute of Bombay - Shock Tunnel

IITG-ST	Indian Institute of Technology Guwahati – Shock Tube
MF	Membership Function
MISO	Multi Input Single Output
NN	Neural Network
PSD	Power Spectrum Density
PSP	Pressure Sensitive Paints
PVDF	Polyvinylidene Fluoride
PZT	Lead Zirconate Titanate
RK5	5th order Runge-Kutta
SSG	Semiconductor Strain Gauges
SWFB	Stress Wave Force Balance
TPS	Thermal Protection System
UDF	User Defined Function

List of Figures

List of Tables

CHAPTER-1

Introduction

Overview

In aviation industry it is often quoted that "you have to do it immediately, before your body realizes it is defying the laws". The recent advancement in aerospace technologies has led to development of numerous extents of manned and unmanned flight vehicles that can operate from transonic to hypervelocity regime. In these flying regimes, usually the aerodynamic vehicles are designed to sustain high drag and surface heating, induced by a strong shock wave in front of it. However, to mitigate the consequences of surface heating, vehicles are designed as a blunt body having large nose radius, which in turn increases the wave drag thereby enhances the fuel consumption. Therefore, accurate estimation of the forces acting on these vehicles will not only provide an estimate regarding the fuel requirement but also will determine the stability of the vehicle. In this regard, various technologies have been evolved and tested in ground based facilities for accurate prediction of forces. Hence, the present investigation is focused towards development of piezofilm based force measurement, which has been evaluated for its effectiveness in several ground based facilities like shock tube and shock tunnel. A brief introduction on aerodynamics of hypersonic flows, available ground based facilities to affirm the new technologies and various force measurement technologies already adopted are briefly reviewed in this chapter. The objectives of the present thesis are concisely elaborated at the end of this chapter.

1.1 Characteristics of Hypersonic Flows

The aviation technology has been an all-time curious wing for the mankind. With the turn of the century, the space age has revolutionized science all over the world. This has further led to development of advanced technologies by many countries in the sector of rocket and satellite design as well as launching. Hence, the development of satellites, space crafts, and re-entry vehicles has undergone a paradigm shift in a short span of time. Thus the recent years' of development in these areas has led to a number of new aerodynamic problems into existence. Majority of the problems encountered during atmospheric re-entry arise due to extremely high flight velocities termed as hypersonic aerodynamics. Typically flow with Mach number greater than 5 is considered as hypersonic flow. The main characteristics of hypersonic flow are thin shock layers, thick boundary layers, regions having strong vortices, dominating viscous interaction and high temperature effects. Existence of these above stated phenomena is solely influenced by the mission requirements which decides trajectory to be followed during the flight and the vehicle configuration. Therefore, the need of aerodynamics, flight dynamics, propulsion, and structures associated with hypersonic vehicles is much more critical than for the conventional aircrafts. Typical flow features observed in case of hypersonic flows are illustrated in **Fig. 1. 1**.

The characteristic features in this flow regime can be well understood from the flow field solutions which can be obtained through numerical methods or using well-established analytical solutions. However, this seems to be a tedious task in case of a complex geometry and necessitates controlled experimental techniques to obtain the flow parameters. Moreover, the affirmation of new evolved hypersonic technologies also needs experimental testing before the actual implementation. Experiments can be carried out either by flight testing or by testing in ground test facilities. But lesser cost and risk provide an edge to the ground testing. The tests include design of propulsion systems, engine performance, and thrust measurements. The vehicle configuration determines the amount of drag force and surface heating that is going to be imposed upon the vehicle. Conventionally, blunt bodies with large nose radius are preferred to reduce the aerodynamic heating. This leads to higher amount of drag force imparting on the model which in turn enhances the fuel consumption. Hence, there should be always a trade-off between stagnation point heat flux and forces acting on the vehicle. Further, accurate estimate of the forces not only provides knowledge of fuel requirement but also helps in determining the trajectory and stability of the vehicle. Many researchers have extended their efforts towards developing analytical relations, numerical simulations and experimental techniques to predict the forces acting on the model. Hence, this work is dedicated to develop new prediction methodologies and experimental approaches to recover the force and moment coefficients from the experimentally measured acceleration or strain signals for various aerodynamic configurations.

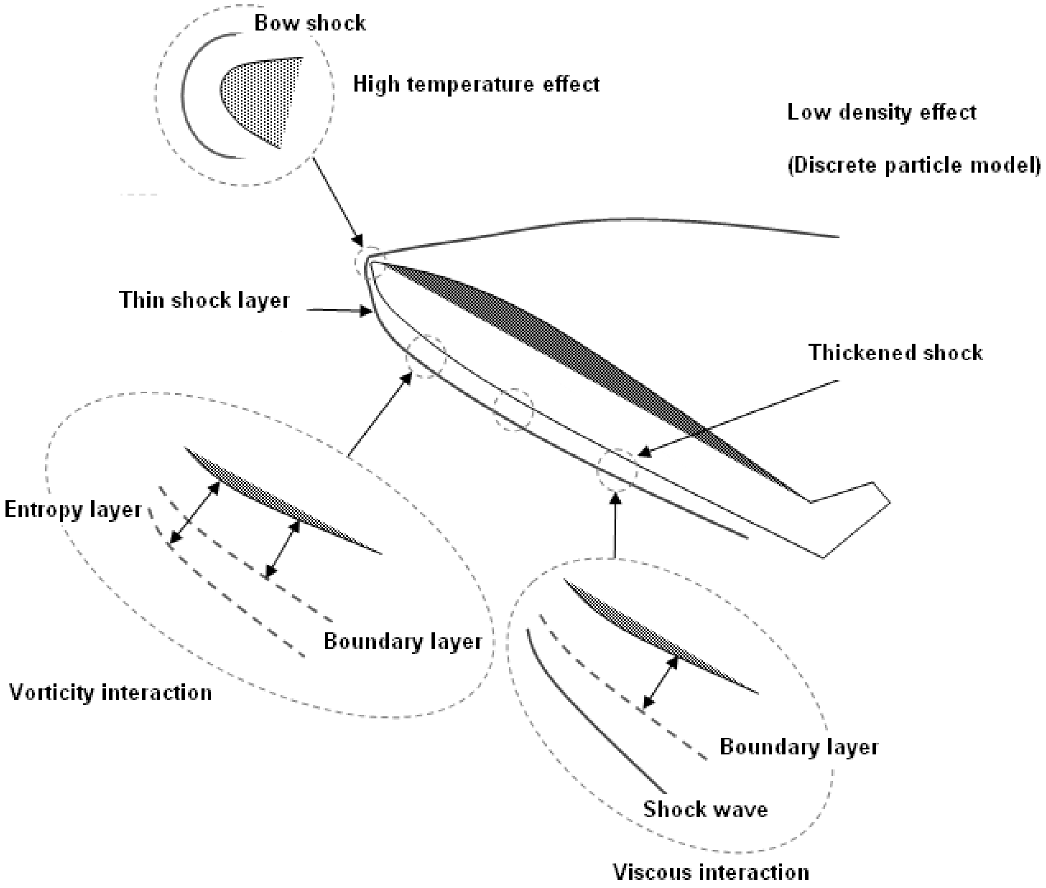

Fig. 1. 1: Flow characteristics of hypersonic regime.

(https://nptel.ac.in/courses/101103004/module4/lec6/3.html)

1.2 Impulse Test Facilities

As described earlier, experimentation is essential to obtain the aerodynamic coefficients for a desired configuration or for affirmation of new aerospace technologies. Ground based facilities are preferred for these experiments due to safety and lower associated cost. This has led to development of several ground based test facilities. Such tests are usually conducted in the supersonic or hypersonic wind tunnels and impulse facilities which include shock tubes, reflected shock tubes, free piston shock tunnels, gun tunnels and expansion tunnels. These test facilities provide the actual condition of the space vehicle in air and it can also simulate the high enthalpy flows of desired test duration for the purpose of providing actual test condition. These facilities can be utilized for external aerodynamic study of space planes as well as internal aerodynamic study of scramjet propulsion systems. Further, these facilities have ultra-short test duration. This short duration should be enough to create flow environment similar to the actual flow conditions. However, measurement of responses during this short duration becomes extremely difficult.

1.2.1 Shock Tube

The basic principle of this impulse facilities commence from sudden release of a highly compressed gas in the driver tube through rupturing a diaphragm. As a result of which a shock wave propagates into the driven section which was initially filled with test gas at low pressure. The shock compresses and heats the test gas to the desired condition. Basically, thickness of the diaphragm, driver gas and driven gas properties determines the strength of the primary shock wave that travels into the driven tube [White (1958)]. In conjunction with the formation of shock wave, expansion fan is also generated which traverse towards the driver section. Afterwards, these waves interact among themselves causing further elevation in temperature inside the test section. Typical set-up and flow features developed in a shock tube facility are illustrated in **Fig. 1. 2.** This impulse facility has been incorporated for various studies related to low supersonic aerodynamics. Typical test duration for this facility lies in the range of few hundred of microseconds.

Shock tube has been implemented as the test facility for measuring drag force on a spherical model by monitoring the displacement during test duration. Here displacement is measured by tracking its location through image-based technique like double exposure holography [Igra and Takayama (1993)]. Drag force on similar spherical configuration is also obtained using a vertical shock tube where output responses are measured using accelerometer [Tanno *et al.* (2003)]. Further, shock tubes in association with laser diagnostics are also used while studying the chemical kinetics during ignition of hydrocarbons [Davidson and Hanson (2009)]. In a similar study, shock tube is used as a tool to quantify ignition delay times for a series of jet and rocket fuels [Davidson *et al.* (2017)]. This impulse facility has also been employed to investigate deformation field of thin steel plates during blast events using digital image correlation technique [Aune *et al.* (2016)]. Finally, an attempt has been made to determine the stagnation heat flux at the end flange of the shock tube [Agarwal and Sahoo (2018)]. Considering the diverse application of shock tube, it can be noted that, this facility can be used for testing of any new technologies in supersonic environment. In the present investigations, shock tube is used as a tool for conducting experiments to measure drag force with usage of strain gauge and piezofilm based balances.

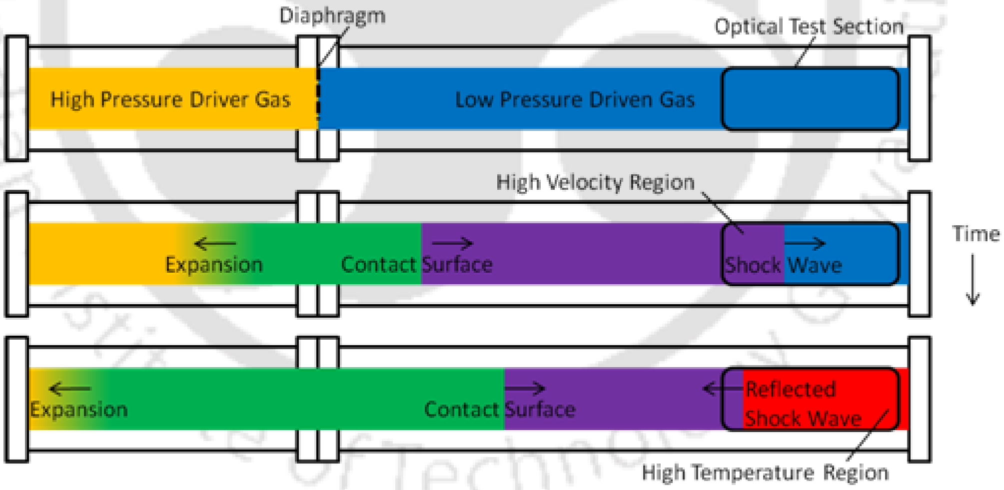

Fig. 1. 2: Schematic of typical shock tube facility and its associated flow features.

(https://www.ucalgary.ca/johansen/research-projects)

1.2.2 Shock Tunnel

In addition to the shock tube section, shock tunnel comprises of a Converging Diverging (C-D) nozzle, test section and dump tank as shown in **Fig. 1. 3**. This nozzle is the most influencing factor which facilitate to obtain the desired hypersonic free stream conditions inside the test section [Jiao *et al.* (2017)]. With variation in the dimensions of the nozzle, it is possible to create any hypersonic condition at the exit. The operational procedure for the shock tunnel is similar to shock tube. Here as well, the experiment initiates with the bursting of the diaphragm due to the pressure difference between driver and driven section. Afterwards, incident shock wave propagates towards driven section and expansion fan towards driver section. Further, this incident shock wave gets reflected from the end flange, which in process bursts the paper diaphragm separating between shock tube and tunnel section. As a result, the reflected shock wave is expelled by the nozzle to a hypersonic condition. The free stream conditions can be obtained through mounting a pitot probe in the test section, which also facilitate in estimating the steady test duration. Usual test time for this impulse facility lies in the range of hundred of microseconds to few milliseconds.

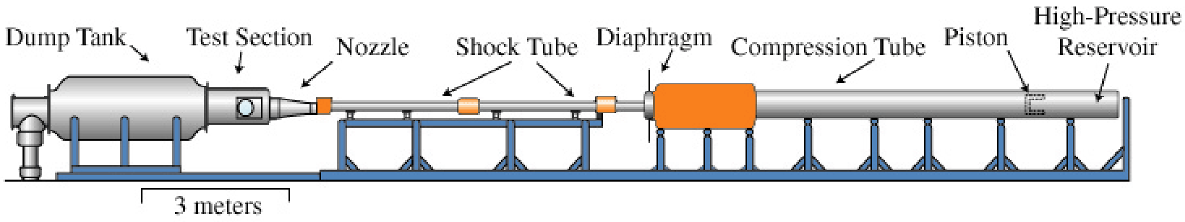

Fig. 1. 3: Schematic of shock tunnel facility.
(http://www.anu.edu.au/aldir/Canberra_Hypersonics/)

Shock tunnel has been incorporated as a tool for several aerodynamic studies. In the preliminary stages, shock tunnel has been used to investigate the behavior of boundary layer transition for a conical model at a free stream Mach number of 5.5 [Rushton and Stetson (1967)]. Further, shock tunnel is used to explore the aerothermodynamic characteristics of Japan's space vehicle HOPE and for testing of its scramjet propulsion systems [Itoh *et al.* (2002)]. Wang *et al.* (2015) has developed and tested a force measurement technique based on pulse-type strain gauge balance which can be applicable to shock tunnel having larger test duration. Afterwards, attempt has been made to measure stagnation heat flux over a blunt body using coaxial surface junction thermocouple at a free stream Mach number of 8.2 [Agarwal *et al.* (2017)]. This test facility has also been employed for study of skin friction coefficient over a flat plate using piezoelectric skin friction balance at a freestream unit Reynolds number of 3.09 x 10^7 [Zhiguo *et al.* (2017)]. Considering the vast application of this impulse facility, it is also considered for the present study for testing of newly developed three-component piezofilm based force balance, that enables deduction of coefficient of drag, lift and pitching moment, at hypersonic conditions.

1.2.3 Expansion Tunnel

The expansion tunnel comprises of driver tube, driven tube, acceleration tube, nozzle, test section and dump tank, as presented in **Fig. 1. 4** The additional entity viz. acceleration tube can accelerate test gas to high velocities analogous to that in the test section of the shock tunnel. But, the temperature and pressure in the acceleration tube is much lower than the shock tunnel free stream conditions. However, to obtain desired velocity range as well as pressure and temperature, again a nozzle has been connected to the end of the acceleration tube. Here, the driven section and acceleration section is filled with same test gas but the pressure maintained inside the acceleration section is lower than that in the driven section. So, all the sections are separated by a diaphragm. Experiment is initiated through rupturing the diaphragm, separating between driver and driven section, resulting in formation of a shock wave that propagates into the test gas, thereby elevating its temperature and pressure. This incident shock further travels down and ruptures the secondary diaphragm separating driven and acceleration tube, causing unsteady expansion of the test gas which further expands in the nozzle and attains desired free stream conditions in the test section. Typical test duration for this impulse facility is few hundreds of microsecond.

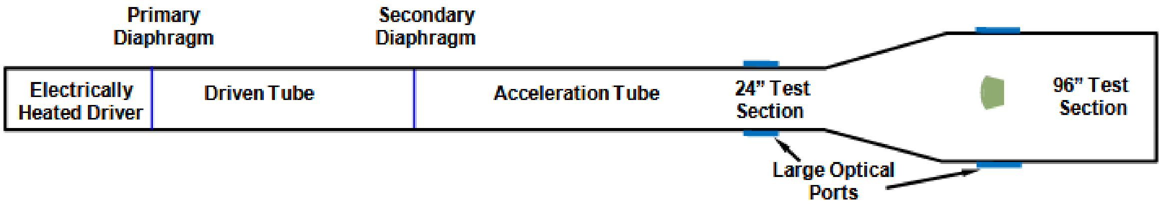

Fig. 1. 4: Typical set-up of an expansion tunnel. [Dufrene *et al.* (2010)]

Mostly this impulse facility has found its application in high enthalpy studies. LENS-XX expansion tunnel facility has been used to study the aerothermal behavior of the Orion heat shield capsule using thin-film and thermocouple for free stream velocities 3 - 8.4 km/s [Dufrene *et al.* (2012)]. Similarly, experiments have been conducted in X2 superorbital expansion tunnel to get an estimate of radiative heat flux and emission spectroscopy for hemispherical and conical models [Porat *et al.* (2017)]. In view of lesser attention to expansion tunnel for force measurement application, it has not been considered in the purview of the current experiments.

1.2.4 Gun Tunnel

Gun tunnel has significant resemblance with the shock tunnel facility except the presence of a piston in the driven section as illustrated in **Fig. 1. 5**. This impulse facility is usually used to produce hypersonic flows having high stagnation pressure and moderate stagnation enthalpy. The operating procedure for the facility is same as the shock tunnel. The experimentation begins with generation of high pressure inside the driver section which in turn bursts the diaphragm separating the driver and driven section. With the rupture of the primary diaphragm, piston accelerates, thereby raises the test gas temperature adiabatically [Ahmed *et al.* (2012)] and also executes the same function as that of the contact surface viz. avoid any mixing between the driver and driven gas. In this facility, mass of the piston plays a vital role, as it determines the time required to attain equilibrium piston speed, which can affect the post-shock conditions of the driven gas. This heated and compressed test gas ruptures the secondary diaphragm and passes through the C-D nozzle, where it expands to desired free stream conditions. For this facility, test duration is the order of several tens of milliseconds.

Gun tunnel has been incorporated to measure the stagnation-point heat-transfer rates at a Mach number of 9.8 using both thin-film gauges and calorimeter [Edney (1967)]. Lewis and East (1995) developed a method for measuring dynamic stability derivatives of a conical model during testing in gun tunnel from the model trajectory obtained during test duration using electro-optical high-speed passive tracking system. Further gun tunnel has been utilized to investigate the shock wave boundary layer interaction for laminar and turbulent flows at different operating conditions [Hillier (2015)]. As, on very rare occasions, force measurements are carried out in gun tunnels and as already it is planned to have testing of developed methodology for current studies in shock tunnel, so this facility is not explored further for experimentation.

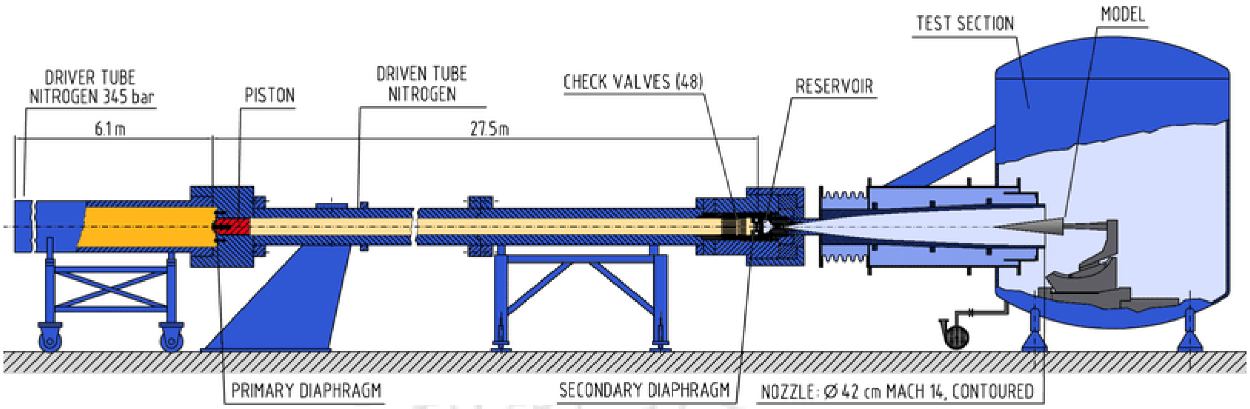

Fig. 1. 5: Diagram showing parts of a gun tunnel. [Ilich *et al.* (2017)]

From the in depth review of all the impulse facilities, it is apparent that as the test duration in these test facilities is very small, therefore, the employed sensors must have less response time than the test flow duration. Due to this restriction in test duration, employable sensors in these domains seem to be very less in number, thereby making the measurement process more complex. The measurement of aerodynamic forces on models in hypersonic impulse facilities has been restricted in the past because of the time taken for the test model to reach a state of force equilibrium with its support mechanism [Bernstein 1975]. Afterwards, it is identified that equilibrium can't be achieved within this short test duration. As a result, it is realized that there is a need of inclusion of the entire system dynamics through proper designing of the force balances. Therefore, the subsequent section describes all the details in regard to the design of force balance, that can be applicable in short duration facilities for force measurement.

1.3 Force Measurement Technique

Mostly the aerodynamic body is subjected to three forces (drag, lift and side force) and three moments (rolling, pitching and yawing) during its motion (**Fig. 1. 6**) and usually the coefficient of these forces and moments are measured. The aerodynamic forces and moments on a moving body are usually due to two basic sources that comprises of pressure i.e. normal to the surface and shear stress distribution which is tangential to the surface of the body. These forces and moments can be either indirectly measured by integrating the local pressure over the model surface or by directly through appropriate sensors and measurement techniques. During the course of indirect measurement, local pressure can be measured by either pressure transducers or pressure sensitive paints (PSP) which can measure two-dimensional pressure distribution [Ardasheva *et al.* (1985)].

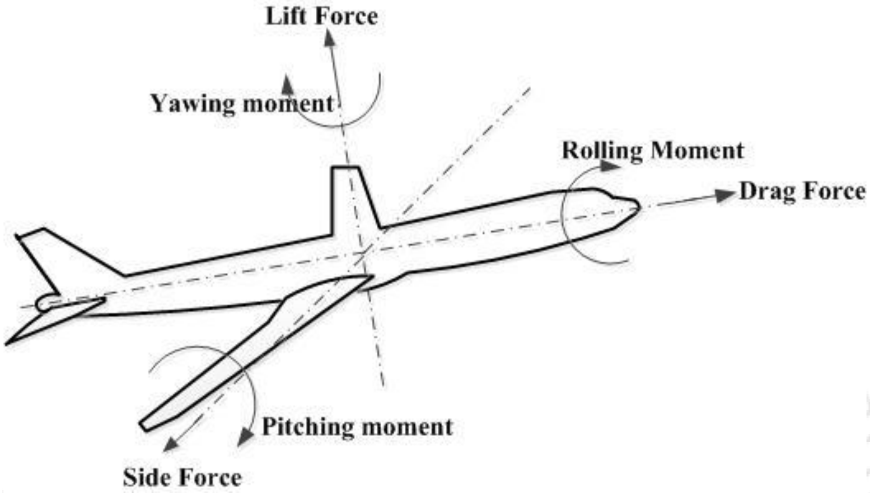

Fig. 1. 6: Forces and moments on aerodynamic body.

These PSPs work based on recording the brightness of the coating luminescence as it varies with pressure but deduction of forces from the measured signals of PSP is not accurate. The reason for the same, can be attributed to the fact that PSP cannot withstand high temperature and pressure gradients produced due to high enthalpy flows and PSPs have more response time. Further, it should be noted that during course of direct measurement, appropriate sensors must have less response time than the test flow duration. Therefore two major techniques adopted during force and moment measurement in impulse facilities i.e. inertia dominated and stiffness based force balance. Mainly these short duration force balances include design, modeling, calibration and prediction of aerodynamic forces and moments. The entire methodology of force recovery for application in short duration impulse facilities is presented in **Fig. 1. 7**.

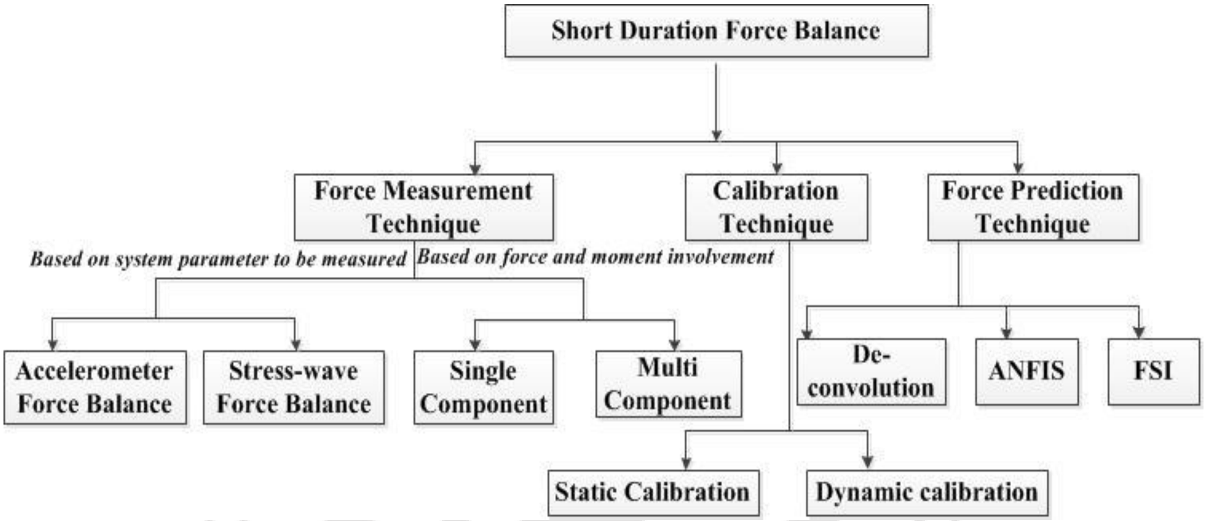

Fig. 1. 7: Flow chart of the process involved with short duration force balances.

1.3.1 Inertia Dominated Force Balance

In this type of force balance the structures associated with it, are considered as lumped parameter elements which rely on measuring the components of transient acceleration during the test. So, it is also called as Accelerometer Force Balance (AFB) system. Acceleration can be measured directly by putting the accelerometers inside the model, which is mounted through flexible support system to consider it as 'unrestrained' and to ensure free flight condition during flow situation. Acceleration can also be measured indirectly through differentiating the velocity signals. Afterwards, the aerodynamic force and moment can be measured from the measured acceleration with prior knowledge of mass and moment of inertia of the model. The location of accelerometers plays a vital role in calculating the various moments in multi component accelerometer balance system. Further, the acceleration responses seems to be affected by the degree of free flight motion, achieved during the test duration. An accelerometer force balance equipped conical model, supported by flexible string for measurement of drag has been illustrated in **Fig. 1. 8.**

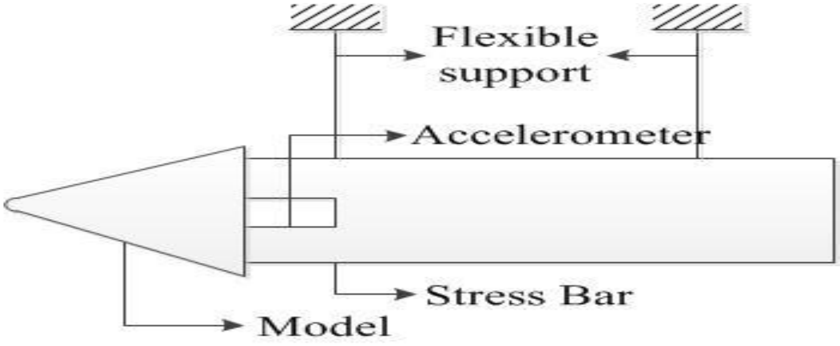

Fig. 1. 8: Accelerometer force balance system.

Several techniques have been developed to attain free flying condition during experimentation. A simple and cost effective method is adopted by Tanno *et al.* (2007), where the model is weakly suspended with the help of thin wires and acceleration responses are obtained for free stream conditions having stagnation enthalpy up to 25 MJ/kg. Similarly, an internally mountable single component accelerometer based force measurement technique has been adopted to attain unrestrained motion through arrangements comprising of steel rings and rubber bushes [Kulkarni and Reddy (2010)]. Joarder and Jagadeesh (2003) made use of a single component free floating balance system where model is mounted on frictionless spherical rollers to ensure free flight motion of model during testing where steel rollers provide point contact between the model and support system and henceforth minimizes the friction. As an advancement for this concern of free flying achievement, Tanno *et al.* (2014) has established a novel technique that incorporates the concept of magnetic releasing and holding of the model in synchrony with the arrival of the test flow. Afterwards, these techniques have been incorporated in various impulse facilities to measure the force and moment coefficients for several aerodynamic configurations.

Sahoo *et al.* (2007) incorporated rubber and steel ring based free flying technique to measure the axial acceleration responses in IISc hypersonic shock tunnel HST2 at Mach 5.75 with test flow duration of $800\mu s$. The same method has been extended for the AGARD model to measure coefficient of drag, lift and pitching moment at a free stream Mach number of 8.0 [Saravanan *et al.* (2009)]. A similar investigation for six component force balance has been done in two fragments, first one is by Menezes *et al.* (2011) in which a flapped, blunt-nosed, triangular lifting body with same soft suspension system as earlier, is tested in a hypersonic shock tunnel (IITB-ST) at free stream Mach number of 8.0 with different angle of attack to measure drag, lift, and roll using AFB system. Secondly, in a similar approach an accelerometer balance was investigated by Trivedi and Menezes (2012) on a blunt triangular model in a hypersonic shock tunnel, IITB-ST for an average test time of 800-1000 μs to measure yawing moment, pitching moment, and side force.

Acceleration can also be measured by differentiating the velocity signal obtained from non-contact type laser-based extrusive technique as developed by Ramesh *et al.* (2014). Velocity based system identification was implemented to predict unknown forces, but an inconsistent behavior of force prediction was observed. So, another technique viz. to find acceleration from the velocity response and usage of it for determining the response function was presented. The modified technique predicts the unknown forces accurately, so necessity of determination of acceleration response from velocity response in case of non-contact type measurements for force prediction has been realized.

It has been observed that most of the literature is concentrated towards incorporation of accelerometer balance in force measurement studies, as the response acquisition procedure is quite lucid and easy to implement. The availability of the analytical relations to obtain the force and moment coefficients from the measured acceleration responses, is also attributed as one of the reasons for widely acceptance of this technique. Practically, this method eliminates the requirement of dynamic calibration before the actual experiments in impulse facilities. However, this in turn affects the force prediction accuracy, as the analytical relation is based on certain assumptions. This method of force measurement is reliable for test models of lower mass. But this technique is not recommended for test models of larger length or higher mass, as it doesn't account system dynamics.

1.3.2 Stiffness Dominated Force Balance

When the model size and mass is large, the effect of unsteadiness becomes more severe between model and its support structure. Hence inclusion of system dynamics to recover transient aerodynamic force becomes necessary. Stiffness dominated force balance is designed according to the above principle and rely on measurement of force from strain signal measured either by semiconductor strain gauges or by piezofilm. Unlike the accelerometer balance systems, there is no requirement of free flying condition, as during fixed condition also, the strain response can be obtained. In this category of force balance, model is assumed to behave as a rigid body. When aerodynamic load is applied to the model, then stress waves are initiated and propagate along the stress bar attached to the end of the model and reflect within the model and its support structure. So, this force balance is also designated as stress wave force balance (SWFB) system. Further, these force balances can be termed as internal or external SWFB system, depending on the sensor location viz. whether housed inside or outside the model. In order to model the system dynamics exactly, the strain sensors should be mounted on the stress bar and most likely close enough to the model such that observation time will be more. Again the stress bar should be long enough, so that it would be difficult for the reflected shock wave to reach the strain measurement location within the test duration. SWFB balance can be categorized depending upon the sensors employed for strain measurement. A typical diagram of the SWFB system having free flying condition is shown in **Fig. 1. 9**.

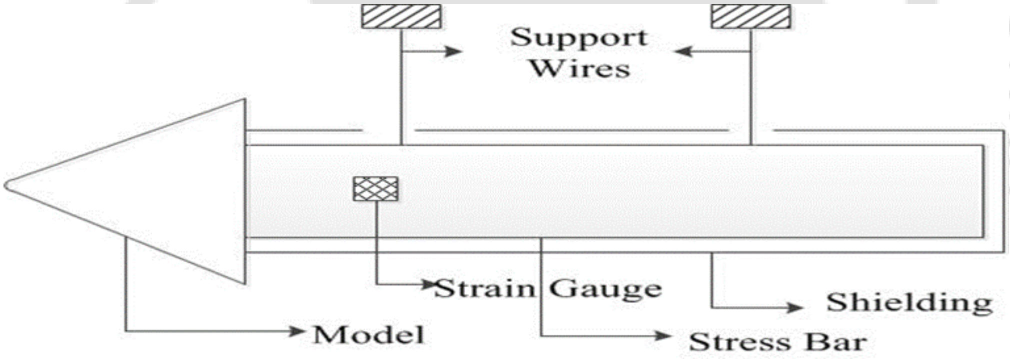

Fig. 1. 9: Stress wave force balance system.

1.3.2.1 Strain Gauge Based Balances

In this category of force balance, strain gauge is incorporated as the sensor which enables in measuring the strain response during the measurement process. Depending upon the magnitude of forces, strain gauges are deformed, thereby altering its resistance. This resistance change can be measured by connecting it to a Wheatstone bridge circuit, comprising of some fixed as well as some variable resistors. This measurement methodology has been adopted in several impulse facilities to predict the coefficient of forces and moments acting on aerodynamic configurations.

Sanderson and Simmons (1991) and Tuttle *et al.* (1995) designed conical models with a stress bar which is supported by vertical threads to ensure an unrestrained motion during testing in the free-piston shock tunnel. Strain response with the help of a strain gauge is recorded and drag force is obtained from the numerically as well as experimentally derived impulse response function. Afterwards, this method has been extended to study the feasibility of three-component force balance applicable in hypervelocity flows, through mounting multiple number of strain gauges on the model and associated stress bar [Mee *et al.* (1996)]. An attempt has also been made to predict the coefficient of forces and moments associated with three component force balance with usage of internal SWFB [Robinson *et al.* (2011)]. Experiments have been conducted for various angles of attack (AOA) at two different enthalpies and the measured coefficients have been compared with the computational results. Jessen and Gronig (1989) proposed a new balance to be used for six component stress wave force balance system. The balance was designed as a cross which comprises of four beams of square cross-section and two semiconductor strain gauges are placed to each side of the beams to acquire the responses. Further, to enhance the effectiveness of this methodology towards force prediction, an acceleration compensated strain gauge balance is employed which results in good agreement of the drag force with the non-equilibrium based Navier–Stokes computations [Marineau *et al.* (2012)].

From the exhaustive literature review, it can be perceived that, this method of force prediction is reliable for application in any of the flow regimes. Also, this method can be employed for all the configurations irrespective of any constraint on its mass and length. Moreover, SWFB system seems to be capturing the system dynamics more accurately in comparison to accelerometer balance, as it incorporates detailed calibration process during force recovery. However, there is no analytical relations available to calculate the force and moment coefficients from the recorded strain responses. Therefore, force prediction using this technique is mathematically intensive. Different calibration techniques that can be associated with the SWFB system, during the process of deduction of force and moment coefficients from the experimentally measured strain responses, are elaborated in the following section.

1.3.2.1.1 Dynamic Calibration Methods

The basic intention of calibration techniques is to exactly evaluate the impulse response or transfer function for a dynamic system that correlates among the input and output responses. Afterwards, using the system identification and some inverse techniques, it is possible to determine the aerodynamic force time history from the measured signals. Mee (2003) emphasizes on various ways of determining the impulse response function. The system identification or the impulse response of a model and its associated balances can be evaluated by recording the output responses corresponding to application of a step or impulse load.

Usually cut weight test (for applying step load) or pulse test (for applying impulse load) is performed as a part of the dynamic calibration process. During the cut weight test (**Fig. 1. 10(a)**), the model and its associated support structure is held vertically and known load is applied to the tip of the model via fine wire. As the wire is cut, the arrangement experiences step loading due to removal of weights and thus using recorded responses, impulse response is derived through incorporating some inverse techniques. In this case the impulse response derived from step load is valid for the time interval taken by the stress wave to travel from the tip of the model to the end of the stress bar and return to the location of measurement. Similarly, pulse test on the model along with the support structure is performed for calibration corresponding to a true impulse (sudden load for very short time duration). It is never possible to produce a true impulse but a short impulse can be produced having same effect. For smaller pulse duration compared to the characteristics time of the system, area under the pulse is important but for a larger pulse duration, shape of the pulse has a great significance. Typically, an impactor or impulse hammer is used to apply impulse load (**Fig. 1. 10(b)**) and the magnitude and trend of the impulse can be acquired by connecting it to a data acquisition system (DAS) which displays the force-time history of the applied load. As a true impulse force can be resolved into harmonic functions of different frequencies [Dieulesaint and Royer (1980)], therefore for the current studies, in all the cases, pulse calibration test using impulse hammer has been performed.

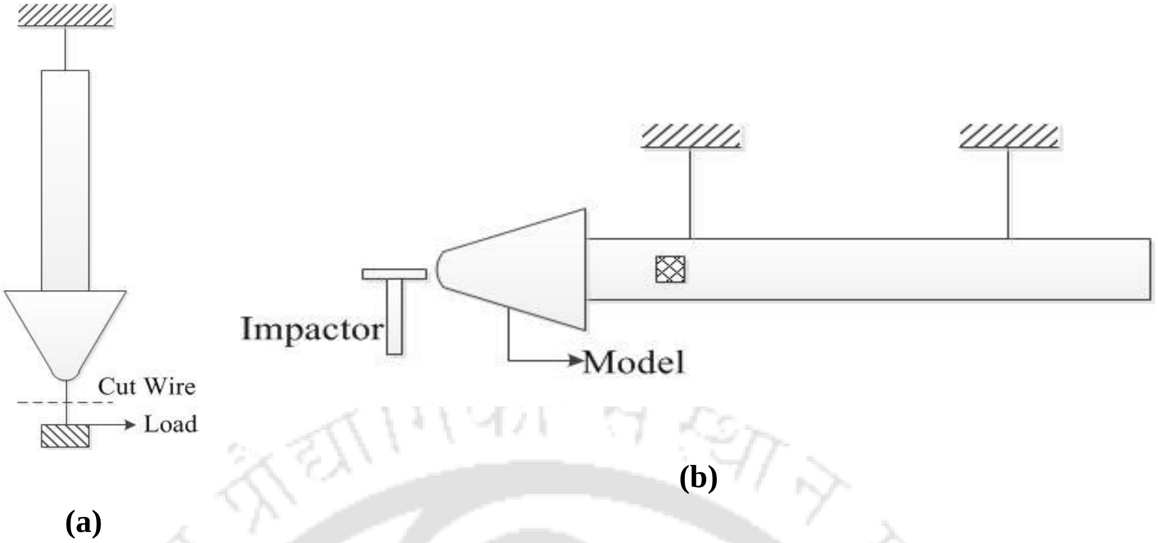

Fig. 1. 10: (a) Cut weight test (b) Pulse test using impactor.

A new pulse test based calibration technique is proposed by Abdel-jawad *et al.* (2007) which is useful for three-component stress wave balance systems where orthogonal forces can not be applied to the model. During this process, de-coupled de-convolution technique was implemented for determining the elements of the impulse response matrix. Reis *et al.* (2013) proposed a method for evaluation of uncertainty present in the calibration process for an external multi-component aerodynamic balance using multivariate polynomial fitting and law of propagation of uncertainty.

The above stated dynamic calibration techniques can be applied to arbitrary models and associated support structures to obtain impulse response function of the system. Further, it can be also noted that these calibration techniques are only limited for the use of strain gauge based balances. These methods can also be applicable for accelerometer as well as piezofilm based balances for obtaining the transfer function of the system. Having information related to the system response function, one may opt for any inverse technique to recover the applied transient force history from the output responses. Details regarding the inverse techniques and other artificial intelligence based force prediction algorithms have been described in the subsequent chapters.

1.3.2.2 Piezofilm Based Balances

This class of force balance incorporates piezofilm for detecting the stress waves propagating inside the model, thereby facilitate measurement of induced dynamic strain [Duryea and Martin (1968)]. Two broad categories of piezo materials viz. lead zirconate titanate (PZT) and polyvinylidene fluoride (PVDF) film is employed for this purpose [Sirohi and Chopra (2000)]. However, only PVDF sensors can be used for high temperature applications. Further, PVDF is preferred over PZT due to its lower value of Young's modulus and it is less likely to affect the dynamics of the parent structure due to its own stiffness [Sahoo and Reddy (2010)]. These piezoelectric or piezoceramic materials are usually polarized in character, hence respond to the forces in a particular direction. These materials rely on converse piezoelectric effect which is based on the fact that they have ability to generate mechanical strain when exposed to electrical field. Hence such sensors can sense the structural deformation generated due to load application. Thus, PVDF piezofilm based force balance has been extensively incorporated in various impulse facilities for force measurement.

Matsumoto *et al.* (2004) demonstrated the use of PVDF film on a structural component for surface strain measurement using theory of piezoelectricity. Vadassery *et al.* (2013) designed a rigid triangular force balance for drag measurement in a shock tunnel at Mach 9.4. Both strain gauge and piezofilm are used for the output response measurement, from which drag force is recovered, using the impulse response function derived during dynamic calibration. An accurate force measurement technique based on acceleration compensated piezo-electric force balance has been developed by Marineau (2011). Applicability of this technique was demonstrated through performing tests in a shock tunnel for prediction of force and moment coefficients. Further, application of PVDF piezofilm has been extended to measure the magneto-hydrodynamic drag force in an expansion tube [Smith *et al.* (2018)]. However, the attempt was unsuccessful due to an unforeseen noise issue which seems to arise from electrical interference of the flow.

In contrary to strain gauges, piezofilms are light, flexible, low cost and can be adhered to any kind of surface irrespective of its electrical and conductive nature. Further, the sensitivity is more for piezofilms in comparison to strain gauges and is likely to be less influenced during harsh environments. However, piezofilm based force measurement were not considered in impulsive testing since these films were not available as compact sensors earlier. Such larger sized films were not suitable for strain measurement since those were not suitable to get local strain time history. Although not in smaller size like strain gauges, but in due course of time, these films are made available as small sensors. Hence present efforts are focused initially on understanding the feasibility of strain measurement using piezofilms and later on devising the strategy for recovering forces from acquired strain signals.

1.4 Summary

Thorough literature review, considering National and International status of work related to aerodynamic force measuring techniques for impulse facilities reveals that, there is still an enormous scope to explore different aspects of the aforementioned topic. The survey was also focused on finding the gaps in literature, which are analyzed and can be summarized in the following points.

- The available literature encompasses various experimental techniques for axial force/drag measurement employing accelerometer and stress wave balance system using shock tube and shock tunnel facility. But, drag measurement and prediction using piezofilm sensor has not been explored in these impulse facilities.
- Multi component force measurement through incorporation of accelerometer balance has been investigated. However, this technique of force prediction needs special attention, as in most of the cases there seems to be much deviation in lift force and pitching moment recovery.
- Stiffness dominated balance, specifically strain gauge based system, need in depth experimental investigation towards electrical connection of the sensors in Wheatstone bridge circuit since this topic is still unexplored. Also, comparative assessment between both types of SWFB balance has not been attempted.
- Necessity of a prediction algorithm other than inverse techniques is realized, as employing calibration methodology for multi-component force prediction is computationally intensive and involves rigorous mathematical formulations.

- Comparative assessment of the capabilities of different balance seems lacking and hence needs attention.

1.5 Objectives of the Thesis

The core objective of the current PhD work involves "**Development and calibration of multi component force balance with execution of soft computing and de-convolution techniques for aerodynamic force prediction**". In order to achieve the key objective, the entire work is delineated into few milestones, which are listed as follows:

- **Design and Fabrication of Force Balance:** Initially two different models viz. a hemispherical model, for experiments in shock tube facility and a slender bi-cone model, for testing in shock tunnel facility have been fabricated. As, the design of a force balance plays a vital role in accurate response acquisition during its test in terms of both magnitude and trend. So different balance designs like accelerometer and stress wave based systems have been planned to implement in impulse facilities. During the design for accelerometer force balance, the necessary requirement of free flight condition in the course of experimentation has been ensured with the usage of rubber bushes of appropriate stiffness. However during the design of stress wave force balance, an internally mountable balance proposed by Robinson *et al.* (2011) has been incorporated with appropriate dimensions so as to press fit inside the model under consideration.
- **Calibration of Model and Associated Balance:** The calibration methodology has to be conducted to get an estimate of the system response function which is a relation between output response and input force. Dynamic calibration for all the fabricated balances is to be carried out with the help of impulse hammer at different locations on the model. Afterwards these responses have to be incorporated in conventional single point calibration methodology and a newly developed multi-point calibration procedure to calculate the transfer function of the system.
- **Real-time application-based study:** The force balances are used to capture transient variation in acceleration/ strain responses in real time experiments. The present work is focused on estimation of the temporal variation of drag force using piezofilm and

strain gauge based balances in a low supersonic environment such as that of shock-tube. Also, attempt has been made to recover temporal variation of coefficient drag force, lift force and pitching moment using an accelerometer balance and piezofilm based balance in the short duration hypersonic facilities such as shock tunnel.

- **Prediction of Forces:** The measured experimental responses and the estimated system response function during calibration are fed to the prediction algorithm for recovery of forces. Conventional de-convolution method and adaptive neuro fuzzy inference system (ANFIS) (which is a soft computing based technique) constitutes the two prediction algorithm that has been implemented during the current study. In some of the cases, numerical studies have also been performed to validate the results obtained from the prediction techniques. Sensitivity study of force measurement and recovery techniques have also been performed in shock tunnel for hemispherical and sharp spike based drag reduction arrangements.

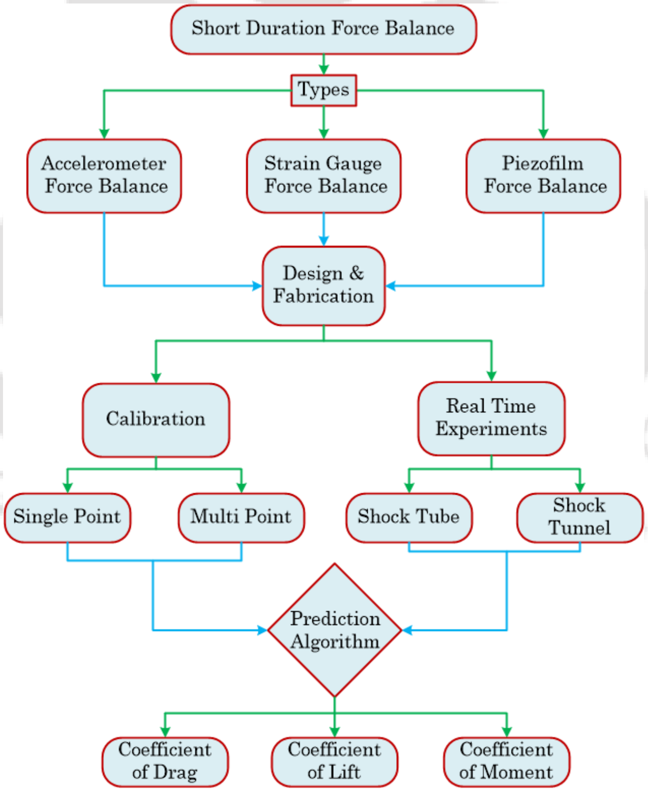

Fig. 1. 11: Flowchart highlighting the overview of thesis work.

Experimental approach followed during the course of the entire curriculum, to achieve the desired objectives is illustrated in **Fig. 1. 11**.

1.6 Structure of the Thesis

Various stages of the current investigation as listed above, are briefly discoursed in the succeeding segments. **Chapter 2** describes the two ground based experimental facilities involved during the current phase of investigation viz. shock tube and shock tunnel. Details regarding working principle of all the sensors that have been implemented during the course of time, have also been elaborated. **Chapter 3** emphasizes on the details of the effect of different circuitry arrangement, necessary for precise measurement of strain time history for impulsive loading applications. **Chapter 4** describes the demonstration of applicability of piezofilm along with the qualitative assessment in regard to the strain gage for force measurement in an impulse test facility. **Chapter 5** dwells on the comprehensive investigation of a new multi-point calibration methodology in association with the soft computing technique for accurate measurement of coefficient of drag, lift and pitching moment using internally mountable accelerometer balance system. **Chapter 6** focuses on comparative assessment of piezofilm based stress wave force balance with the established accelerometer force balance through experimentation in shock tunnel. It is highly desirable to compare two measurement philosophies since basic way of instrumentation and working principle are different. The core theme of **Chapter 7** remains to investigate the sensitiveness of the accelerometer balance system as well as the prediction methodology viz. ANFIS in hypersonic flow regime. **Chapter 8** encompasses the concluding remarks obtained during the present investigations and scope for further studies in this domain.

CHAPTER-2

Experimental Facility & Instrumentation

Overview

Recent years' of development in aviation technology has led to new aerodynamic problems into existence, among which effect of extremely high pressure and temperature encountered during atmospheric re-entry has been evolved as a prime zone of interest for the researchers. Thin shock layers, thick boundary layers, regions having strong vortices and dominating viscous interaction can be used to characterize the flow physics during this stage. Therefore, proper conceptualization of aerodynamics and flight dynamics associated with these vehicles is highly desirable. The evolution and affirmation of new technologies in this regard can be assessed through experimentation in ground based facilities due to low cost and less risk. Also for better understanding of the flow physics these facilities can be utilized. In line with the application of ground based facilities, shock tube in IIT Guwahati (to simulate supersonic flow condition) and shock tunnel in IIT Bombay (to simulate hypersonic flow condition) has been developed. With incorporation of these impulse facilities, various force measurement techniques are also established which will put a light on stability and trajectory related information of the aerodynamic vehicles. This chapter deals with various types of experimental facilities that have been incorporated in due course of time as well as the force balances that have been developed in view of force measurement in these facilities. Elaborated description regarding the assumptions and theory of force estimation from the experimentally measured responses has also been presented.

2.1 Introduction

The development of satellites, space crafts, and re-entry vehicles and the associated technologies have undergone a paradigm shift in recent times due to the never ending race for exploring better technological capabilities. Though various mission deliverables have been accomplished with the help of these vehicle configurations, the success rate of these missions is very less. The major aspect of the successful executions can be endorsed to the enhancement of computational capability to simulate the flow features over complex aerodynamic configurations. However, CFD simulations are limited with the modelling technique for flow complexities and meshing difficulties for geometric complexities. Lack of validation of the CFD result with the experimental and unavailability of the computational solution for some of the flow conditions also accounts for unsuccessful attempts. Hence, the necessity of ground based facilities to replicate the flow situation becomes intensive. Evolution and affirmation of new aerodynamic technologies can be assessed through experimentation in these test facilities. However, measurement procedure must be sophisticated in case of ground based test facilities due to very short test time. Flight based tests can also be opted as an alternative tool to substantiate the innovations, but the low cost and less risk makes the ground based tests affordable for extensive experimental prototype flight testing. Usually, tests are conducted using wind tunnels [Whitecomb, 1976] and impulse facilities that include shock tubes [Tanno *et al.*, 2003], free piston shock tunnels [Stalker, 1967] and expansion tunnels [Holden, 2004] which are capable of reproducing the actual flow condition experienced by the space vehicles. These facilities can also generate high enthalpy flows of desired test duration for the purpose of providing actual test condition for both external and internal aerodynamic study of various aerodynamic configurations. The ground based facilities are usually equipped with pressure sensors at different locations for accomplishment of exact flow conditions. The test facilities are also often equipped with additional instrumentation for flow visualization.

Moreover for aerodynamic force measurement in impulse facilities, test models are equipped with some sensors like accelerometers, strain gauges and piezofilms to quantify the output response which will be usable afterwards for proper estimation of the forces and moments acting on the model. As explained by Bernstein (1975), application of these techniques has been restricted in the past because of the nonexistence of the appropriate sensors and higher time requirement than test duration to achieve equilibrium between model and its support structure. Nevertheless contemporary research work is focused towards development of force balances which can acquire the output responses in microsecond scale, so that it can be applicable to any of the ground based impulse facilities. The performance of force balances solely relies on the frequencies of the system as a whole viz. upon the model, balance, and support structure. Among various developed force balances, AFB system is typically incorporated due to its simplicity in instrumentation, but it is limited to lower mass and smaller length models. Naumann *et al.* (1991) developed a fast acting support system which ensures free flight motion while measuring output response through accelerometer. Simultaneously, Sanderson and Simmons (1991) established SWFB technique with an intention to relax the constraint of size or weight of the model imposed by AFB, thereby including the system dynamics more accurately.

In view of the intense obligation towards development of force balance systems for accurate force prediction, few ground based facilities have been developed to assess the performance of these balances. In this regard, shock tube and shock tunnel facilities are established to generate supersonic and hypersonic flow conditions respectively. In conjunction with the impulse facilities development, various force balance system has been designed and performance has been checked through experimentation in these flow conditions to assess the applicability of the employed sensors. All the details, in regard to the experimental facilities, associated instrumentation and working principle of force balance systems along with the sensor details have been elaborated in the subsequent sections.

2.2 Experimental Facility

To evaluate the performance of various force balances, experiments have been conducted in different impulse facilities such as shock tube and shock tunnel. This evaluation aids in ensuring the applicability of the force balances in different operating conditions and flow regimes. The facilities that have been implemented during course of time, their working principle and the free stream conditions generated during the test, have been emphasized in the succeeding sections.

2.2.1 Shock Tube Facility

In view of assessing the force balance in supersonic flow condition, shock tube facility as illustrated in **Fig. 2. 1** has been developed at IIT Guwahati. A shock tube having driver section of 2m and driven section of 5m, is made out of stainless steel tubes of length 1 m. Deliberately the driven section is made longer than the driver section to ensure the proper generation of incident planar shock wave. The outer diameter of the tube is 77 mm having a thickness of 11 mm. Driver and driven sections are separated by an aluminum diaphragm of 1.2 mm thickness. This diaphragm is grooved to obtain its controlled rupture [Takayama *et al.* (2014)]. During normal operation of the shock tube, high pressure section is continuously filled with nitrogen or helium until the diaphragm ruptures. Bourdon tube pressure gauge has been installed in this section to measure bursting pressure (P_4). Simultaneously, the driven section is filled with test gas viz. air maintained at low pressure (P_1). Rotary type vacuum pump (Make: HHV Pumps Private Ltd) is connected in the driven section to generate low pressure which is monitored by a vacuum gauge (**Fig. 2. 1**). Due to pressure difference across the two sections, abrupt rupturing of the diaphragm occurs resulting in formation of compression waves which then coalesce to form a strong shock front that propagates towards the driven section. Trailing to the incident shock wave movement, the interface between the driver gas and test gas, termed as contact surface also travel towards low pressure section. Simultaneously, a series of expansion waves propagate to the driver section. Afterwards, as the incident shock wave reaches the end wall, it reflects and moves back into the driven section.

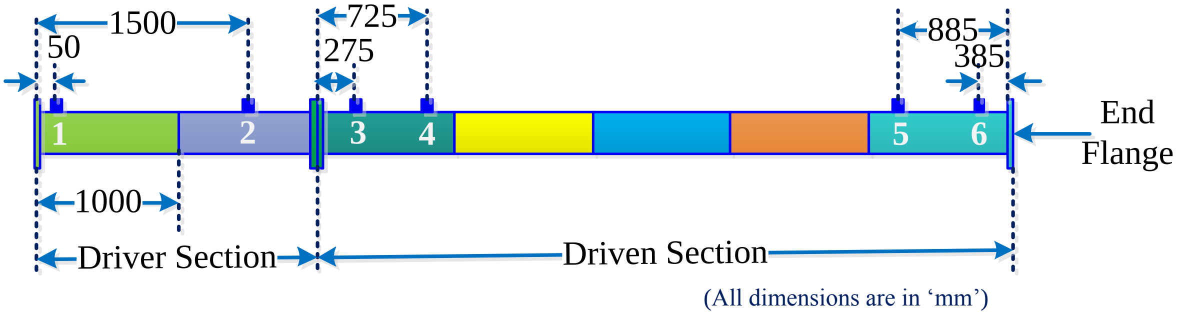

1- Driver Gas Inlet Valve
2- High Pressure Gauge
3- Vacuum Pressure Gauge
4- Port for Vacuum Pump
5- Pressure Sensor 1
6- Pressure Sensor 2

Fig. 2. 1: Schematic diagram of the shock tube facility-IIT Guwahati.

As a part of the calibration test of the shock tube, the pressure rise across the incident and reflected shock wave needs to be captured. In this regard two pressure transducers, PCB Piezotronics made (Model: 113B22) have been mounted in the driven section (**Fig. 2. 1**), which is connected to DAS through signal conditioner. Typical pressure signal obtained during the experiment is shown in **Fig. 2. 2**. With value of the sensitivity of both the pressure transducers, the recorded voltage signals can be processed to get an estimate of the pressure jump across the incident as well as reflected shock wave. These experimentally obtained parameters can be further validated by comparing the flow properties with 1-D theoretical relation, based on multiple gas dynamics namely "Rankine-Hugoniot relation" represented by **Eq. 2.1** [Anderson, 2004]. Further, incident shock Mach number ($M_{s,e}$) is calculated from the distance between both pressure transducers (ΔS) and time taken by the shock wave (Δt) to travel the same distance using **Eq. 2.2**.

$$\left.\begin{array}{l} \dfrac{p_2}{p_1}=1+\dfrac{2\gamma_1}{\gamma_1+1}\left(M_{s,t}^2-1\right);\dfrac{T_2}{T_1}=\dfrac{1+\left(\dfrac{\gamma_1-1}{\gamma_1+1}\right)\dfrac{p_2}{p_1}}{1+\left(\dfrac{\gamma_1-1}{\gamma_1+1}\right)\dfrac{p_1}{p_2}} \\ \\ \dfrac{p_4}{p_1}=\left(\dfrac{p_2}{p_1}\right)\left[1-\dfrac{(\gamma_4-1)(a_1/a_4)\left(\dfrac{p_2}{p_1}-1\right)}{\left(\sqrt{2\gamma_1}\right)\left(\sqrt{(2\gamma_1)+(\gamma_1+1)\left(\dfrac{p_2}{p_1}-1\right)}\right)}\right]^{\dfrac{-2\gamma_4}{(\gamma_4-1)}} \end{array}\right\} \qquad (2.1)$$

$$V_s = \frac{\Delta S}{\Delta t}; \;\; a_1 = \sqrt{\gamma R T_1}; \;\; M_{s,e} = \frac{V_s}{a_1} \tag{2.2}$$

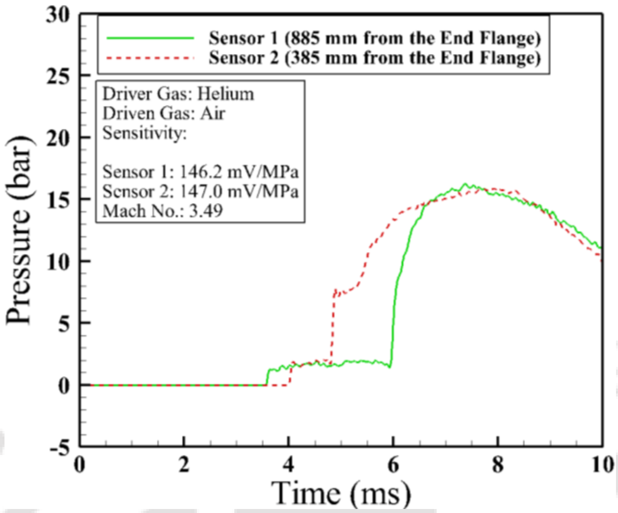

Fig. 2. 2: Pressure signal acquired in the shock tube using helium as the driver gas.

Afterwards based on the recorded values of P_4/P_1, using the above relation, theoretical shock Mach number ($M_{s,t}$) is also calculated and compared with the experimentally obtained induced Mach number ($M_{s,e}$). Calibration of the shock tube is performed with consideration of driver gas as nitrogen and helium, as shown in **Fig. 2. 3** and **Fig. 2. 4**. It can be observed that, in case of nitrogen as driver gas, the incident Mach number and pressure ratio for pressures across the primary shock wave are in good agreement with the theoretical values. However, in case of helium, significant deviation in pressure ratio is perceived. It can be attributed to the fact that use of lower molecular weight of the driver gas leads to higher primary shock Mach number and hence higher temperature rise of the test gas [Persico *et al.* (2005)]. Due this enhancement, viscous effects become prominent during experiments. As a result of this, more difference between the pressure ratio is noticed between the prediction from inviscid shock tube relation and the experimental findings.

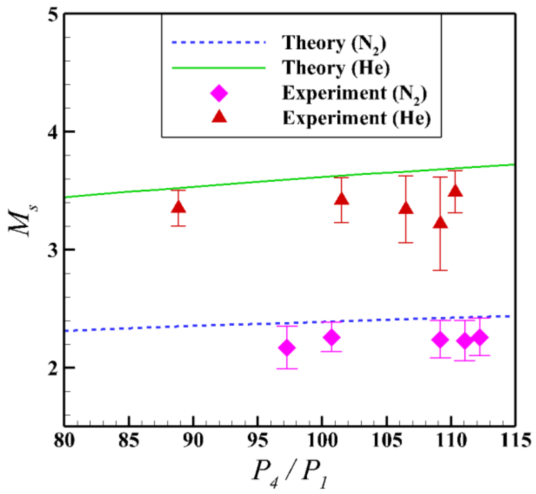

Fig. 2. 3: Comparison of incident shock Mach number for different driver gas.

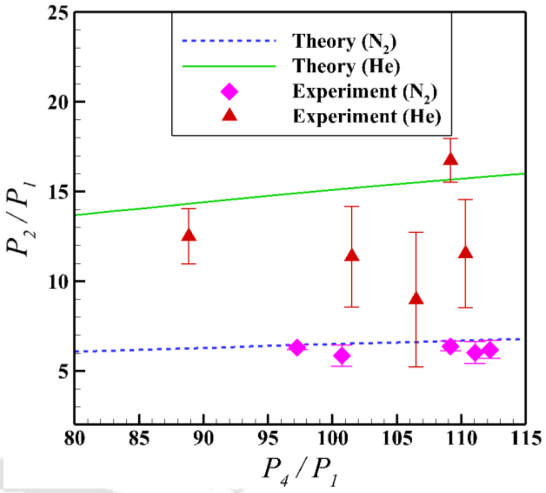

Fig. 2. 4: Comparison of pressure rise across incident shock wave.

2.2.1.1 Numerical Validation

In addition to the theoretical validation, numerical simulation of the same is necessary as it provides a clear visualization of the flow inside the domain. Also it offers essential information about magnitude of signals to be acquired and associated data acquisition settings. Hence inviscid simulation of complete shock tube is carried out for a better insight. Present investigations make usage of the commercial CFD solver ANSYS FLUENT 14.5 where governing equations of continuity, momentum and energy are solved using finite volume approach. To incorporate the effect of different driver and driven gas, species transport equations are also solved herein. The computational domain along with its associated initial and boundary conditions is shown in **Fig. 2. 5**.

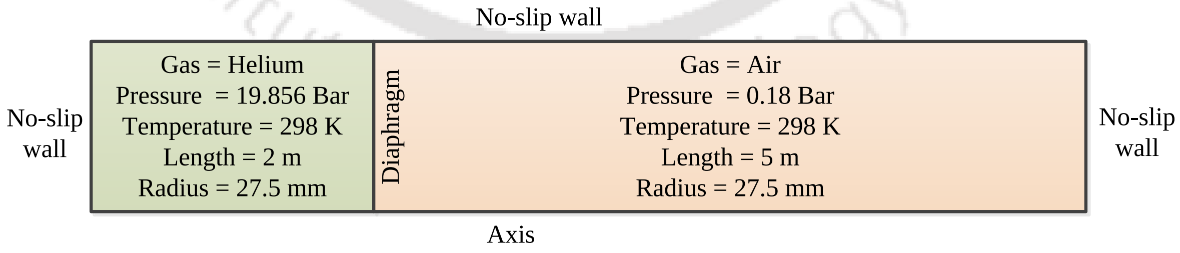

Fig. 2. 5: Computational domain and its boundary conditions.

As the axisymmetric approach is sufficient to render an accurate description of the real flow configuration, so the shock tube is modeled as an axisymmetric body. Structured mesh is opted for this computational domain. Density based implicit solver with fourth order Runge-Kutta scheme has been chosen for transient analysis of the flow field. For the current numerical simulation, “advection upstream splitting method (AUSM)” flux vector splitting scheme has been adopted to compute the convective fluxes. User defined function (UDF) has been incorporated in the present situation to initialize the computational domain into two different sections viz. driver and driven sections. Bursting of the diaphragm is not the prime concern, so the diaphragm is assumed to be ruptured instantly at time t = 0. Initial conditions set in the computational domain are as given in **Fig. 2. 5**. This figure also describes the boundary conditions for the present problem. Simulations are performed for different time steps and mesh sizes so as to arrive at an optimum combination. Finally chosen mesh and time step have fetched the results which are independent of the mesh size and time step with adequate resolution of the flow field. Finally, chosen mesh has 320000 nodes in the computational domain. Pressure contours after 0.9ms of the rupture of the diaphragm are shown in **Fig. 2. 6**. It gives clear visualization of a right-running incident shock wave and a left-running expansion fan. The incident shock hits the end wall and reflects back creating high temperature and pressure zone behind it, which is evident in **Fig. 2. 7**.

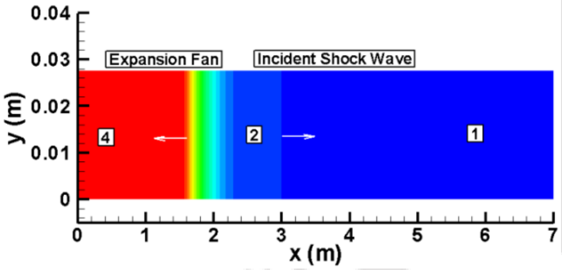

Fig. 2. 6 : Pressure distribution after diagram rupture.

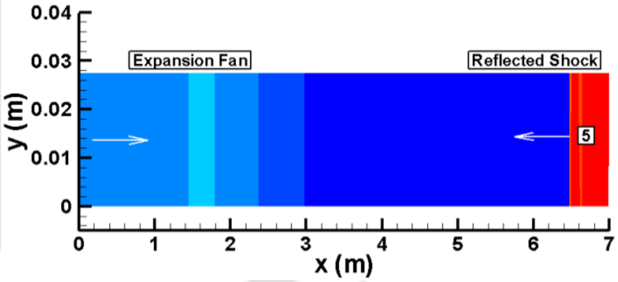

Fig. 2. 7: Pressure distribution after reflection from end wall.

As both primary and reflected shocks are the concerned factors during experiments, so jump across these shocks is the critical information acquired as an outcome of computational efforts and has been compared with the theoretical values. For the current initial conditions, pressure behind the primary shock is estimated to be 3.23bar from the CFD simulation. Primary shock Mach number calculated from the simulation is noted as 3.6. Similarly, primary shock Mach number and pressure behind it, predicted from exact Riemann solver are 3.68 and 2.81 bar respectively. Good agreement between these values strengthens the numerical ability to capture the flow phenomena inside the shock tube. Thus this numerical model can be used further for the estimation of the force coefficients on any test model under certain flow conditions.

After the successful numerical and experimental validation of the flow parameters associated with shock tube, further it is planned to test the performance of SWFB. In accordance with the proposed experiments to be conducted, a hemispherical model along with its associated support structures has been fabricated. The model along with the force balance in conjunction with the employed sensor is mounted in the end flange for response measurement during the test duration. Comprehensive details of the measurement procedure for the sensors viz. strain gauge and piezofilm, have been briefly elaborated in the subsequent sections.

2.2.2 Hypersonic Shock Tunnel Facility

In line with the sole objective of assessing the force balances in various flow conditions, experiments have been also conducted in hypersonic facility present at IIT Bombay as illustrated in **Fig. 2. 8** This shock tunnel is an integration of shock tube and wind tunnel. Shock tube portion is same as descried in the earlier section, which consists of a driver and driven section separated by 1.2mm thick aluminum diaphragm. The driver and driven section is having constant outer diameter of 76mm and thickness of 12mm. Further the wind tunnel section comprises of a C-D nozzle, test section and dump tank. The throat and exit diameter of the C-D nozzle is 23 mm and 300 mm respectively. The exit of the C-D nozzle is further connected to a test section having square cross section of 300 mm x 300 mm with 450 mm length. The final portion viz. dump tank is connected to the rotary pump for evacuating the wind tunnel portion to a vacuum level of ~ 1mbar, before conducting each experiment. Experiments have been performed with nitrogen as driver gas and air at atmospheric pressure as driven gas. Due to the pressure difference between the sections, sudden rupture of the aluminum diaphragm occurs, resulting into generation of incident shock wave that propagate towards to the low pressure driven section. To monitor the primary shock Mach number, two pressure transducers with sensitivities of 5 mV/psi and 1 mV/psi respectively have been installed in the driven section, separated by a distance of 505mm.

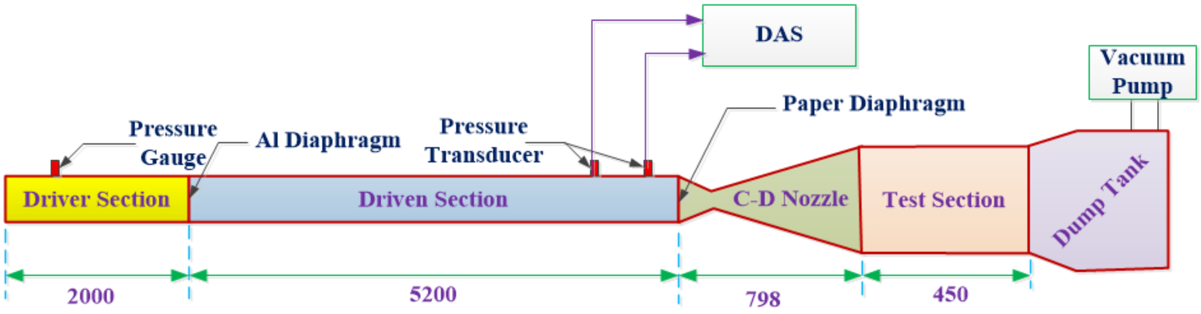

("All Dimensions are in mm")

Fig. 2. 8 : Schematic of the experimental facility present at IIT Bombay.

Typical signal captured by the pressure transducers has been shown in **Fig. 2. 9**. Further, this incident shock wave gets reflected and travel back into the medium elevating the pressure and temperature of the test gas. As the induced mass motion velocity behind the reflected shock wave is almost zero, so the slug of test gas momentarily acts as a reservoir of high temperature (T_5) and pressure (P_5), thereby ruptures the paper diaphragm that separates the shock tube and wind tunnel portion. The test gas is further expanded through the C-D nozzle to attain desired free stream conditions in the test section. A rake of pitot sensor is mounted in the test section during one of the tests with an intention to quantify the free stream conditions and steady test duration. The sensitivity of the employed pitot sensor is 14.91mV/kPa and the typically obtained response from the pitot sensor is portrayed in **Fig. 2. 10.** Usually the steady portion of the pitot signal indicates the available test time which lies around 500-700μs for the current set of experiments.

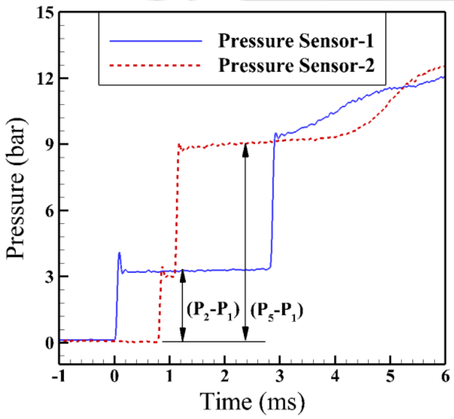

Fig. 2. 9: Temporal variation of pressure traces obtained from pressure transducers.

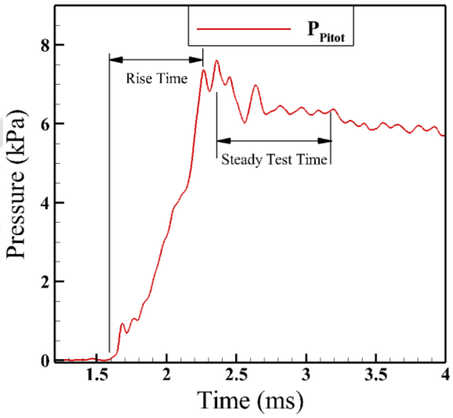

Fig. 2. 10 : Typical pitot signal obtained at the test section.

2.2.2.1 *Determination of freestream conditions*

The free stream Mach number (M_∞) at the test section can be deduced using **Eq. 2.3,** with available information regarding the magnitude of pressure at the nozzle entry and the pitot transducer response (P_{02}). The pressure at the nozzle entry is same as the pressure behind the reflected shock wave (P_5), as the test gas has zero velocity behind the reflected shock.

$$\frac{P_{02}}{P_5} = \left\{ \frac{(\gamma-1)}{2} \frac{M_\infty^2}{\left(1+\frac{(\gamma-1)}{2}M_\infty^2\right)} \right\}^{\gamma/(\gamma-1)} \left\{ \left(\frac{2\gamma}{\gamma+1}M_\infty^2\right) - \left(\frac{\gamma-1}{\gamma+1}\right) \right\}^{-1/(\gamma-1)} \tag{2.3}$$

After quantification of free stream Mach number, assuming isentropic expansion through C-D nozzle, the free stream pressure (P_∞) and temperature (T_∞) can be estimated using isentropic relations. Further based on the free stream conditions, freestream dynamic pressure (q_∞) can be attained using the following expression.

$$q_\infty = \frac{\gamma}{2} P_\infty M_\infty^2 \tag{2.4}$$

The freestream Reynolds number (Re_∞) also can be can be estimated using **Eq. 2.5** where the dynamic viscosity (μ_∞) is calculated using Sutherland's law given in **Eq. 2.6**.

$$\mathrm{Re}_\infty = \frac{\rho_\infty v_\infty}{\mu_\infty} \tag{2.5}$$

$$\frac{\mu_\infty}{\mu_{ref}} = \left(\frac{T_\infty}{T_{ref}}\right)^{1.5} \left(\frac{T_{ref}+S}{T_\infty+S}\right) \tag{2.6}$$

where, the reference quantities are: μ_{ref} = 1.789 x 10^{-5} kg/ms, T_{ref} = 288K and S = 110K. Typical freestream conditions available in the test section are given in **Table 2. 1**. Subsequently, after obtaining the free stream conditions, test model and its associated support structures are mounted in the test section to acquire the temporal variation of output responses over the test duration.

Table 2. 1: Free-stream conditions in the IITB-shock tunnel.

Pressure (Pa)	74.05 ± 2.66
Temperature (K)	43.91 ± 0.26
Mach Number	8.36 ± 0.16
Reynolds No. (m^{-1})	$(2.4 \pm 0.07) \times 10^6$

2.3 Types of force balances

As already mentioned, two major techniques are usually adopted during force and moment measurement in impulse facilities, namely inertia dominated and stiffness based force balances. However, inertia dominated balance bank upon analytical relations to estimate the force coefficients from the experimentally measured acceleration responses.

2.3.1 Accelerometer force balance theory

As free flight motion of the balance and associated support structure is the necessary condition for accurate measurement of acceleration magnitude, so various procedures of attainment has been reported in the literature. The estimation of the force and moment coefficients from the acceleration responses has been demonstrated by Vidal (1956), through replacement of force balances by spring-mass system having single degree of freedom as illustrated in **Fig. 2. 11**. During the design of this system, assumptions like linear characteristics of spring, no effect of damping have been considered. It is also assumed that the net axial force imparting on the model passes through the center of gravity (C.G) of the model.

In regard to deduce the analytical relation for coefficients of forces and moment, *m* and *I* is considered as the mass and mass moment of inertia respectively of the test model and $K_1, K_2,\ K_3$ are the spring constants for the axial and two normal springs that have been incorporated. For the current analysis it is also implicit that axial force $\left(C(t)\right)$ passes through C.G of the model and normal force $\left(N(t)\right)$ acts at center of pressure, which is located at a distance 'e' from the C.G of the model. During flow over the model mounted at an AOA, the model is assumed to have three degrees of freedom in x, y and θ orientations. However, the model and the springs connected in normal direction viz. K_2 and K_3 constitute a two degrees of freedom system with combined angular and rectilinear mode of motion as shown in **Fig. 2. 12** It is evident from the figure that during the flow over the model (t > 0), the spring K_2 is compressed by a distance $\left(y+a\theta\right)$ whereas the spring K_3 is compressed by a distance of $\left(y\text{-}b\theta\right)$.

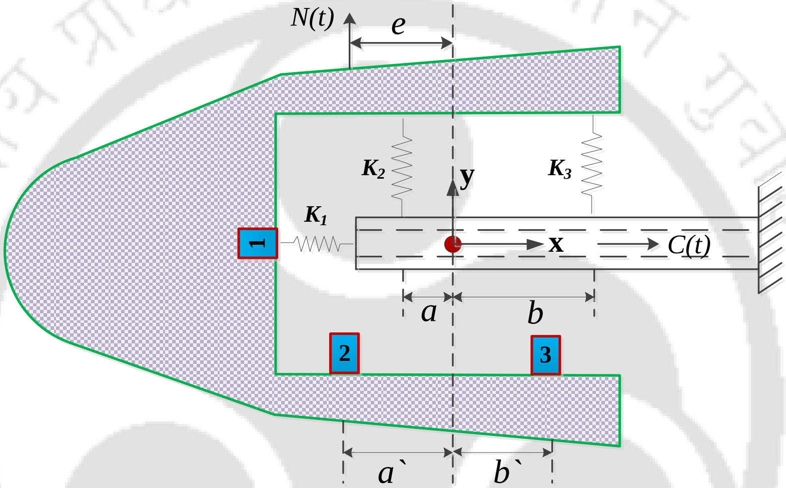

Fig. 2. 11: Simplified schematic diagram of the three-component AFB system

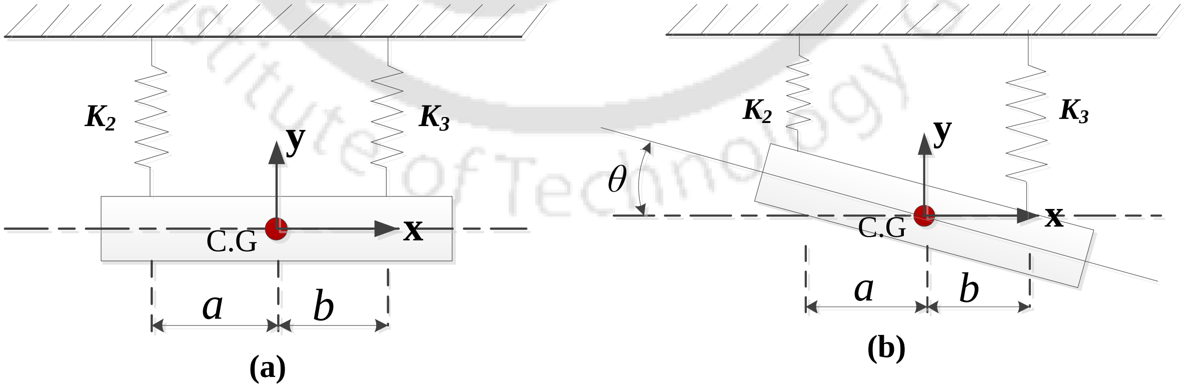

Fig. 2. 12: Combined rectilinear and angular mode system (a) t = 0 (b) t > 0

The simplified free body diagram for the present configuration of two degrees of freedom system is portrayed in **Fig. 2. 13.**

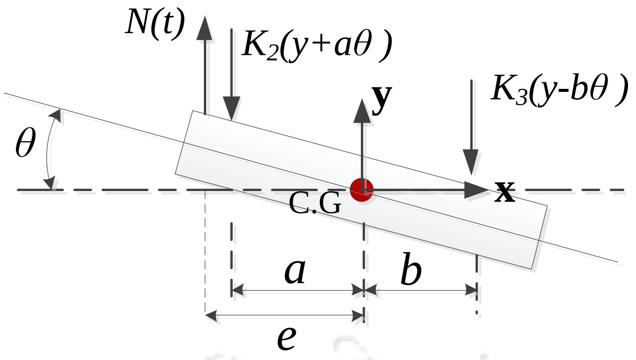

Fig. 2. 13: Free body diagram for combined rectilinear and angular motion of the system.

From this figure, the force acting along y-direction and equation of motion in θ direction can be deduced, as represented by the **Eq. 2.7** and **Eq. 2.9** respectively.

$$m\ddot{y} = N(t) - K_2(y + a\theta) - K_3(y - b\theta) \tag{2.7}$$

Rearranging the equation will result in,

$$N(t) = m\ddot{y} + (K_2 + K_3)y + (aK_2 - bK_3)\theta \tag{2.8}$$

Similarly the equation of motion in θ direction about C.G will be,

$$I\ddot{\theta} = N(t)\cdot e - K_2(y + a\theta)a + K_3(y - b\theta)b \tag{2.9}$$

On rearrangement, the normal force will be,

$$N(t) = \left(\frac{I}{e}\right)\ddot{\theta} + (aK_2 - bK_3)\frac{y}{e} + \left(a^2K_2 + b^2K_3\right)\frac{\theta}{e} \tag{2.10}$$

In a similar manner, the spring connected in axial direction (K_1) with the model, constitutes a single degree of freedom system with only linear motion, as shown in **Fig. 2. 14**.

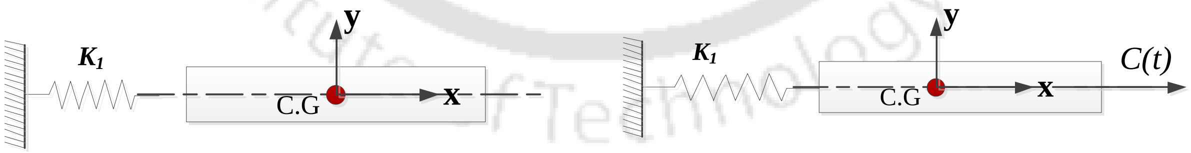

(a)

(b)

Fig. 2. 14: Representation of rectilinear mode system (a) t = 0 (b) t > 0.

The free body diagram is also illustrated in **Fig. 2. 15**, based on which the axial force is estimated, as given by **Eq. 2.11**.

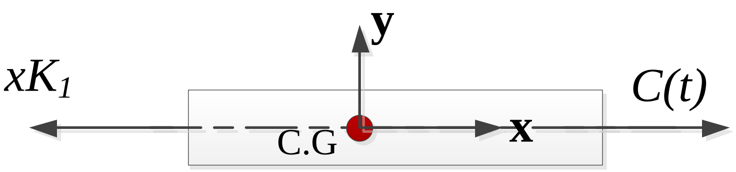

Fig. 2. 15: Free body diagram for rectilinear motion of the system.

The axial force is given by the expression:

$$m\ddot{x} = C\left(t\right) - K_1 x \tag{2.11}$$

$$C\left(t\right) = m\ddot{x} + K_1 x \tag{2.12}$$

The boundary conditions for the equations (3.8), (3.10) and (3.12) are as follows:

$$\text{At } t \le 0,\ N = 0,\ C = 0$$

$$t > 0,\ N = N(t),\ C = C(t)$$

The above equations and the associated boundary conditions are solved using Laplace Transforms, which results in expression for acceleration in three different directions, as given below.

$$\ddot{y} = \left(\frac{N\left(t\right)}{m}\right)\left\{1 - t^2\left[\left(\frac{K_2 + K_3}{m}\right) + \left(\frac{e\left(aK_2 - bK_3\right)}{I}\right)\right]\right\} \tag{2.13}$$

$$\ddot{\theta} = \left(\frac{eN\left(t\right)}{I}\right)\left\{1 - t^2\left[\left(\frac{aK_2 - bK_3}{em}\right) + \left(\frac{a^2K_2 + b^2K_3}{I}\right)\right]\right\} \tag{2.14}$$

$$\ddot{x} = \left(\frac{C\left(t\right)}{m}\right)\left[1 - t^2\left(\frac{K_1}{2m}\right)\right] \tag{2.15}$$

If experimentally obtained acceleration responses are substituted in the equations (2.13), (2.14) and (2.15), then the unknown forces viz. $N\left(t\right)$ and $C\left(t\right)$ can be estimated. Further, as the test duration in the impulse facilities lies in a range of few milliseconds, hence the term associated with 't^2' can be neglected. However larger test time may enhance the error in force measurements and also may become excessive if stiffer springs are used. Incorporation of the above stated fact of neglecting the factors associated with 't^2' will result in following expression for calculation of forces acting on the model.

$$N\left(t\right) = m\ddot{y} \tag{2.16}$$

$$N(t) = \ddot{\theta}\left(\frac{I}{e}\right) \tag{2.17}$$

$$C(t) = m\ddot{x} \tag{2.18}$$

In order to accurately estimate the unknown forces from the above equations, it is essential to measure the three accelerations $\ddot{y}, \ddot{\theta}$ and $\ddot{x}$. Instead of measuring linear and angular acceleration, it is simpler to acquire linear accelerations at two different locations in order to calculate the pertinent body accelerations, using the following relations.

$$\ddot{x} = \xi_1 \tag{2.19}$$

$$\ddot{y} = \frac{b'\xi_2 + a'\xi_3}{a' + b'} \tag{2.20}$$

$$\ddot{\theta} = \frac{\xi_2 - \xi_3}{a' + b'} \tag{2.21}$$

where, ξ_1, ξ_2 and ξ_3 are the accelerations measured by the axial, front lift and aft lift accelerometers respectively, mounted at the locations indicated in the **Fig. 2. 8**. Consequently, the axial force, normal force and moment acting on the model can be expressed in terms of the measured acceleration responses as,

$$C(t) = m\xi_1 \tag{2.22}$$

$$N(t) = m\left(\frac{b'\xi_2 + a'\xi_3}{a' + b'}\right) \tag{2.23}$$

$$M(t) = eN(t) = I\ddot{\theta} = I\left(\frac{\xi_2 - \xi_3}{a' + b'}\right) \tag{2.24}$$

Therefore, the aerodynamic coefficients (C_d, C_l and C_m) can be computed using following relations which incorporates accelerations measured by three accelerometers.

$$C_d = \left({C(t)} \big/ {\left(q_\infty A_{ref}\right)} \right)\cos\alpha + \left({N(t)} \big/ {\left(q_\infty A_{ref}\right)} \right)\sin\alpha \tag{2.25}$$

$$C_l = \left({N(t)} \big/ {\left(q_\infty A_{ref}\right)} \right)\cos\alpha - \left({C(t)} \big/ {\left(q_\infty A_{ref}\right)} \right)\sin\alpha \tag{2.26}$$

$$C_m = \left(M(t) \Big/ q_\infty A_{ref} L_{ref} \right) \tag{2.27}$$

As the measured responses from the accelerometer solely affect the level of deviation in coefficient of forces and moment acting on the model; hence, the accelerometers capable of acquiring responses at higher frequencies must be preferred. Consequently, PCB Piezotronics make accelerometers are equipped inside the model to measure the axial and normal accelerations. The output of the accelerometer is further connected to the signal conditioner for data acquisition purpose.

2.3.2 Stiffness based force balance

Stiffness dominated force balance relies on measurement of strain signal either by semiconductor strain gauges or by piezofilm. Theoretical approach to calculate the coefficients of forces and moment from the steady state magnitude of the measured strain responses are not available. Therefore, system identification and inverse technique is implemented to determine the aerodynamic force time history from the measured signals. Brief description about theory of SWFB has been presented in the subsequent section.

2.3.2.1 Theory of stress wave balance

On application of aerodynamic forces on a model, initiation of stress wave propagation and reflection occurs inside the model and support structure. These stress wave activities can be detected through measuring the transient strain responses induced in the model. Assuming a linear dynamic system, relationship can be devised between the applied force and measured strain history as schematically presented in **Fig. 2. 16**.

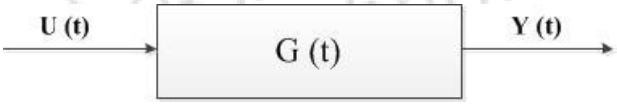

Fig. 2. 16 : Schematic of stress wave balance.

The relationship viz. transfer function of the linear system can be represented mathematically using convolution integral as shown in **Eq. 2.28**.

$$y(t)=\int_{0}^{t} g(t-\tau).u(\tau)\,d\tau \tag{2.28}$$

$$y(f)=g(f)\times u(f) \tag{2.29}$$

Where *y(t)* represents output response, *u(t)* is the input force and *g(t)* is the impulse response function of the system. This impulse response is usually derived from the response obtained during dynamic calibration performed through application of step or impulse load. However, for calculation of impulse response function for all the case studies, dynamic calibration is performed through application of impulse forces through an impactor and capturing the strain response of the system. Further, if the system response function can be estimated, then deconvolution technique can be adopted to determine time history of input load from the measured strain responses. But, time domain based convolution and de-convolution involves rigorous mathematical formulations. As, convolution in time domain is equivalent to multiplication in frequency domain (**Eq. 2.29)** and similarly de-convolution in time domain acts like division in frequency domain; therefore, frequency based techniques are employed in this regard for current studies. To convert the temporal responses into frequency domain, inbuilt FFT command of MATLAB has been used. Various strain sensors employed for response acquisition in the experimental test facilities is described in the following sections.

2.3.2.2 Strain gauge based force balance

This force balance method for force recovery employs strain gauges for output response measurement, during experimentation in impulse facilities. The working principle of strain gauge is based on change of resistance of the sensor developed due to the applied load. This change in voltage can be further converted to corresponding strain magnitude using empirical relations. Various types of strain gauges viz. semiconductor strain gauges (SSG) and metallic foil gauges are available. However, usually SSGs are preferred due to their fast response time. For the current set of studies encapsulated SSGs (Kulite Make) have been incorporated as they have an extra encapsulation of protective glass matrix on the sensing element. Also higher sensitivity, higher resistance and smaller size make this sensor suitable for application in impulse facilities. Present choice of SSG has a resistance of 350 Ω and gauge factor of 130, which in turn resembles higher sensitivity of the sensor.

As the test duration in the impulse facilities is very small, capturing the change in resistance within due course of time is a challenging task. Therefore, the strain gauges need to be connected to some circuitry elements, to convert this change in resistance to corresponding voltage variation. Again this generated voltage change seems to be very less which needs amplification before acquiring responses in DAS. In this regard, SSG is connected to one of the terminal of Wheatstone bridge circuit and output of this circuit is connected to an amplifier. Commercial INA 128 amplifier is employed for this purpose in which, provision of varying the amplification factor is also available through alteration in gain resistor. Typical Wheatstone bridge arrangement for strain response acquisition is illustrated in **Fig. 2. 17**.

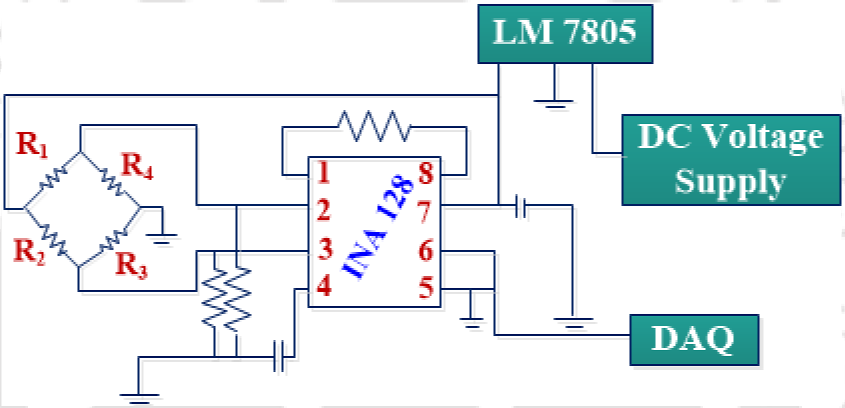

Fig. 2. 17: Wheatstone bridge circuit arrangement for acquiring the strain response.

2.3.2.3 Piezofilm based force balance

Similar to the strain gauge based balance, piezofilm based force balance is also implemented with an intention to measure the output response in terms of induced strain inside the model. Piezofilm is an active dynamic sensor for measuring strain response as it produces charge in proportion to applied mechanical stress which in turn can be related to voltage. Foremost characteristic of piezofilm includes utilization of converse piezoelectric effect to actuate the structure. Both piezoceramic (PZT) and piezoelastic (PVDF) films can be employed for strain response measurement, but PZT films are brittle in nature and thus can only be used on flat surfaces. Hence, for the current set of experiments a PVDF piezofilm (Measurement specialties make) having capacitance 0.5nF and sensitivity 12mV/µ-strain has been incorporated during the force balance design.

The charge produced by the piezofilm is usually in the order of few Pico-coulombs having high output impedance. But to capture this response in DAS, it should be converted from high impedance charge to low impedance voltage. Charge amplifier can be utilized to cater this, through transferring the input charge to another reference capacitor, thereby producing an output voltage same as the voltage across the reference capacitor. During assessment of this force balance in shock tunnel facility a charge amplifier of Measurement Specialties make (Model No. 1007214), has been incorporated. However, it may be noted that in some of the cases, the output of the sensor can be directly connected to the DAS which can be further converted to strain magnitude using the sensitivity relation.

Summary

The chapter deals with different ground based facilities viz. shock tube and shock tunnel that have been considered for the current studies. In conjunction with the experimental facilities, the force balance techniques which have been employed for measuring coefficients of force and moment are also explained explicitly. Shock tube present at IIT Guwahati is successfully calibrated considering driver gas as nitrogen and helium. In a similar approach, shock tunnel facility developed at IIT Bombay is also calibrated and free stream condition, prevailing in the test section is also estimated. Theoretical aspect of three component accelerometer force balance for calculating the coefficients of forces and moment from the acceleration responses is analyzed. In regard to involving system dynamics more accurately, stiffness based force balance systems are also explored and working philosophy in association with requisite instrumentation for response acquisition is also presented.

CHAPTER-3

Qualitative Assessment of Strain Gauge Balance for Impulsive Loading Applications

Overview

In the preliminary stage of study, strain gauge balance described in the previous section is analyzed through various qualitative as well as quantitative aspects. Present investigations address the necessity of precise measurement of strain time history for impulsive loading applications, specifically with usage of the shock tube facility present at IITG. Finite element modeling is initially carried out for a hemispherical test model and stress bar assembly to arrive at an appropriate location for strain measurement irrespective of the boundary condition for the end of the stress bar. During dynamic calibration experiments, performance assessment of two wire and three wire quarter bridge arrangements along with half bridge circuit is carried out. Usefulness of these arrangements has been verified by analyzing strain signals in time and frequency domains. Comparison of recovered force time histories obtained through frequency based de-convolution technique proved that the half bridge circuit is the most suitable for such applications. Actual shock tube testing of the instrumented hemispherical test model also confirmed the applicability of half bridge circuit for short duration strain measurements. Drag force acting on the model during experiment has also been recovered from the transient strain signal using de-convolution technique.

3.1 Introduction

Ground based facilities such as shock tubes or shock tunnels where supersonic, hypersonic and hypervelocity testing is generically carried out, can be used to generate short duration impulsive loading condition. In such experiments, test model and dynamic response measurement systems are subjected to loading which can be detrimental and may lead to failure of structural components. Therefore, in such situations, precise measurement becomes challenging and hence remains a topic of research. The response of impulsive force can be acquired using intrusive [Sahoo *et al.* (2003)] or non-intrusive techniques [Ramesh *et al.* (2014)]. Among the intrusive techniques, accelerometer based systems are usually preferred but those are limited to application for small scale models. Stiffness dominated force balance is therefore proposed by group of researchers from University of Queensland, Australia [Simmons and Sanderson 1991]. This technique overcomes such limitations by measuring the stress wave propagation in the model and support structure. In this case, the associated force balance comprising of model and support structure can be termed as internal/external balance depending upon the sensor location.

Two types of strain sensors viz. strain gauge and piezofilm can be effectively implemented in impulse facilities to detect stress wave propagation. However, as seen in literature, strain gauge is preferred over alternative sensors due to its small size and long term stability. Therefore, local strain measurements for impulsive loading are generically carried out using high gauge factor strain gauges. Mounting of the strain gauge on the test model and its integration in the associated electrical circuit are the major tasks before actual strain measurement experiments. Such importance is justifiable since magnitude and trend of the recorded strain are highly sensitive to the circuit arrangement. Major reason for this can be attributed to the fact of “lower signal to noise ratio” in case of strain gauge force balance unlike the accelerometer force balance where acceleration magnitudes are very high. Second important fact is the nature of strain signal which has relevance with the force prediction. Thus, although numerical value of steady state acceleration is the lone requirement for force estimation using accelerometer force balance and hence the strain signal needs to be captured properly. Importance of these features of strain signals is based on the fact that the recorded strain signal is required for deconvolution and convolution programs for applied force recovery in temporal domain. Therefore choice of configuring strain gauge in Wheatstone bridge circuit has prime importance in strain measurement for impulsive loading applications. There are few configurations with which it is possible to connect the strain gauge to Wheatstone bridge circuit. Those are two-wire quarter bridge circuit, three-wire quarter bridge circuit, half bridge circuit and full bridge circuit [Hoffman (1989)]. Usually the type of circuit is named according to the number of strain gauges connected in the Wheatstone bridge circuit. Vadassery et al (2013) implemented quarter bridge circuit on a triangular force balance attached to a conical model, for drag measurement during shock tunnel testing at Mach 9.4. Jessen and Gronig (1989) proposed a balance in form of cross bars where semiconductor strain gauges were placed on each side of the beams of the cross. Wheatstone bridge circuit with strain gauge in each arm was used for response measurement.

For precise measurement of strain, present efforts are dedicated to the development and implementation of various circuits associated with stress wave force balance. Assessment of those arrangements is also planned through force measurement experiments. Execution of the above objectives is made possible using a hemispherical model integrated with a stress bar. In the initial phase, emphasis has been given to determine the location of the strain gauge with the help of finite element analysis (FEA) so as to ensure accurate measurement of dynamic strain. Dynamic calibration of the test model using impulse hammer and subsequent testing in shock tube are the major milestones of present studies.

3.2 Preliminary Investigation

Details of the initial efforts about numerical simulations and dynamic calibrations are elaborated in the following section.

3.2.1 Transient Finite Element Simulation

A hemispherical model, shown in **Fig. 3. 1**, is designed and fabricated specially for force measurement experiments. This test model of 15 mm radius is made out of aluminum. It is attached with a stress bar of brass having diameter 14 mm, thickness 1 mm and length 41 mm. Choice of brass as material for the stress bar is to ensure that the stress wave propagation takes place at lower acoustic speeds. Thus, it enables to capture the response for longer test duration [Sahoo and Reddy (2010)]. Initially, FE simulations are carried out in order to arrive at an optimum location of strain gauge position where higher magnitude of the strain can be expected. These transient FE simulations are conducted using commercial solver (ANSYS 14.5) for simulation time of 2ms. During mesh generation for the test model, 10-noded tetrahedral (solid 187) element is used. Final mesh of 115872 nodes is selected after detailed mesh independence studies (**Fig. 3. 2**). Material properties assigned to the model and stress bar during simulation are given in **Table 3. 1**. During FE simulation bonded contact is provided between the internal part of the model and corresponding external part of the stress bar. Simulations are performed for two types of boundary conditions. In one of the types, rear end of the stress bar is given "zero displacement boundary condition" in any direction as shown in **Fig. 3. 2.** This simulation would provide the response under the constraint where model is held firmly during testing. Other simulation is performed without any constraint on the "free rear end of the stress bar" in order to get the reaction under free flying condition. Inner surface of a 6 mm thick rubber is glued to the concerned end of the stress bar and the outer surface of the rubber is restricted to move in any direction. Rubber bushes having Young's modulus of 3 MPa are chosen, so as to imitate the free flying condition [Sahoo et al. (2007)].

During the simulation, different magnitudes of impulse forces are applied at the tip of the model. Care is taken to apply an impulse of lower width and in most of the cases width of such applied impulse is noticed to be 300μs. As no permanent deformation of the model is expected during impulse hammer based calibration test and also in the shock tube, therefore the FE simulations are restricted in the linear regime only.

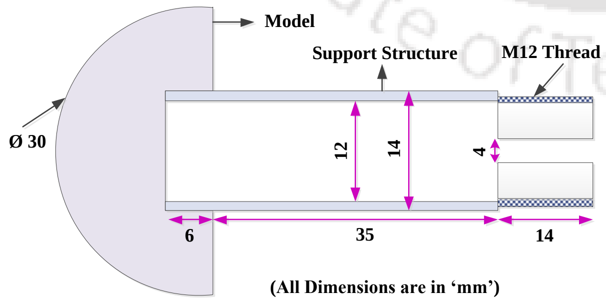

Fig. 3. 1: Schematic diagram of the model.

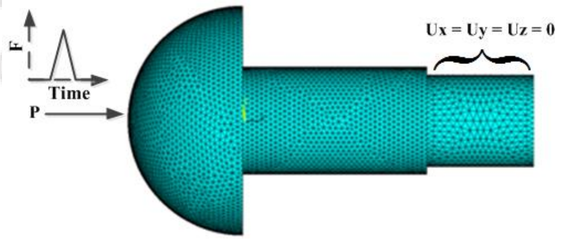

Fig. 3. 2 : Meshed model generated from FE during fixed condition analysis.

Table 3. 1: Material properties assigned during simulation.

Material	Young's modulus (E) in GPa	Density (ρ) in kg/m^3	Poisson's Ratio (υ)
Aluminum	70	2700	0.32
Brass	100	8400	0.3

Dynamic strain along the axial direction, at discrete points on the stress bar, is computed for both types of boundary conditions. Comparison of maximum magnitude of strain obtained from simulation, for 20 N loading, is as shown in **Fig. 3. 3**. From the figure, it can be concluded that the strain gauge should be mounted at a distance of 5 mm from the rear end of the hemispherical model for ensuring a larger magnitude of strain. As the nonlinear behavior is not taken into account for simulation, higher magnitude of impulse loading on the model is also seen to yield similar results as those of the earlier case.

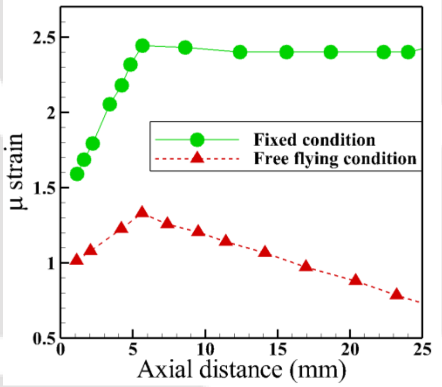

Fig. 3. 3: Comparison of strain magnitude over the length of the stress bar.

Explicit dynamic simulations are performed for "surface loading" instead of "point loading". Here as well, objective is to arrive at the maximum strain location during the test duration. Therefore hemisphere surface is considered to have force applied upon, so as to imitate the experimental testing where object gets exposed to surface forces. The meshed model considered for these simulations is as shown in **Fig. 3. 4** comprises of 139867 nodes for free flying boundary condition. Strain variation on the stress bar at different time instances obtained from the simulation is illustrated in **Fig. 3. 5.** This simulation also asserts about the same location as decided earlier for maximum strain location.

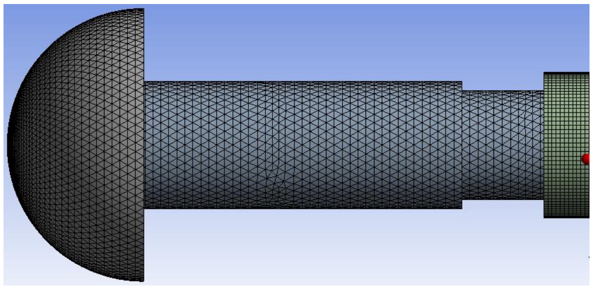

Fig. 3. 4: Meshed model generated during Explicit dynamics

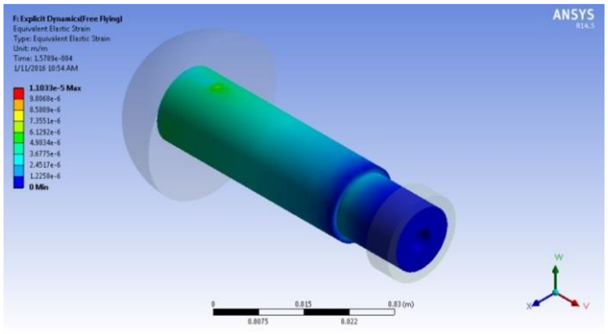

(a)

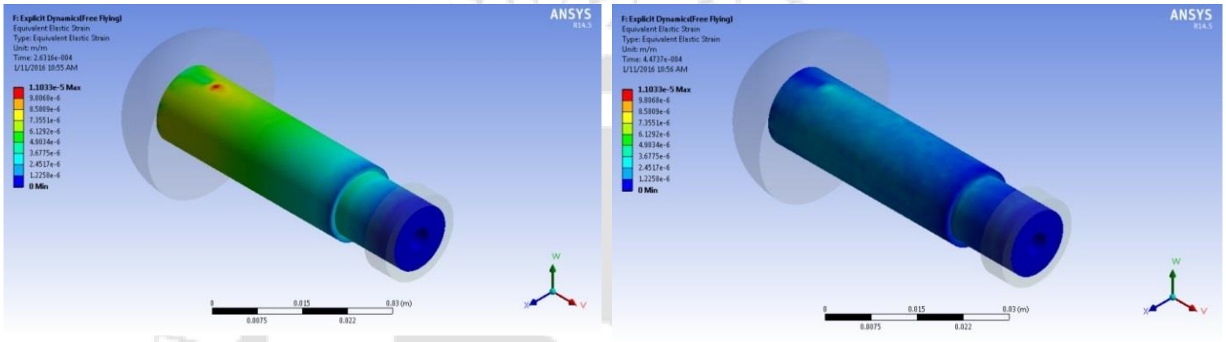

(b) **(c)**

Fig. 3. 5: Strain concentration over the stress bar at (a) 110 µs (b) 263 µs (c) 447 µs.

3.2.2 Exploration of circuit configuration for strain measurement

As described in the previous chapter, Wheatstone bridge is generally used as the sensing circuit for strain gauge instrumentation due to its inherent ability to detect the small resistance changes. Three variants of this circuit are considered in present studies. In an arrangement for strain measurement, one of the resistive elements is replaced by a strain gauge. This configuration is termed as “two wire quarter bridge circuit” as shown in **Fig. 3. 6.** Such arrangement is preferred where accurate measurement of strain magnitude is not desired. Limitation of this circuit arrangement is the possibility of measuring bending and axial strains where axial strain measurement is only required. Besides, the wire resistance also adds its impression on strain measurement since two wires have to be attached to the strain gauges. This wire effect cannot be completely eliminated but can be minimized with the addition of a third wire as shown in **Fig. 3. 7**. Here, the extra wire is connected between the one of the terminals of the strain gauge and the output terminal of the Wheatstone bridge circuit. There is no significant voltage drop across the additional wire since it doesn’t carry any current. This arrangement is termed as “three-wire quarter bridge circuit”. It contributes half of the wire resistance in series with the gauge in comparison with the earlier arrangement. Further, the chances of inclusion of bending strain can be reduced by using half bridge circuit as illustrated in **Fig. 3. 8**. This arrangement encompasses two strain gauges as its active arms and as an effect, this circuit gives twice the output voltage for a particular strain. Therefore, the sensitivity of the circuit would enhance twice than earlier. In the present studies, SSG with high gauge factors are used for strain measurement (**Sec. 3.3.2.1**). In all the cases, output strain response of the semiconductor strain gauge is expected to be low and an amplifier is used for magnifying the response. This voltage amplifier has provision of gain factor 500 and 1000 with an operating bandwidth frequency in the range of 1- 40 kHz. The relation between output of the Wheatstone bridge and the local strain produced in the test model, is given by the **Eq. 3.1** [Cimbala (2011)] where ‘n’ can be 1, 2 or 4 depending upon the type of circuit implemented viz. full bridge, half bridge or quarter bridge circuit respectively.

$$Strain = \frac{V \times n}{GF \times E} \tag{3.1}$$

An experimental arrangement as shown in **Fig. 3. 9,** is considered for testing all the circuits. During these experiments, an impulse hammer (PCB Piezotronics Make) is used to apply a point load on the tip of the hemispherical part. Time history of the applied force is recorded in the DAS. All the strain measurement circuits are tested separately and the strain signals are also recorded. Specific attention is given to apply force of similar magnitude along axial direction in each experiment.

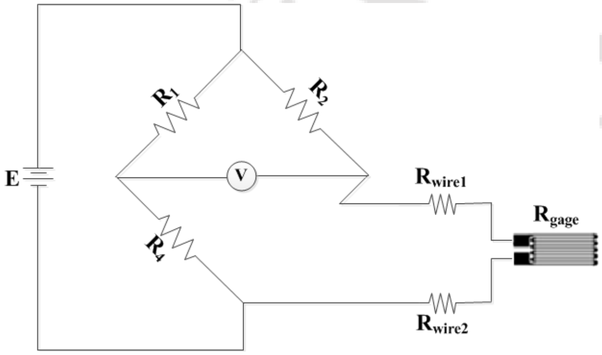

Fig. 3. 6: Two-wire quarter bridge circuit

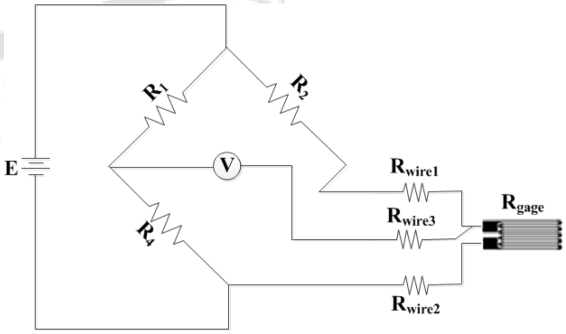

Fig. 3. 7: Three-wire quarter bridge circuit

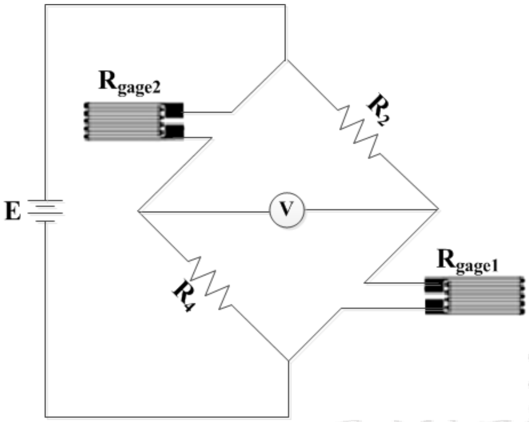

Fig. 3. 8: Half bridge circuit.

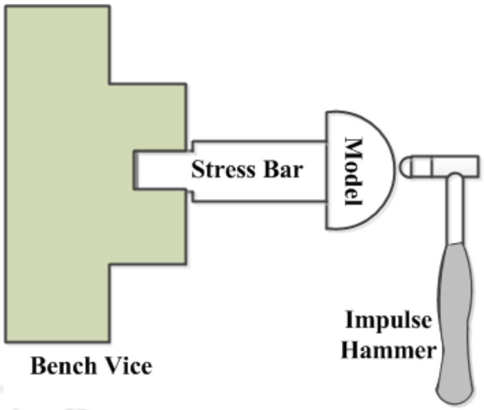

Fig. 3. 9: Dynamic calibration setup for fixed condition.

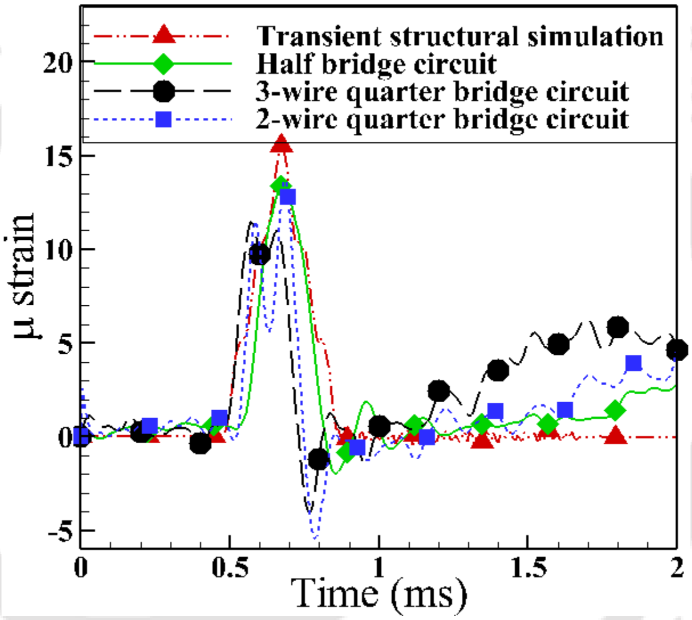

Fig. 3. 10: Comparison of strain signal obtained from different circuits due to impulse loading.

However minor deviation of ± 1.6% in applied forces is noted. Numerical simulations are then carried out using the known force time variation for the fixed end boundary condition of the stress bar. The transient strain signals obtained in impulse hammer tests with different circuit configurations and their comparison with the structural simulation results for an impulse load of around 122 N has been shown in **Fig. 3. 10.** It is evident from the figure that both two-wire and half bridge circuit is having a peak magnitude deviation of 10.5% as compared to the transient simulation result. Further, three-wire quarter bridge circuits portray deviation of 22.6% as compared to corresponding simulation results due to the shortcomings of the circuit configurations, as discussed earlier.

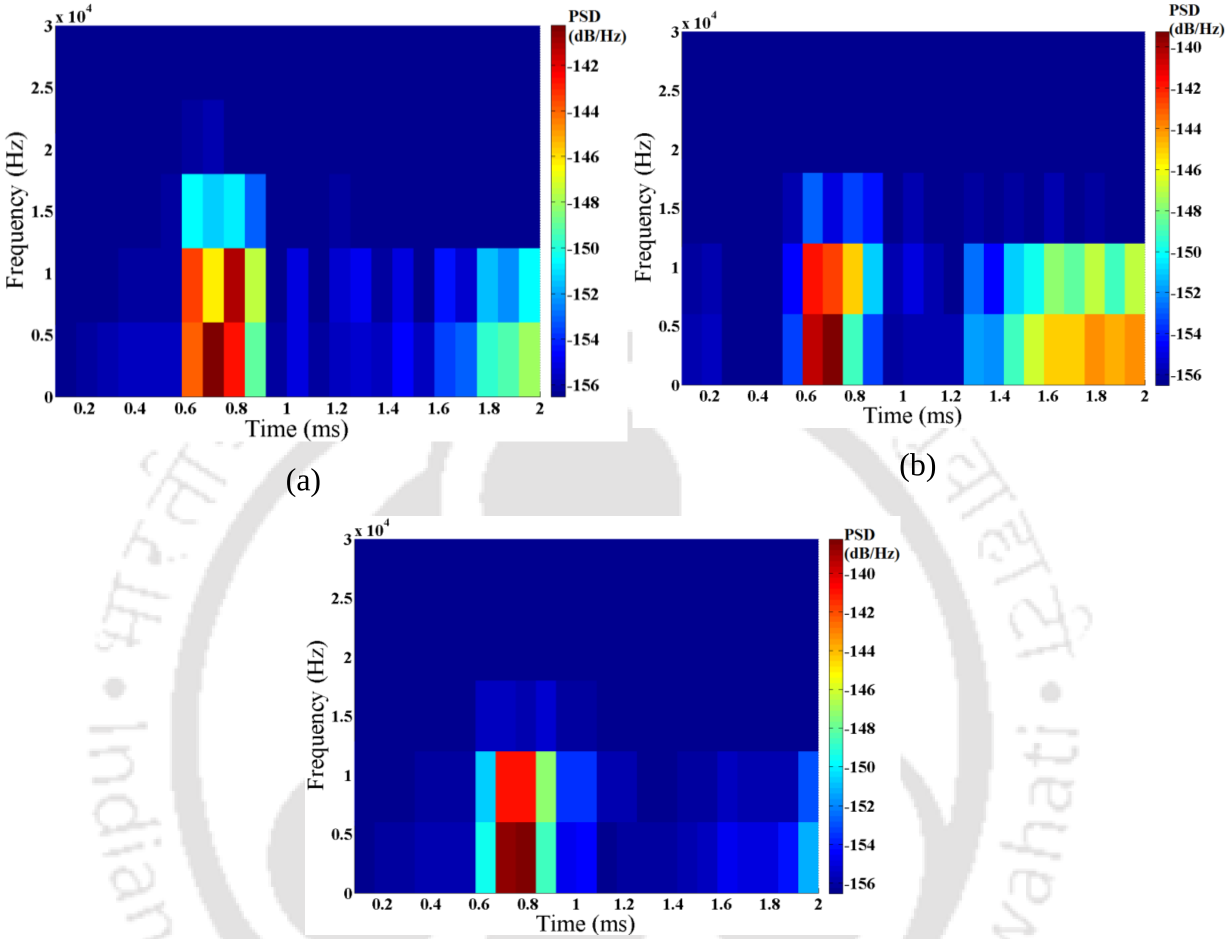

(a) (b)

(c)

Fig. 3. 11: Spectrogram for (a) Two-wire quarter bridge (b) Three-wire quarter bridge (c) Half bridge circuits.

It has been observed that the signal obtained from the half bridge circuit is less noisy as compared to that of other two circuits. Therefore, this signal (half-bridge circuit) is noticed to have more closeness with the results from transient simulation. It can be clearly indicated from **Fig. 3. 10** that two peaks are present in case of strain response obtained from two-wire quarter bridge circuit. All the strain responses are then considered to compare for their frequency content using spectrograms (**Fig. 3. 11**) by representing in the form of contours called as “Power Spectrum Density (PSD)”. In general, PSD provides an estimate of the energy content of the signal over a specified frequency range. As it can be seen from **Fig. 3.**

11(a), two high magnitude regions are existing at two different frequency bandwidths in case of 2-wire quarter bridge circuit. But the applied force, upon spectrogram analysis, is seen to have high magnitude frequency region only below a frequency bandwidth of 6 kHz. However, spectrogram for three-wire quarter bridge circuit, **Fig. 3. 11(b)**, does not portray such anomalous spectrum. But, it is seen to have disadvantage of increasing frequency magnitude with respect to time. However, it should not have been for the applied impulse because after the impulse width frequency content of the signal must be very low. Further, the use of half bridge circuit is found to have merits since its spectrogram, **Fig. 3. 11(c)**, shows high intensity region only during application of force and minor increment in frequency with time as compared to contemporary cases.

3.2.3 Dynamic calibration of force balance

The experimental set-up shown in **Fig. 3. 9,** is used for dynamic calibration of the SWFB. All the circuit arrangements are used for strain measurement experiments in these calibration tests. Force history of applied impulse using impulse hammer and corresponding strain signal of each test are recorded in the oscilloscope. Major objective of this calibration experiment is to evaluate the system response function using these known force and strain signals. Such calibration is highly desirable since the obtained system response function would then be useful to recover the unknown force history from the experimentally measured strain. This usefulness will be verified in case of shock tube tests. The associated unsteady behavior of the test model and support system during short testing duration of the order few milliseconds is the inherent characteristics of such stress wave force balance. Hence, the calibration experiments will essentially justify the prediction of unknown forces during real time tests (Mee 2003). Typical force and corresponding strain signals for half bridge circuit are shown in **Fig. 3. 12** and **Fig. 3. 13** respectively. Similar experiments are conducted with other circuit arrangements also. Force and strain signals obtained from any of the calibration experiments using each arrangement are then used for estimation of corresponding system response function. The selection of calibration test is purely arbitrary, as all the applied force and the corresponding response can be replicated within deviation of ± 1.6%. Fast Fourier Transform (FFT) based convolution algorithm of MATLAB is employed for this estimation. Thus obtained system response function and the strain signal from other calibration test are then used in the FFT based de-convolution procedure of MATLAB to recover the corresponding applied force. The recovered impulse forces for each strain gauge arrangement are shown in **Fig. 3. 14**.

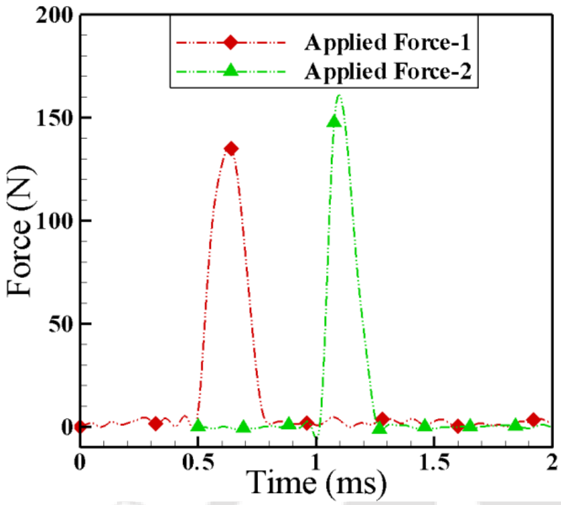

Fig. 3. 12 : Typical force signal obtained during dynamic calibration

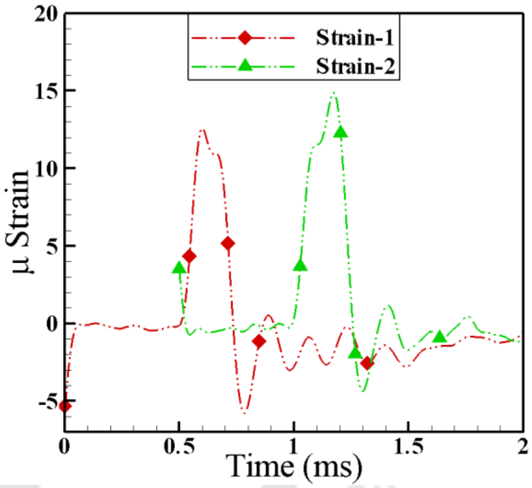

Fig. 3. 13: Typical strain signal obtained from half bridge circuit.

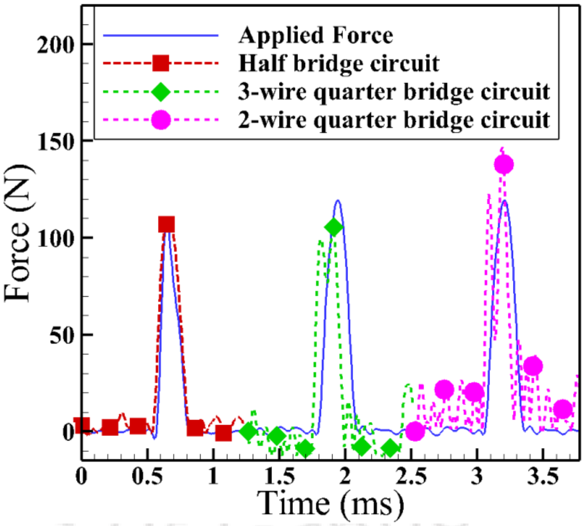

Fig. 3. 14: Comparison of applied and recovered force signals for different circuit arrangements.

Further confirmation of improved performances of the half bridge circuit for response measurement is evident during comparison of the predicted forces in this figure. It is clear that a noisy and higher magnitude of force is predicted using the response of two-wire quarter bridge circuit. Further, the peak magnitude of predicted force seems to be decreased in case of three-wire quarter bridge circuit along with the noise. However, in case of half bridge circuit, the noise seems to be reduced significantly and encouraging match is observed between the recovered and applied load in terms of trend and peak magnitude. Uncertainty in predicting the peak magnitude, for half bridge circuit, is found to be ± 8%. Thus, the present calibration experiments also validate the use of half bridge circuit for force measurement.

3.3 Force measurement in shock tube

The present experiments for force measurement are planned in the shock tube facility described in the earlier chapter. The test model integrated with the stress wave force balance along with half bridge circuit is mounted at the driven side end of the shock tube. Pressure transducers and strain gauges are connected to oscilloscope. Experimental set up and final circuit implementation is shown in the **Fig. 3. 15** and **Fig. 3. 16** respectively. Experiments are carried out with nitrogen as driver and air as driven gas. During the actual force measurement experiments, driven section is maintained at a pressure of 0.18bar. Shock tube pressure and strain signals are recorded in each experiment for same settings. Typical pressure signals obtained from both the pressure transducers are shown in **Fig. 3. 17**. All the experiments are found to have repeatability in terms of acquired strain responses as shown in **Fig. 3.18**.

These plots show the unfiltered data of the measured variables in Volts. Further, present acquisition is performed with gain settings depending upon the signal strength. Due to this fact the measured variables have different magnitudes. In this case the calculated shock Mach number is 2.17. This figure confirms the repeatability of the present measurements. Minor discrimination in strain magnitude is observed, but it is attributed to the standard repeatability issue of shock tube experiments. Further, this deviation found in magnitude of strain responses is noticed in the acceptable uncertainity range. Ideally after certain duration after the shock wave crosses the 2nd pressure transducer, the strain gauge should be activated which can also be verified from **Fig. 3. 19**. It portrays the rise time of the sensor as 250 μs and the steady force duration as 1.15ms. The experimental strain response is then provided to the de-convolution algorithm along with the system response function to recover the applied force and the predicted force history is shown in **Fig. 3. 20**.

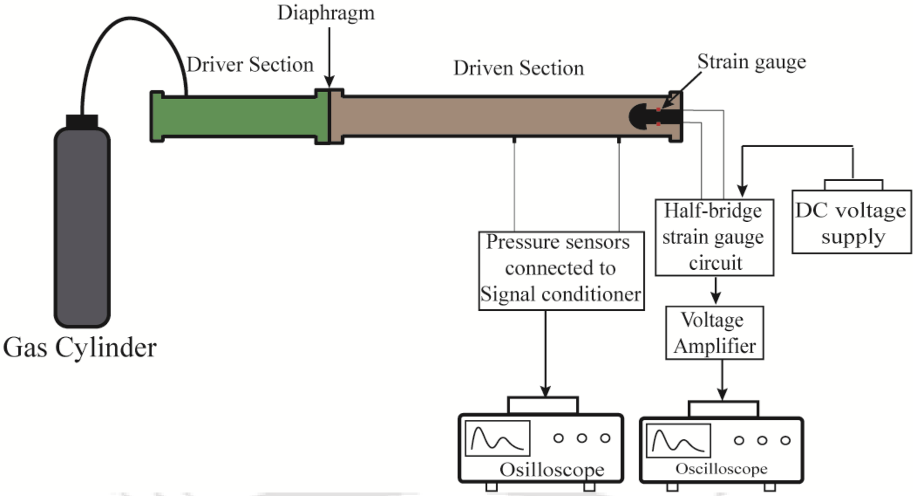

Fig. 3. 15: Exhaustive representation of the experimental setup.

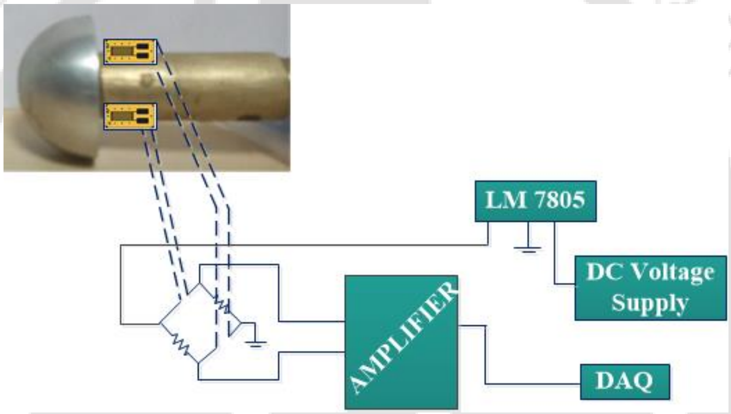

Fig. 3. 16: Circuit diagram for the hemispherical model used in shock tube experiments.

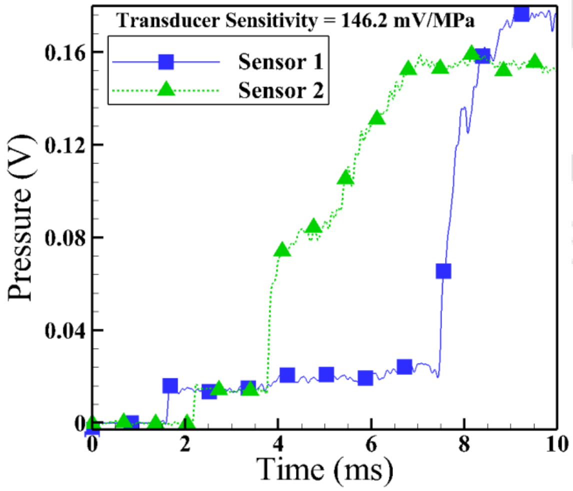

Fig. 3. 17: Typical pressure signal obtained during experiment.

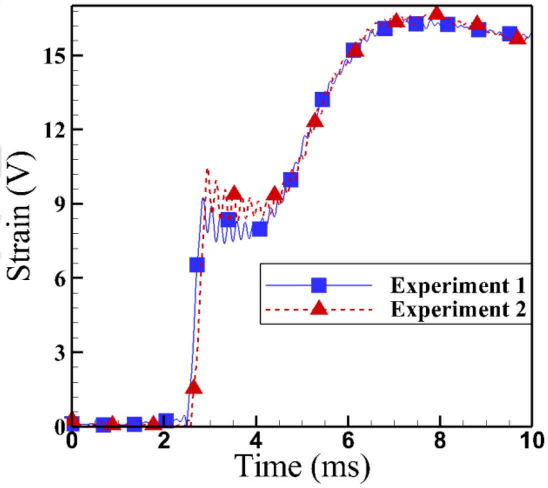

Fig. 3. 18: Strain histories obtained during shock tube experiments.

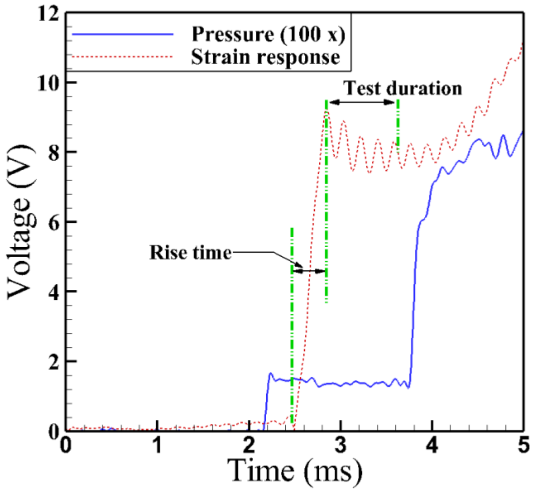

Fig. 3. 19: Comparison of pressure and strain signal for proper estimation of test duration.

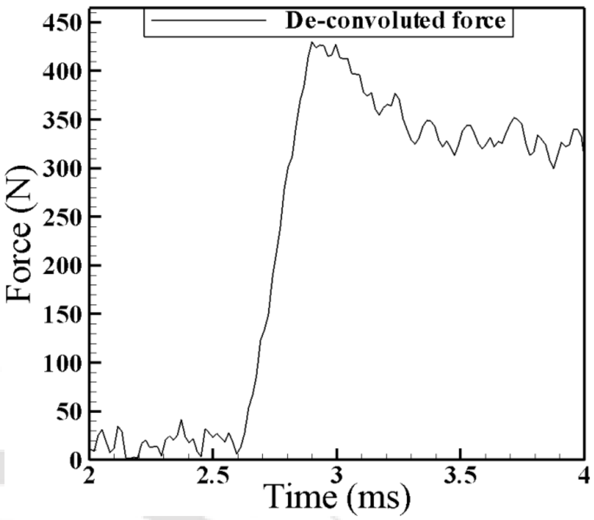

Fig. 3. 20: Transient drag force predicted through de-convolution technique.

Summary

Initially, numerical simulations are performed to estimate best location of the strain gauge mounting, on a hemispherical test model integrated with stress bar. Finite element simulations showed that higher magnitude of strain will be acquired at a distance of 5 mm from rear end of the test model. Different circuit arrangements are successfully made and implemented for impulsive force applications. Response of various types of Wheatstone bridge circuits is recorded during dynamic calibration experiments. These temporal strain signals when analyzed for trend and magnitude in time and frequency domain, resulted in a deviation of 10.5% and 22.6% for half bridge and quarter bridge circuit respectively, as compared to the transient simulation results. Prediction of the applied impulse force from the strain signal of half bridge circuit using de-convolution technique is observed to have expected trend and peak magnitude with ± 8% uncertainty, which depicts that the half-bridge circuit has an edge over the other arrangements. Usefulness of this arrangement is proven during force measurement experiments by mounting the same test model in the end flange of the shock tube. Transient responses are successfully captured and force prediction technique is also employed to recover the drag force acting on the model during test duration. Henceforth, current study emphasizes the use of half bridge circuit and its associated instrumentation for strain based force measurement in impulsive applications.

CHAPTER-4

Piezofilm as a Potential Sensor for Force Measurement in Short Duration Impulse Test Facilities

Overview

Successful implementation of the strain gauge in impulse facilities has been the influencing aspect to explore the other strain sensors which can be used in dynamic environments. Therefore, present investigations are focused towards employing piezofilm for force measurement in an impulse test facility. In view of achieving the above stated objective, SWFB system which employs semiconductor strain gauge and piezofilm for dynamic strain measurement has been considered. Initially, dynamic calibration experiments are carried out using impulse hammer tests on a hemispherical test model and stress bar assembly with an intention to estimate the system response function. However, the same calibration data is also used for calculation of model weights for a soft computing architecture through training of force and strain signals. Then, force measurement experiments are conducted on the same test model by fixing it at the end flange of the shock tube. Drag force acting on the model during the experiment is recovered from the strain signal using de-convolution technique and ANFIS. Simulations using in-house solver are also performed to predict the temporal variation of drag force. Encouraging match in steady state magnitude of drag force between the numerical prediction and recovered force from piezofilm and strain gauge response clearly depict piezofilm as a potential sensor for stress wave force balance. However, discrimination is found while recovering the temporal force history from the output responses. Therefore, present studies recommend the use of piezofilm for force measurement in short duration test facilities since it is a low cost alternative and it needs lesser supportive instrumentation.

4.1 Introduction

In view of less attention and advantages of stress wave force balance in comparison to accelerometer balance, this study has been focused towards assessment of different sensors that can be opted for measuring dynamic strain in impulse facilities. Essentially, strain gauge or piezofilm is usually incorporated to monitor the strain variation. High gauge factor strain gauges are effectively implemented in the impulse facilities to detect the stress wave while employing the SWFB for force measurement. Piezofilms can also be thought as an alternative to the strain gauges for strain measurement. Anjana *et al*. (2013) considered film developed from the composite of piezo ceramic and piezoelectric materials to measure the strain. These developments inspired present studies for the possible use of piezofilm to measure forces in the short duration impulse facilities since it has not been explored adequately. Such investigations are highly desirable to establish an alternative accurate measurement technique with lesser instrumentation as compared to the existing options. In addition to this, piezoelectric sensors are usually self-excited and possess the property of high frequency noise rejection with involvement of less signal conditioning [Sirohi and Chopra (2000)]. Further, associated cost of these sensors is also less in comparison with the high gauge factor strain gauges.

Therfore knowing these advantages of the piezofilms and noting lesser attention to its usage for force measurement application in short duration test facilities [Vadassery *et al.* (2013)], experiments are planned to assess their applicability for force measurement in an impulse test facility. In an extension to this, it is also planned to have qualitative and quantitative assessment of strain gauge and piezofilm responses. Hence the hemispherical model with a stress bar, described in the previous chapter is instrumented with strain gauge and piezofilm force balances to test for drag force measurement in shock tube. During dynamic calibration of these balances, system response function is estimated using frequency based convolution technique whereas the same calibration signals are also fed to ANFIS network for evaluation of model weights. Thereafter, the trained architecture and de-convolution technique are used for recovery of temporal variation of drag force by using experimentally measured responses from both the balances. In aid with experiments in shock tube, CFD simulation is also carried out to predict the time variation of force acted on the hemispherical model subjected to experimental conditions. Details of the test model, force balances, recovery techniques, CFD simulations and shock tube testing are discussed in the following sections.

4.2 Test Model, Instrumentation and Experimental Set-up

Hemispherical test model and associated stress bar assembly, described in the earlier chapter, have been utilized for the current sets of investigations. Stress bar of brass material is generally preferred, as the stress wave propagation speed is less for this material which will result in maximum duration of the response acquisition before any interaction between stress waves. Thereafter, this assembly of test model and stress bar is considered for force measurement purpose using strain gauge. Schematic of the model and stress bar assembly is shown in **Fig. 4. 1**. The same model with stress bar of slightly higher length of 50 mm is used for experiments with piezofilm balance so as to get an adequate space for mounting this piezo sensor to measure the strain at the same location as that of strain gauge. Therefore, sensor mounting location is adjusted in such a way that CG for both the sensors is located at the same distance from the rear end of the test model. Hence, for the force measurement with strain gauge balance, a strain gauge having length 7 mm is mounted at a distance of 5 mm from the rear end of the hemispherical model. As the length of the piezofilm is 18 mm, it is mounted closer to the end of the model to mimic the same location of the CG of the sensor as earlier. Thus same test model, integrated with two strain sensors in the leeward side, is used to measure the wave drag. Here, in one set of experiments, strain is measured with the help of Kulite encapsulated strain gauges of gauge factor 130 and resistance 350 Ω. These strain gauges have an extra encapsulation wherein the gauge is embedded in a protective epoxy/glass matrix. Half bridge circuit arrangement of Wheatstone bridge is adopted while considering the strain gauge for strain measurement as it eliminates the chances of inclusion of strain produced by the lateral forces during measurement of axial strain induced in the body [Nanda *et al.* (2017)]. In the other set of experiments, strain is measured with help of piezofilm (Make: Measurement Specialties) having capacitance 0.5 nF, which is capable of capturing response in a frequency range of 0.001 Hz to 10^9 Hz. This film has sensitivity factor of 12 mV/μ-strain and it can be directly exposed to a maximum temperature of 100° C. However, during actual experimentation the film has been wrapped with proper insulation to eliminate the effect of electro-magnetic radiation and direct exposer to the flow. **Fig. 4. 2a** and **Fig. 4. 2b** give the details of test model with mounting of sensors.

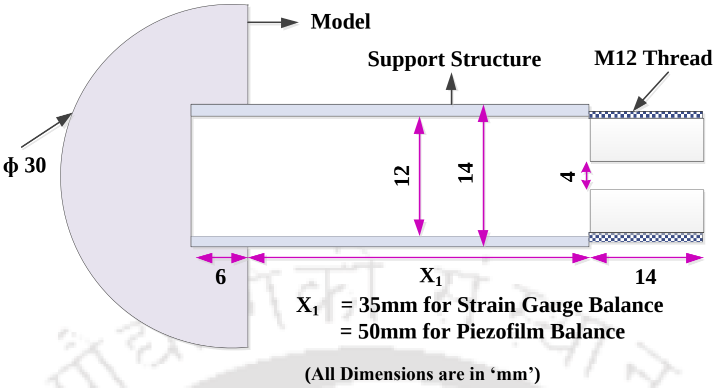

Fig. 4. 1: Schematic drawing of the hemispherical model.

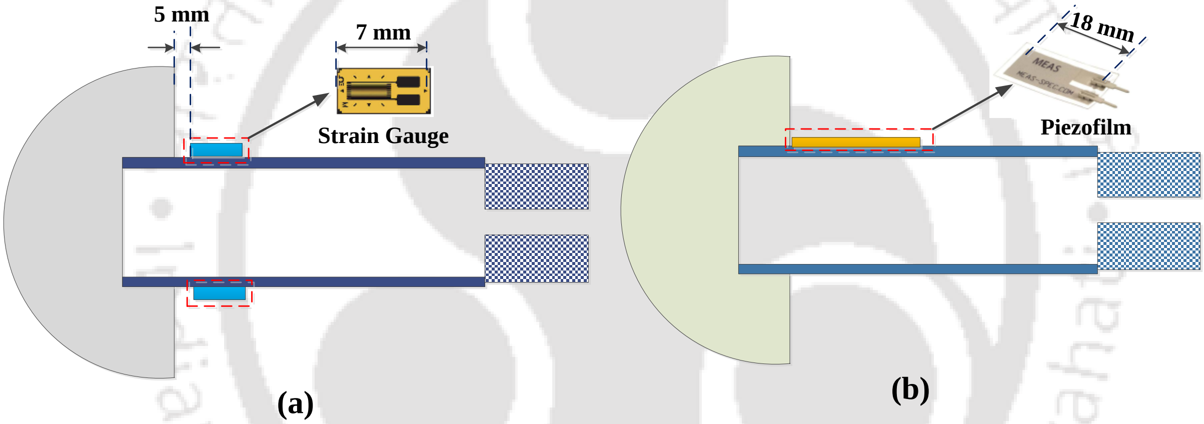

(a) (b)

Fig. 4. 2: Test model with mounting of (a) strain gauge (b) piezofilm.

The present experiments for force measurement are planned in the shock tube situated at Indian Institute of Technology, Guwahati, India (IITG-ST) [Nanda *et al.* (2017)]. The entire shock tube assembly and its working procedure have been briefly described in **Chapter 2**. Two pressure transducers are mounted in the driven section to monitor the primary and reflected shock wave strengths. The test model-stress bar assembly, equipped with the strain sensor, is mounted at the center of the driven section end flange. Two strain gauges are mounted opposite to each other on the stress bar and are further connected to half bridge circuit arrangement for measuring resistance change during the experiment. Since output of the Wheatstone bridge is of the order of few microvolts, a voltage amplifier, INA128 with gain factor of 500, is employed during data acquisition. Conversely, acquisition of piezofilm response is quite simple; this sensor is directly connected to the DAS .This experimental set up is shown in **Fig. 4. 3**.

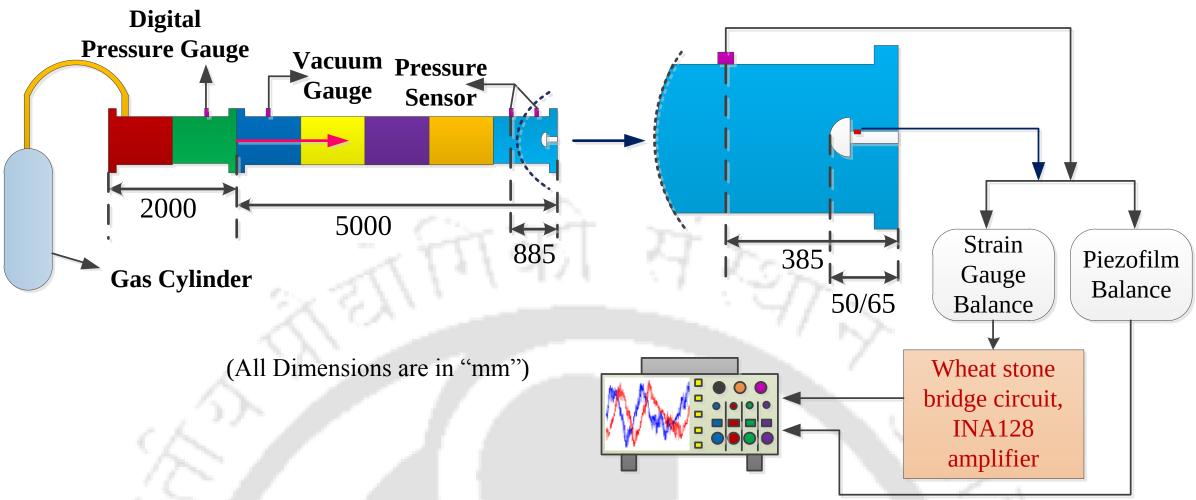

Fig. 4. 3: Representation of the experimental set-up.

All the experiments in IITG-ST reported herein are carried out with nitrogen as driver and air as driven gas. During initial shock tube calibration experiments and for the actual force measurement experiments, driven section is maintained at a pressure of 0.18 bar while diaphragm rapture pressure in the driver section side is noted to be 20.2 bar. Incident shock Mach number for this experimental setting is 2.48 while the pressure and temperature behind the primary shock are 1.15 bar and 569K respectively. During experimentation, axis of the test model is aligned with the axis of the shock tube. Such mounting eliminates the possibility of introduction of lateral forces on the model in the test duration. Thus, such mounting results in exposure of the hemisphere to only the drag or axial force. Further, this drag force has major contribution from the high pressure acting on the model surface due to presence of shock wave. Such wave drag, which creates high pressure on the windward side of the test model, depends on shape of shock wave and hence on the model geometry. Therefore the model geometry being same in both the measurement techniques (**Fig. 4. 2**), force imparted on the test model would remain same in either cases. Afterward, in line with experiments, space-time (x-t) diagram (**Fig. 4. 4**) is obtained using x-t diagram plotter where S_1 and S_2 represents the location of pressure transducers in the driven section [Anderson *et al.* (2000)]. It is analysed to get an insight on the spatial and temporal position of the flow features originating after the diaphragm rupture. This diagram also puts light on the zone of interaction between flow features and also the available test duration. It is evident from the x-t diagram that the reflected shock and contact surface interact with each other after 7.39 ms of diaphragm rapture and at 527 mm from the driven section end. Therefore, though the length of stress bar is different for strain gauge and piezofilm experiments, both the balances in reality are located in a zone of non-interaction of flow features. Therefore, the flow conditions experienced by the test model are same and hence the force experienced.

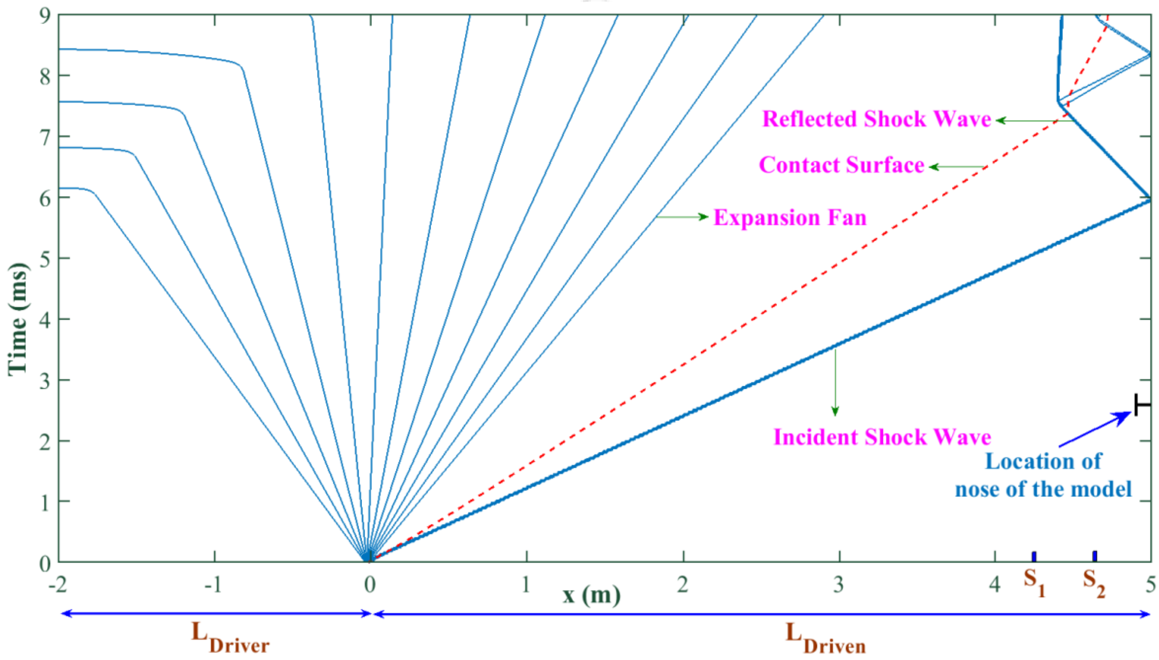

Fig. 4. 4: Space-time diagram for shock wave propagation during running condition of the shock tube without model mounting.

4.3 Computational Methodology

4.3.1 Fluid Flow Simulation

Present efforts are centred on prediction of wave drag, which originates mainly from high pressure on the windward side of the model in the presence of strong shock wave. Hence, CFD simulation using Euler solver is sufficient to predict the wave drag on a supersonic or hypersonic configuration. In view of this, the in-house developed non-equilibrium inviscid flow solver is employed for shock tube flow simulations to predict the time varying force applied on the test model [Desai *et al.* (2016), Desai *et al.* (2017)]. This solver accounts presence of five species (N_2, O_2, N, O, and NO). The governing equations of this two-dimensional (2-D) axi-symmetric Euler solver, considered to solve in finite volume formulation, are given by **Eq. 4.1** in vector form.

$$\frac{\partial U}{\partial t} + \frac{\partial F}{\partial x} + \frac{\partial G}{\partial y} + S + S_I = 0 \tag{4.1}$$

where,

$$U = \begin{bmatrix} \rho \\ \rho u \\ \rho v \\ \rho E \\ C_1 \\ C_2 \\ C_3 \\ C_4 \end{bmatrix} \quad F = \begin{bmatrix} \rho u \\ \rho u^2 + p \\ \rho uv \\ (\rho E + p)u \\ uC_1 \\ uC_2 \\ uC_3 \\ uC_4 \end{bmatrix} \quad G = \begin{bmatrix} \rho v \\ \rho uv \\ \rho v^2 \\ (\rho E + p)v \\ vC_1 \\ vC_2 \\ vC_3 \\ vC_4 \end{bmatrix} \quad S_I = \frac{1}{y}\begin{bmatrix} \rho v \\ \rho uv \\ \rho v^2 \\ (\rho E + p)v \\ vC_1 \\ vC_2 \\ vC_3 \\ vC_4 \end{bmatrix} \quad S = -\begin{bmatrix} 0 \\ 0 \\ 0 \\ 0 \\ S_1 \\ S_2 \\ S_3 \\ S_4 \end{bmatrix}$$

Polynomial expressions, as given by Gordon and McBride (1994) are used to account for specific heat variation with temperature. While considering the eleven reactions among the five species, specific reaction-rate constants mentioned by Dunn and Kang (1973) are used to develop this solver [Desai et al. (2017)]. Details of these reactions are associated chemical kinetics are available in the literature [Desai et al. (2017)]. Convective flux calculation scheme, AUSM with second order spatial accuracy is adopted herein along with the 5th order Runge-Kutta (RK5) scheme for higher order time accuracy. For accurate estimation of the temporal variation of drag force, the computational domain should be chosen judiciously, which should mimic the actual flow conditions experienced by the model during the test time. Flow in shock tube set-up, illustrated in **Fig. 4. 3**, is planned for simulation, but only for computational domain which is 250 mm from the end flange of the driven section. The domain restriction information can be deduced from the x-t diagram (**Fig. 4. 4**) for the current operating parameters. Sketch of the computational domain and the boundary conditions are shown in **Fig. 4. 5**. Free-slip (or inviscid) wall boundary condition is applied for the top wall and the driven section end (right) wall. Accounting the flow to be axi-symmetric, only half of the domain is considered for simulation by implementing symmetry wall boundary condition to the bottom wall of the domain. Further, left vertical wall is set as an inlet. This computational domain is initialized with two distinct initial conditions by accounting the primary shock location as 70 mm from the driven end of the shock tube. Driven section conditions of pressure, temperature and velocity are set ahead of this primary shock and post shock conditions of pressure, temperature and velocity are given as initial guess behind this shock. These post shock conditions are also applied as inlet conditions for the left vertical wall which has inlet boundary condition.

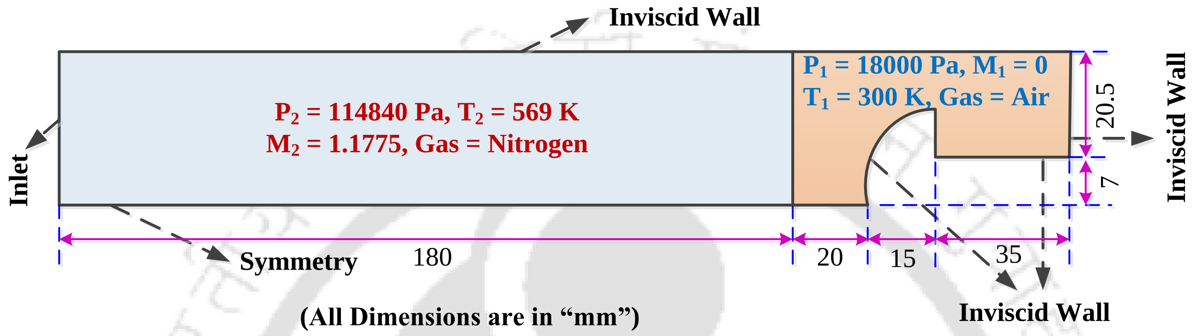

Fig. 4. 5: Schematic of the computational domain with boundary and initial conditions.

4.3.2 Transient Structural Simulation

For the present studies, FE simulations are carried out using ANSYS as mentioned in the previous chapter. These simulations are performed for the test model and its associated balance for experimental test duration of 1.2 ms. Computationally obtained drag force or the experimentally recovered one can be applied as input force at the nose of the model. Major intention of these structural simulations is to estimate the dynamic strain at the location of the strain sensor.

4.4 Results and Discussion

At first, the above mentioned hemispherical model equipped with strain gauge and piezofilm is calibrated dynamically to estimate the impulse response function of the system which is incorporated in frequency based de-convolution technique for force prediction. Simultaneously, the same calibration data is also fed to the soft computing based ANFIS network for obtaining the model weights of the optimum architecture which can be also employed for force recovery. Experiments are then carried out in the IITG-ST for earlier mentioned shock tube operating conditions.

4.4.1 Dynamic Calibration

Here as well, dynamic calibration is carried out in a similar manner as described in previous chapter. Impulse forces of different magnitude are applied manually at the nose of the test model during the calibration tests and responses have been obtained. Care is taken to apply the force with its orientation aligned along the longitudinal axis of the model and stress bar assembly. Such care in force application is essential to bypass the interaction of forces in different direction and also for the associated responses. As a result, it reduces the complicacies involved in evaluating the system response function or estimating correlation between force and its associated response. Practically, the nine components of system response function desired for accurate estimation of the behavior of the model and balance system, simplifies to evaluation of a single transfer function that relates the axial force and its corresponding response [Abdel-Jawad *et al.* (2007)]. Sample recorded force and strain signals obtained in case of strain gauge are shown in **Fig. 4. 6**; while those for piezofilm case are given in **Fig. 4. 7**.

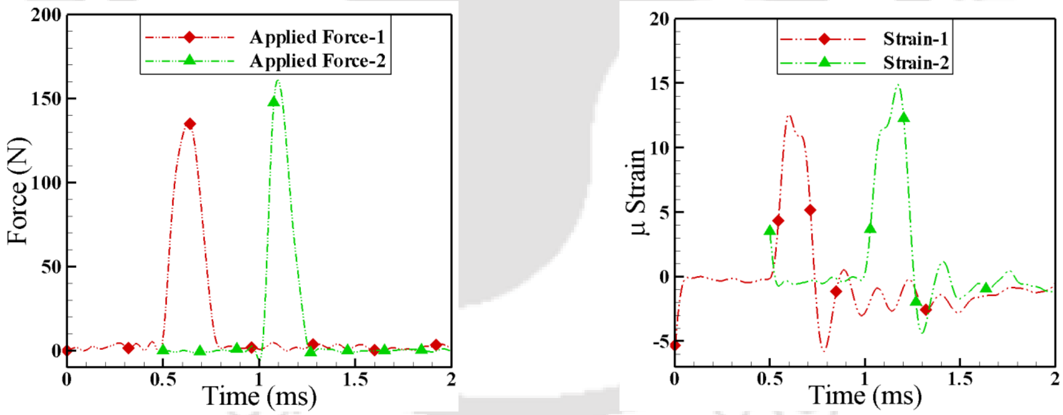

(a) **(b)**

Fig. 4. 6: Sample applied (a) force signals and (b) corresponding strain signals of two calibration tests using strain gauge balance.

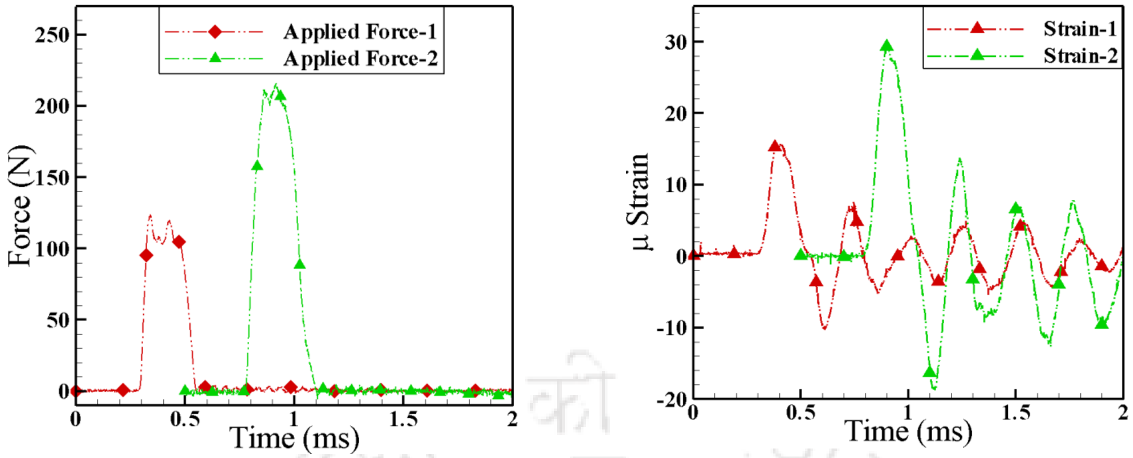

(a) **(b)**

Fig. 4. 7: Sample applied (a) force signals and (b) corresponding strain signals of two calibration tests using piezofilm balance.

4.4.1.1 System Response Function Estimation

The strain and corresponding impulse force signals are initially used to calculate the transfer function of the system which will be incorporated in frequency based de-convolution technique for force prediction. Here, the instrumented model and the mounting system are assumed to follow linear dynamics. Hence, force input)u)t ((and the strain output)y)t((can be correlated through the system response function)g)t((, as presented in **Eq. 4.2.**

$$y(t)=\int_{0}^{t} g(t-\tau).u(\tau)\,d\tau \tag{4.2}$$

The above stated convolution in time domain can be transformed to simple multiplication in frequency domain. Therefore, the transient responses acquired as an outcome of calibration experiments, are considered in frequency domain using FFT and then the system response function is obtained [Mee (2003)]. In case of frequency domain convolution, peak impulse of 80 N along with its corresponding strain signal is chosen to evaluate the system response function for strain gauge, whereas, for piezofilm based recoveries, impulse force of 120 N is employed for the same. Before incorporating it for experimental force recovery, responses obtained during other calibration tests are provided to assess the prediction capability. The response acquired from both the balances for impulse force of 190 N is used for evaluating the accuracy of prediction, which is illustrated in **Fig. 4. 9**. Reasonable accuracy in terms of both magnitude and trend is evident from the figure.

4.4.1.2 Force Prediction Using ANFIS

The established soft computing technique, ANFIS has also been incorporated to arrive at a correlation between the input and output time histories [Pallekonda *et al.* (2017)]. Presently opted soft computing technique is unification of Fuzzy Logic (FL) and Neural Network (NN) as a result of which, it has universal approximation capability as well as a sense of adaptability for tuning the fuzzy controlled parameters. ANFIS is a Multi Input Single Output (MISO) system which comprises of one input layer, one output layer and four hidden layers and each layer is connected through model weights as presented in **Fig. 4. 8**. In this method, an initial fuzzy model containing input and output variables along with the rules extracted from input output data is created. This is further fine-tuned to optimize the model weights through optimizing the consequent and premise parameters using neural network. Therefore, parametric variation can be performed to obtain optimum network architecture. ANFIS tool box of MATLAB is employed during accomplishment of the present objectives. Existing ANFIS module of MATLAB usually handles normalized input and output data, so different type of input and output membership function (MF) are available for normalization. These MFs more often normalize the data between 0 and 1 which basically relays on the shape of MF. The input MFs are categorized into five groups viz. Piecewise linear, Gaussian, Bell-shaped, Sigmoidal and Polynomial based whereas linear and constant MFs are also available for normalizing the output data. The input and output MF to be considered depends upon the type of data to be trained. It can also be chosen based upon user's experience. Incorporating either of the MFs for training, back propagation and hybrid training methods are available through which the training of the input and output data can be carried out. Back propagation method uses gradient descent algorithm whereas hybrid method follows gradient descent algorithm along with least square method to evaluate the model weights. As hybrid training strategy incorporates both the techniques, it seems to be converging to the global optimal model weights. But the back propagation is slow and likely to be trapped in local optimal solution. Also output of the back propagation training strategy depends upon the number of epochs whereas hybrid training method seems to be independent of it. The number of iteration up to which training is performed is designated as epochs.

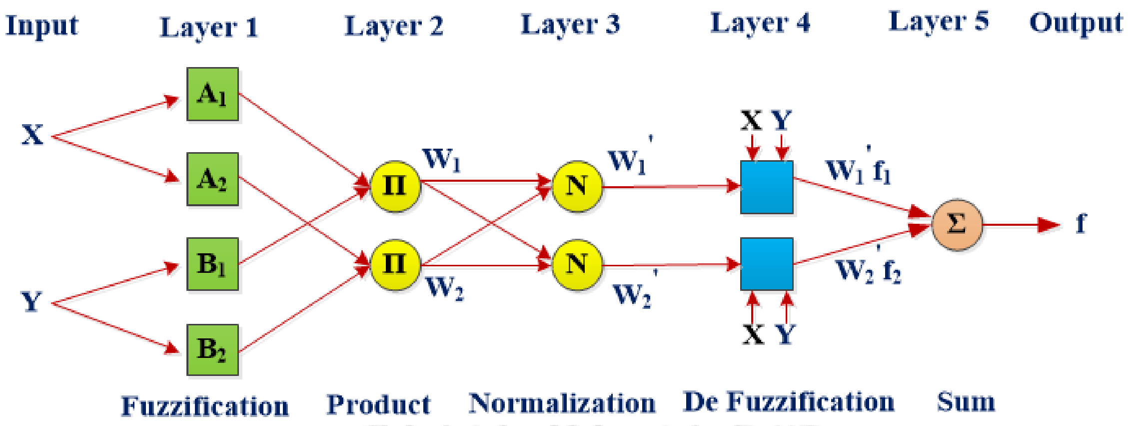

Fig. 4. 8: Elementary ANFIS architecture**.**

Such training results in optimized parameters of the network which relates between input and output data. For the current analysis, the temporal variation of responses acquired during calibration experiments are fed as input to the network whereas the corresponding transient force are considered as the output. Then, the obtained optimized parameters of the network and the recorded experimental strain signal are used to predict the time history of unknown force experienced by the test model in the shock tube testing. Before conducting actual shock tube tests, the recovery methodology needs to be assessed. In view of this, other impulse forces, applied during dynamic calibration tests, are recovered to validate the calibration methodology. For strain gauge balance, impulse force of peak magnitude 80 N and 250 N along with their respective strain signals are used to train the ANFIS network. Similarly for piezo sensor based balance, impulse of peak value 120 N and 350 N are considered for training the ANFIS architecture. Inbuilt MATLAB based functions are employed to train and test the ANFIS network [Pallekonda *et al.* (2017)]. In this planned recovery process, recorded strain signals from both the balances corresponding to impulse force of 190 N is used. Thus recovered peak impulse of 190 N is shown in **Fig. 4. 9**.

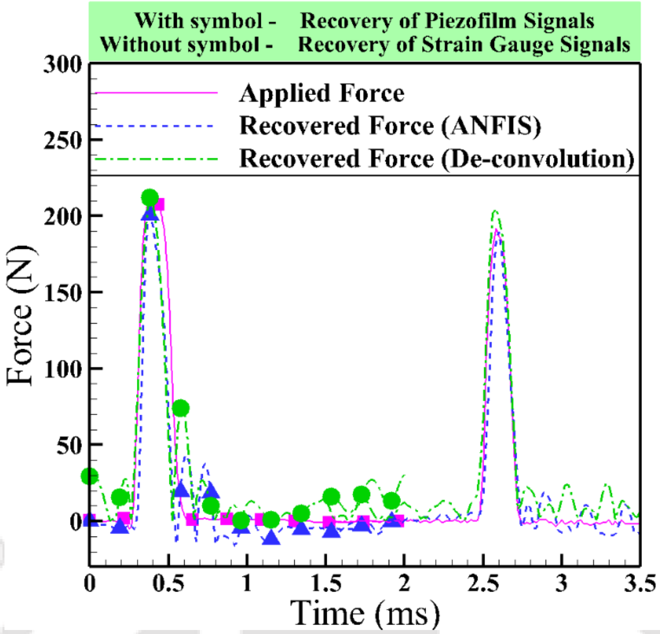

Fig. 4. 9: Recovery of a sample force time history for strain gauge and piezofilm based measurements.

It is evident from the **Fig. 4. 9** that, not only peak magnitude but also the trend of the impulse force is recovered nicely using either force recovery methodologies. Uncertainty in prediction of peak is calculated as the deviation of the peak magnitude of the recovered forces with respect to the applied force and it is noted to be ± 6.8% for strain gauge and ± 4.76% for piezofilm based measurements. Therefore, these measurement strategies can be confidently used to recover the time trace of force applied on the test model during shock tube testing. Both the strategies of inverse prediction are employed to recover or predict the force experienced by the model in the shock tube tests.

4.4.2 Shock Tube Experiments

Shock tube experiments are conducted for the same operating conditions as discussed earlier. Typical pressure signals from the driven section mounted pressure transducers are shown in **Fig. 4. 10**. It should be noted that these sensors are 500 mm apart from each other. Therefore, this known distance and the time difference between arrival of primary shock at the location of pressure transducer (noted from the first jump in pressure signals) are used to calculate the incident shock wave speed which is noted to be 2.48.

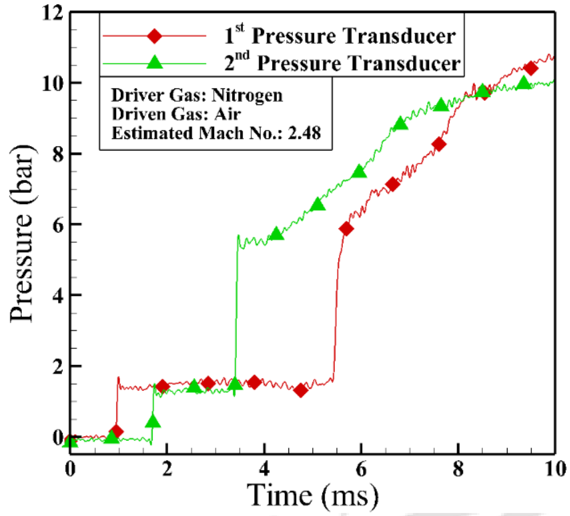

Fig. 4. 10: Typical pressure signals from pressure transducers mounted in the driven section of the shock tube.

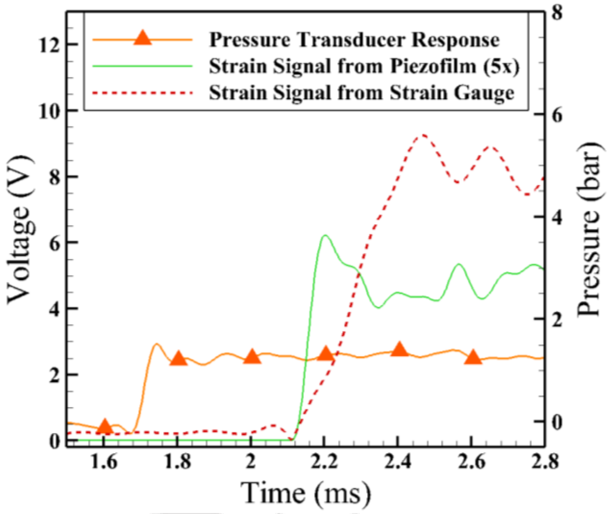

Fig. 4. 11: Strain signals from strain gauge and piezofilm during shock tube testing.

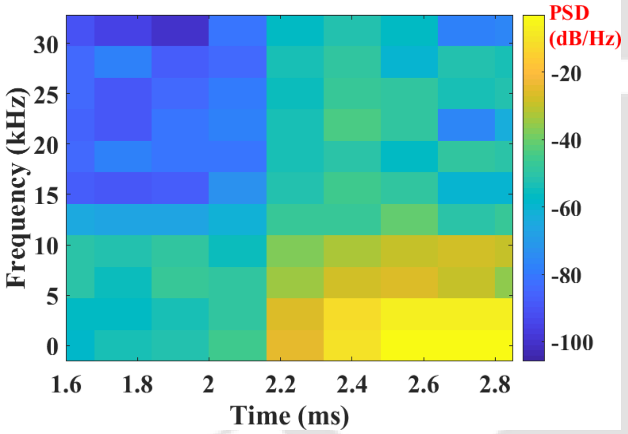

Fig. 4. 12: Spectrogram for strain response obtained from strain gauge balance.

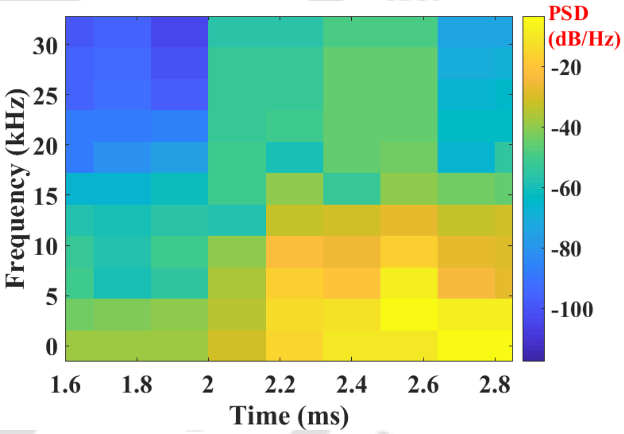

Fig. 4. 13: Spectrogram for strain response obtained from piezofilm balance.

Temporal variation of strain induced in the model, in response to the shock tube flow, captured using strain gauge and piezofilm are shown in **Fig. 4. 11**. Some regular oscillations case of strain gauge balance, where the time duration in time during the test are observed between the trough and crest,corresponding to a single fluctation , is 64 μs. Physically, this time corresponds to the time required by the incident and reflected stress wave to travel a distance from the sensor location to the end of the stress bar or vice versa .Nevertheless, these oscillations are not observed in case of piezofilm balance, as the sensor is glued to a larger area of the stress bar; hence it diminishes the chance of measurement of such fluctuations. imate of this Transient FE simulation are also performed to arrive at an est period. The time required to traverse this distance is caluclated during this simulation which is found to be 43 μs . The FE simulation provides same order of magnitude estimate for the travel of stress waves in the stress bar and thus it explains the nature of strain signal of the strain gauge shown in **Fig. 4. 11**. Further the recorded responses are also analyzed in frequency domain in terms of their energy content using spectrogram feature of MATLAB and are illustrated in **Fig. 4. 12** and **Fig. 4. 13**, respectively. It has been perceived that the piezofilm has a capability of capturing the responses at higher frequency levels as compared to strain gauges. However, both the responses seem to have same energy content as revealed by the power spectrum density in these figures. As these signals are having most of the energy below frequency of 12 kHz, so the obtained responses are filtered using Butterworth low pass filter having cut-off frequency of 12.5 kHz. As a qualitative estimate of the sensors incorporated in impulse facility, lag time of both the sensors are compared. Here, "lag time" is defined as the difference between the time at which flow exerts force on the model and actual time when the sensors start responding. For the present shock tube operating conditions, speed of the primary shock wave is 784 m/s. So, the theoretical time required for the shock wave to travel between second pressure transducer and the tip of the test model is 427.3 μs for strain gauge balance; whereas the same is 408.16 μs for piezofilm balance. Referring to **Fig. 4. 11**, strain gauge responds after 444.78 μs upon starting the response of the second pressure transducer. Hence it is expected that the flow would reach the test model in 427.3 μs from the second pressure transducer and then would apply the load on it. But the strain gauge is seen to respond after 17.48 microseconds upon application of the load. Similarly, piezofilm is seen to respond after 459.33 microseconds of first response of the second pressure sensor. Accounting these finite times, the lag time of the presently used strain gauge is 17.48 microseconds and the piezofilm is 51.17 microseconds.

This small lag makes both the sensors perfectly applicable for force measurements in short duration impulse facilities. During shock tube tests, it is expected that the primary shock upon interacting with the model allows the induced driven gas to flow over it. Later, this primary shock reflects from the tube end wall and stagnates the induced mass motion of driven gas. It leads to further rise in the pressure. Such motion of the shock and pressure variation in the vicinity of the test model are computed using earlier discussed inhouse solver and are shown in **Fig. 4. 14**. The time instances mentioned in this figure have reference zero corresponding to diaphragm rupture time**.** So, these instances are consistent with x**-**t diagram in **Fig. 4. 4.** Computed pressure on the model surface is integrated to evaluate the drag force acting on it at any time instance. Thus, predicted force time history from the CFD simulations and the experimental predictions using ANFIS as well as de-convolution technique are shown in **Fig. 4. 15a** and **Fig. 4. 15b** for strain gauge and piezofilm force balances respectively. Steady state value of the force is noted to be 334 N from CFD and it has encouraging agreement with the experimentally recovered force from strain gauge (362 N) and piezofilm (354 N) based strain signals using both recovery techniques.

Minor difference noticed in the way this steady force is reached, since in case of CFD, there is sudden rise in force but the sensors invest finite amount of time for reaching the steady value. Further, computationally obtained force time history is provided as the input to the transient structural simulation. As an outcome of this simulation, strain signal is recorded at the strain gauge location **(Fig. 4. 2)**. Comparison of the strain signal from the experiments and the structural simulation is portrayed in **Fig. 4. 17**. Here magnitude as well as trend of strain signal has encouraging agreement. However as piezofilm has ability of responding to higher frequencies, so initially it rises to a higher magnitude than strain gauge balance, but due to the same energy content for both the signals during test duration (**Fig. 4. 12**and **Fig. 4. 13**), the steady state shows a quiet good match. Thus it is evident from **Fig. 4. 15** and **Fig. 4. 16** that**,** strain measurement and force recovery using piezofilm are comparable with the established strain gauge based measurement. Therefore, present studies clearly depict that the piezofilm, which is a low cost sensor and needs lesser supportive instrumentation, can be employed for measurement of short duration forces. Thus it can comfortably replace the strain gauge or can be used as an alternative sensor for force measurement in short duration impulse facilities. Further, piezofilms can also be considered instead of strain gauges to design a multi-component force balance by employing multiple piezofilms at different orientations for response acquisition [Mee (2003), Abdel-Jawad *et al.* (2007)]. Then, these responses can be post-processed using force prediction methods described earlier for recovering the forces and moments acting on the test model.

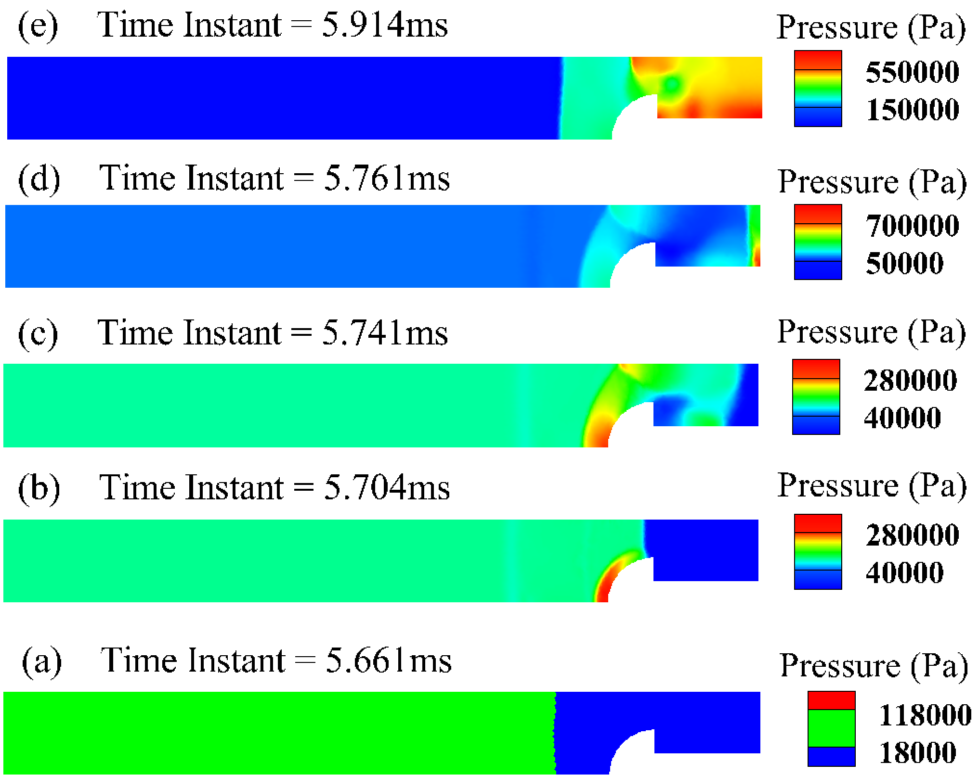

Fig. 4. 14 : Time evolution of pressure and movement of shock in the shock tube

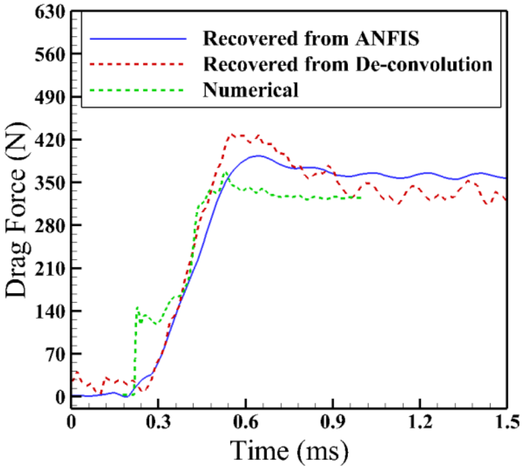

Fig. 4. 15: Transient drag force obtained through various techniques for strain gauge.

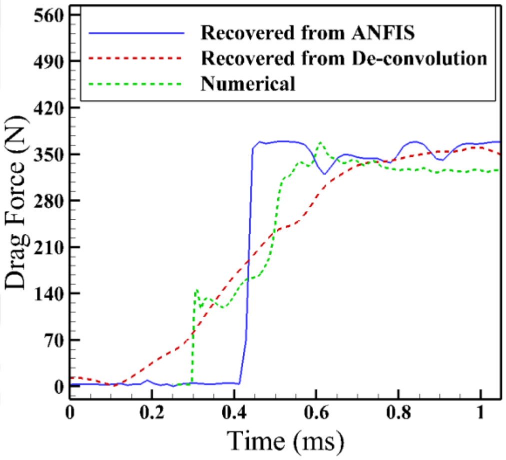

Fig. 4. 16: Transient drag force obtained through various techniques for piezofilm.

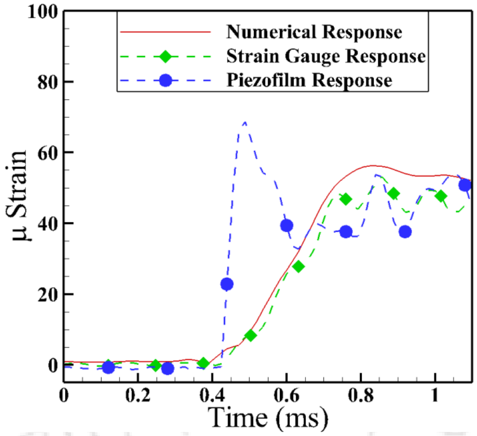

Fig. 4. 17: Comparison of strain response obtained from experiment and numerical simulation.

Summary

A sophisticated experimental set-up of IITG-ST is considered to demonstrate the applicability of piezofilm for force measurement in short duration experimental test facilities . For these tests, a hemispherical model, integrated with the stress bar, is equipped with a high gauge factor strain gauge and piezofilm for strain measurement .Initial calibration tests, using an impulse hammer, and associated force recovery using ANFIS and de-convolution, clearly showed the encouraging match between applied and recovered force signals .Then, force measurement experiments are successfully carried out in the IITG-ST and strain signals are recorded using strain gauge and piezofilm .In the interim, CFD simulations are performed using in-house solver for shock tube operating conditions to predict the time varying force and pressure on the model surface .Experimentally recovered force for both the balances is found to be in good agreement with the predictions from numerical simulation. In case of strain gauge balance the devaiation is found to be ± 8.3% whereas in case of piezofilm balance the error is estimated to be ± 5.9%. Further, strain signal is also predicted using the structural simulations and it also falls in line with the experimentally recorded strain signals in terms of peak magnitude. However some discrepancy in the trend is observed, which can be attributed to the sensor characteristics. Thus, present efforts consolidate that it is possible to use a low cost piezofilm for strain measurement and onwards for force recovery during experiments in the short duration impulse facilities. Besides, requirement of lesser instrumentation makes it a potential alternative sensor for stress wave force balance to measure aerodynamics forces and moments in an impulse facility.

CHAPTER-5

New Multi Point Calibration Methodology for Force Prediction in Shock Tunnel Testing Using Soft Computing Techniques

Overview

After the successful implementation of stress wave balance in low supersonic environment, it is further planned to assess the balance performances in hypersonic facilities through comparison with an AFB system. However, due to some technical incapability of the previously employed calibration and prediction methodology, deviations are observed for accelerometer force balance at higher angle of incidence. Therefore, this chapter focuses on way of improvising the force prediction for the AFB system. A blunt bi-conic aluminum model, integrated with a three component accelerometer force balance system, is tested in the IITB-Shock Tunnel at various angles of inclination with an intention to measure aerodynamic coefficients. Initially, Genetic algorithm (GA) is employed to deduce the orthogonal inputs and their responses from distributed point loads applied on the test model during calibration experiments. Time histories of these loads and their responses are then used to train the architecture of ANFIS. This ANFIS architecture is further employed for force prediction from the acquired acceleration responses during shock tunnel experiments. Testing of the experimental acceleration responses of 0º and 10º angle of attack experiments showed encouraging agreement for recovered time averaged aerodynamic coefficients with the accelerometer balance theory based predictions. These results clearly showed the necessity to consider multiple point loads and their acceleration responses for training the soft computing algorithm or calibration of force balance. Further, use of only one point force and its responses, for training ANFIS, is not only seen to have discrepancy in prediction but also is noted to be non-unique due to choice of the loading point. Moreover, it is recommended to choose the loading point near the center of pressure for the tested experimental conditions to incur lower discrepancy in prediction using single point loading data for ANFIS training.

5.1 Introduction

Estimates of unsteady aerodynamic force acting on any space vehicle can be deduced through testing of force balance system integrated models in ground based facilities. However, as seen from literature, due to simple acquisition procedure, accelerometer balances are preferred, but necessity of free flying condition during test duration makes it a bit sophisticated. Various researchers have opted steel ring and rubber bush based method to achieve the free flight motion. In this regard, Trivedi and Menezes (2012) have attempted to incorporate the effect of rubber bushing for estimation of force and moment coefficients; however, no significant improvement is reported. Thus, it is evident that the accelerometer based force measurement demands improvisation for better prediction. Therefore, it is highly desirable to enhance the prediction capability of the measurement technique rather than focusing on the acquisition methodology. In line with this, as an alternative, the force recovery can also be achieved from the measurements using de-convolution algorithm which involves complex mathematical modelling or by implementing some artificial intelligence technique.

But, prediction of forces, using the aforesaid methods, requires dynamic calibration to be executed for calculating the system response function, before the actual experiments. Kulkarni and Reddy (2010) first time considered dynamic calibration of the accelerometer force balance by accounting suggestions of Abdel-Jawad *et al.* (2007). But it was applicable for the measurement of drag only. It is possible to integrate acceleration measurement and the calibration methodology used for stress wave force balance [Abdel-Jawad *et al.* (2007)], but this integration becomes numerically intensive. Sahoo and Reddy (2010) reviewed various methods of static and dynamic calibration for calculating the transfer function; however, these methods seem to have a wide confidence range for axial force prediction as compared to normal force. Ramesh *et al*. (2018) proposed a new approach with use of soft computing method, ANFIS, to predict the forces and moment from the acquired acceleration responses of a generic hypersonic test model. This proposition is better than the earlier suggested improvisations but with certain limitations. The major drawback of this suggestion is that the researchers have considered impulse forces applied at a point during calibration for the ANFIS training, which is equivalent to obtain the system response function of the dynamical system. Such calibration or training strategy does not account for complete dynamics of the system; thus obtained system response function would not be unique due to its dependence on choice of point to be considered for calibration. Therefore, it would inherently introduce errors in prediction of actual aerodynamic loading which is mainly due to surface forces while the calibration of the force balance banks on a point force based response. Besides, though multi-point loading is desirable for calibration, literature reported procedure [Abdel-Jawad *et al.* (2007)] needs rigorous computations and also strategic choice of loading points so as to arrive at the desirable orthogonal inputs and corresponding responses for evaluating system response function or training of any soft computing technique.

In view of the noted limitations, a new multi-point calibration methodology is proposed as an attempt to improve the reliability of the accelerometer based force measurement technique. This proposal is also expected to mathematically simplify the training process or method of obtaining system response function. In this method, initially forces are applied at various locations on the blunt cone model and corresponding acceleration responses are recorded during calibration. Further, in view of obtaining responses due to orthogonal forces, these force time histories and corresponding acceleration signals are clubbed together with incorporation of associated weightage factor. These weights for the calibration location is estimated through use of optimization technique and afterwards the resulted responses are fed to ANFIS for training purpose. Thus, obtained training parameters and the same ANFIS architecture are employed to recover the forces and moments acting upon the blunt cone model during actual shock tunnel tests. A single point calibration methodology is also considered to assess the effect of location on calibration and to demonstrate the advantages of multipoint calibration proposal. Details of the calibration process, its integration with optimization process, shock tunnel tests and actual force recovery are discussed in the subsequent sections.

5.2 Model and Force Balance

A blunt bi-conic re-entry configuration has been considered for investigating the effect of calibration methodology on force prediction. This model consists of a front hemispherical part having radius of 16.76 mm and two aft conical portions having cone angle 44° and 10.8° respectively as shown in **Fig. 5.1**. This test model is fabricated from aluminum. It is equipped with internal three-component accelerometer force balance to capture accelerations in different directions. The force balance is comprised of steel rings and rubber bushes [Sahoo *et al.* (2007), Kulkarni *et al.* (2010)] in order to achieve free flying motion during the experiments. Two Rubber bushes of thickness 6 mm, having inner diameter 12 mm and outer diameter 32 mm are glued to the steel rings having inner diameter 32 mm and outer diameter 46 mm. Further, the steel ring and rubber assembly is screwed to the model. Also, the core part of the rubber bushes is attached to a stainless steel sting which would be fastened in the test section of the shock tunnel. This balance design along with the major dimensions is illustrated in **Fig. 5. 2** For monitoring the accelerations during calibration or tunnel experiments, one axial accelerometer and two normal accelerometers viz. front lift (One before C.G) and aft lift (after C.G) are equipped inside the balance assembly. Here axial accelerometer is mounted to sense the axial acceleration (A_{axial}). Acceleration measured by the front lift accelerometer is termed here as front normal acceleration ($A_{front\ Normal}$) while the measurement of later is referred as aft normal acceleration ($A_{aft\ Normal}$). Uniaxial accelerometers having sensitivity as given in

Table 5. 1 have been used for the current study.

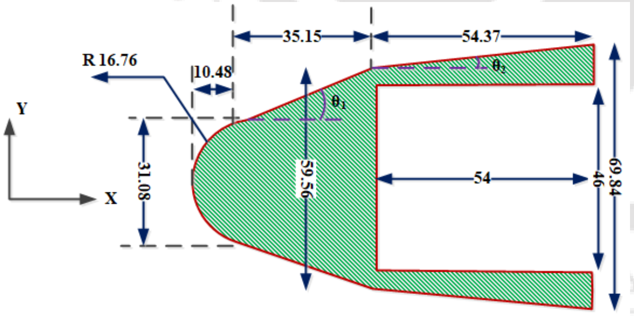

(All Dimensions are in "mm")

Fig. 5. 1: Schematic of the model.

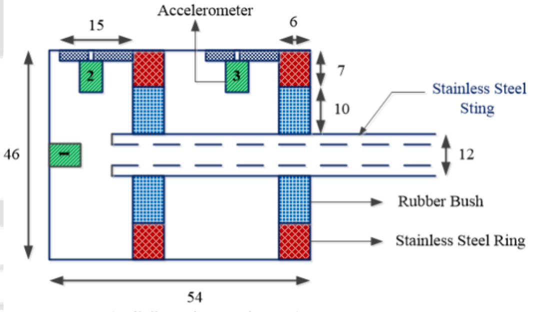

("All dimensions are in mm")

Fig. 5. 2: Major dimensions of the balance.

Table 5. 1: Specification of the accelerometers.

Location	Sensitivity (mV/(m/s^2))	Frequency Range (kHz)
1	10.15	10
2	9.97	10
3	10.05	10

5.3. Calibration and Prediction Methodology

5.3.1 Calibration Experiments

Prior to the actual experiments in the shock tunnel, calibration of the test model needs to be carried out for training the ANFIS architecture from known force and acceleration signals [Mee (2003)]. As mentioned earlier, such training of any soft computing technique is equivalent to finding the system response function of the dynamical system. Further, multi point calibration strategy is adopted herein since the accuracy of force prediction can be improved if multiple points are considered for application of force during calibration. Again, in case of a multi component calibration methodology, deriving the responses corresponding to pure forces and moments is a bit sophisticated task for the model where orthogonal forces can't be applied. So, there is requirement of a simple and efficient prediction algorithm for accurate force recovery at any AOA. During such calibration, model integrated with the force balance assembly, is fixed in a bench vice. An impulse hammer is used to apply a point load at various locations on the model as shown in **Fig. 5. 3**. It is evident from the figure that, choice of all the locations lies in one plane passing through the axis of the test model. Such choice is helpful in obtaining three aerodynamic coefficients for three degree of freedom systems. Care has been taken to apply local normal loads at all the locations. As an outcome, forces and corresponding accelerations are recorded in the acquisition system.

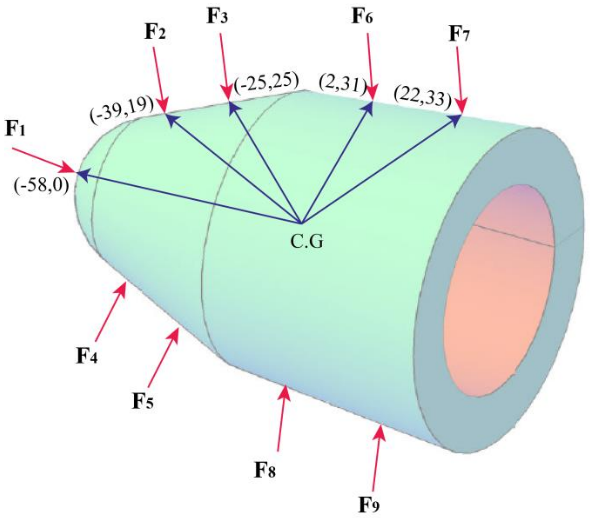

Fig. 5. 3: Calibration location on the model along with their coordinates.

5.3.2 Optimization for Orthogonal Inputs of Calibration

Calibration experiments necessarily give the acceleration response to the locally normal impulse forces. But, it is always desirable to note the responses for orthogonal inputs like axial force and normal force. Hence this section deals initially with evaluating orthogonal inputs, in the frame of reference fixed with the model, from the applied local normal forces and then to deduce the corresponding responses for those orthogonal inputs. Thus, it becomes a milestone of the new approach for force balance calibration through the usage of a well-established optimization algorithm namely Genetic Algorithm (GA). This method is essentially implemented to calculate weights corresponding to different calibration locations (**Fig. 5. 3**) with an intention to obtain pure axial and normal forces from distributed point forces. **Equation 5.1** shows functional relation between pure axial force, pure normal force and induced moment in terms of co-ordinates of the force application locations during the calibration experiments (**Fig. 5. 3**) and cone angles of the model.

$$\left.\begin{aligned}
F_x &= F_1 + \sum_{i=2}^{i=5} \alpha_i F_i \sin\theta_1 + \sum_{i=6}^{i=9} \alpha_i F_i \sin\theta_2 \\
F_y &= \sum_{i=2}^{i=5} \alpha_i F_i \cos\theta_1 + \sum_{i=6}^{i=9} \alpha_i F_i \cos\theta_2 \\
M_z &= \sum_{i=2}^{i=5} \alpha_i F_i (x_i \cos\theta_1 + y_i \sin\theta_1) + \sum_{i=6}^{i=9} \alpha_i F_i (x_i \cos\theta_2 + y_i \sin\theta_2)
\end{aligned}\right\} \quad \textbf{Eq. (5.1)}$$

Here, angles and directions are consistent with those given in **Fig. 5. 1,** while forces of different subscripts are given in **Fig. 5. 3.** Further, α_i is the weight of the force F_i which is applied in local normal direction. It is obvious from the above stated equation that the resultant normal force is zero if the force is applied at location 1, as it is a purely axial force. Thereafter, GA is employed for calculation of the weights, corresponding to calibration locations, which eventually helps to estimate the pure axial force and pure normal force. Consequently, the objective function for the GA is set to maximize the axial force (Fx) while accounting the constraint of making the normal force (Fy) and induced moment (Mz) as zero. In a similar manner, GA is again used to evaluate the weights for maximizing the normal force (Fy) along with the constraint of restricting the magnitude of axial force (Fx) and induced moment (Mz) to zero. Subsequently, GA can also be implemented to maximize the value of induced moment (Mz), however it is not desirable, as estimate of the pure axial force and normal force can in turn predict the coefficient of drag, lift and pitching moment with the help of conventional accelerometer force balance theory. Optimization tool box available in MATLAB is implemented for achieving the abovementioned objective. For the current investigations, GA having population size of 20, crossover fraction as 0.8, selection function as stochastic uniform, crossover function as scattered and mutation function with constraint dependent is used. Thus, calculated weights corresponding to different calibration are provided in **Table 5. 2:** Optimized weights for various calibration locations.. As the entire system can be assumed to have linear characteristics during the experimental time scale [Mee (2003)], the force as well as acceleration responses can be combined to evaluate the effective inputs and corresponding responses. In view of this, pure axial and normal forces as well as their associated acceleration responses are estimated by superposing all the input and output responses obtained from calibration test at each location along with their corresponding weights. These forces and responses now are fed to train the prediction technique, ANFIS, to monitor its performance. During the course of training the system, network parameters are varied to reach an optimized structure of the ANFIS network.

Table 5. 2: Optimized weights for various calibration locations.

occasion / **Location**	**Weights**								
	α_1	α_2	α_3	α_4	α_5	α_6	α_7	α_8	α_9
Pure Axial	1	1	1	1	1	1	1	1	1
Pure Normal	-	-0.298	-1	0.298	1	-1	-1	1	1

5.3.3 Force Recovery Algorithm

Present investigation emphasizes implementation of an extensively used soft computing technique ANFIS [Nayak *et al.* (2014)] for prediction of temporal force and moment histories. Details of the architecture and basic philosophy of force prediction has been explained in the previous chapter. As already explained, various parameters of the network can be chosen suitably according to the data to be trained. Now considering the varying parameters as input MF, output MF and training strategy, a parametric study is done using the data sets obtained from the multi-point calibration methodology. This helps in assessing the parameters which will be efficient for accurate prediction of coefficient of forces and moments, using the acquired experimental responses. The entire flowchart of the adopted calibration procedure has been shown in **Fig. 5. 4**. Temporal responses obtained along the orthogonal directions are fed as input to the network whereas the corresponding forces as the output. Various parameters viz. input MF, output MF and training strategy have been varied so as to optimize an ANFIS structure. Accuracy of the prediction of the training data is monitored to arrive at the optimized parameters. So, for the current analysis sigmoid (psig) type of input MF, constant type of output MF and hybrid training strategy with 500 epochs i.e. iterations have been selected.

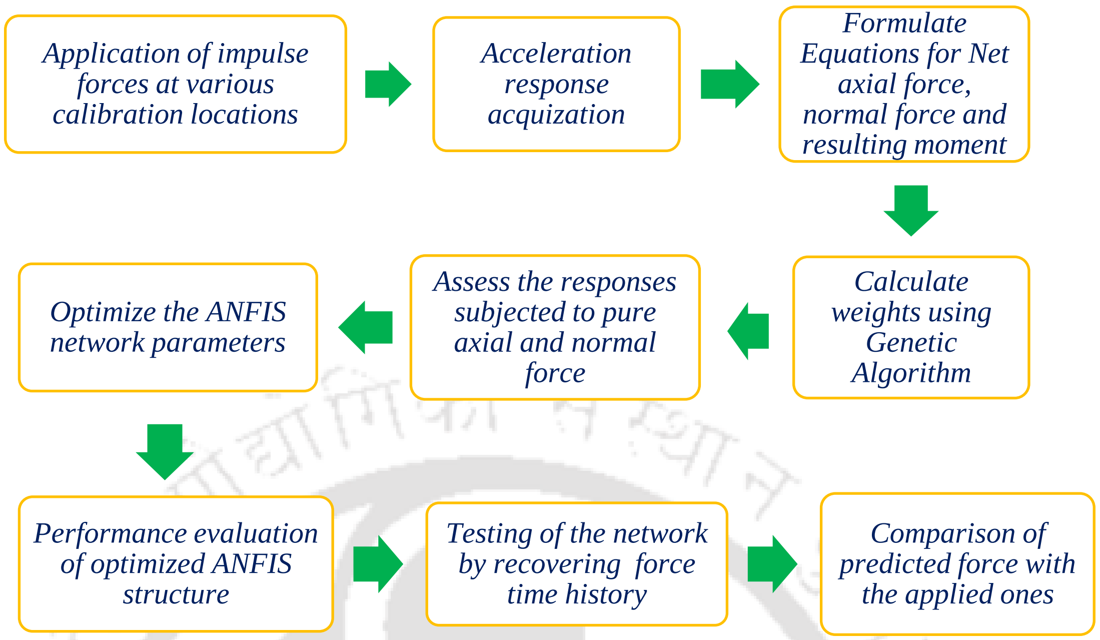

Fig. 5. 4: Flowchart of the multi-point calibration methodology.

5.4 Experimental Facility

Experimental investigations are carried out in IITB shock tunnel [Menezes *et al.* (2011)] using three component accelerometer force balance system. The schematic of the experimental facility and the free stream conditions have been presented in **Chapter-2**. For all set of experiments, nitrogen is used as the driver gas and air as test gas. The pressure inside the driven section is kept as 1 bar, while the dump tank is evacuated to pressure 10^{-3} mbar. As already mentioned, a pitot sensor is mounted in the test section for accurate estimation of the test conditions and duration. Steady portion of the pitot pressure signal (P_{pitot}) indicates the available test time and it lies around 500-700 μs for the present experiments.

5.5 Results & Discussion

5.5.1 Validation of Calibration Process

As explained earlier, initially, three acceleration signals are acquired for each impulsive loading at each location shown in **Fig. 5. 3**. Further, these signals are processed to calculate the effective responses of pure axial and pure normal loads by employing the weights determined by genetic algorithm. Before using these signals, they are filtered using low-pass Butterworth filter at a frequency of 10 kHz. Thereafter, the orthogonal inputs (axial and normal forces) and corresponding acceleration responses are fed to the ANFIS algorithm of MATLAB for training purpose. Thus, the inputs to the architecture are chosen to be three acceleration time histories viz. axial, front lift and aft lift; whereas the outputs are the corresponding time histories of axial and normal forces. Further, accuracy of a recovered impulse force from any of the calibration experiments, applied at a point, is checked without altering parameters of the ANFIS structure. The comparative assessment of these predicted axial and normal forces with the applied forces as recorded during calibration is presented in **Fig. 5.5.** The recovered forces closely match with the actual ones in terms of both magnitude and trend which is apparent from this figure. It has been noticed that there is a nominal deviation of ± 2.3% for peak magnitude of axial force and ± 1.8% for peak magnitude of the normal force. In light of encouraging prediction of the calibration forces, ANFIS settings of same parameter is extended further to predict the experimental forces obtained during shock tunnel tests.

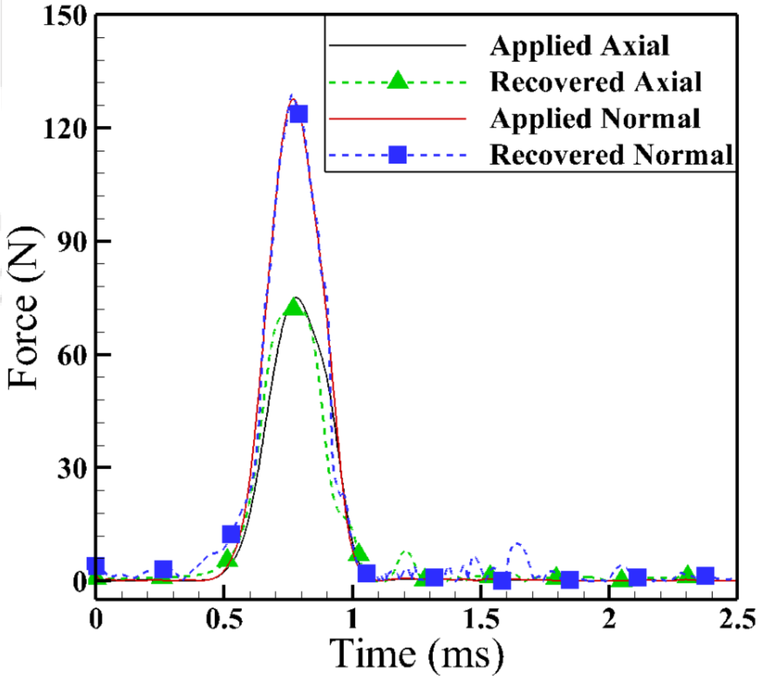

Fig. 5. 5: Applied and recovered force comparison for calibration.

5.5.2 Force Recovery of Shock Tunnel Experiments

Experiments are conducted in the hypersonic environment generated in IITB-shock tunnel for free stream conditions given in **Chapter 2**. Responses are recorded for model mounted at AOA 0º and 10º in the test section. The accelerometer signals acquired for 0º and 10º AOA are plotted in the **Fig. 5. 6**. In this figure, these acceleration responses are shown along with the pitot signal so as to get a proper estimate of the steady state acceleration magnitude from these signals. The horizontal dotted lines in this figure represent the possible steady state duration of the acceleration response corresponding to shock tunnel experiment. These steady state acceleration magnitudes and the conventional accelerometer force balance theory [Truitt (1959)] are used to evaluate the steady state magnitudes of axial and normal forces. Further, acquired transient acceleration signals are fed as the test data to the ANFIS algorithm with same premise and consequent parameters considered in previous section. As stated earlier, one of the objectives of the present studies is to assess the single and multi-point recovery techniques and to analyze the dependence of recovered force on the choice of calibration point. In view of this, training data of either of the calibration methodologies are used. Training data for the ANFIS architecture, in multi-point calibration case, are the forces along the orthogonal directions and their responses obtained during multi-point calibration methodology. However, for the single-point calibration case, the recorded responses and corresponding forces applied at ‘Point-3’ and ‘Point-7’ are provided separately as training data while predicting the aerodynamic coefficients for 10º AOA experiments. But, in order to recover the drag force for 0º AOA, using single point calibration technique, loading at Point-1 is only considered.

The recovered axial force for 0º AOA through ANFIS architecture using two training data sets is presented in the **Fig. 5. 7(a)**. In this figure, the steady axial force (F_{Axial}), obtained from conventional accelerometer force balance theory, has been indicated with horizontal dotted lines and its magnitude is 7 N. Steady state value of the recovered force using multi point calibration data set is estimated to be 6.99 N whereas the usage of single point data set results in a magnitude of 7.16 N. It can also be perceived here that the ANFIS prediction is more convincing as it provides both time averaged aerodynamic coefficients and temporal variation of orthogonal forces as deliverables rather than only the steady magnitude of the forces as in case of force balance theory. But, it is evident that either (single and multi-point) recovery algorithms are successful in predicting the axial force, hence the coefficient of drag (**Table 5. 3**) is seen to be in the acceptable bound. It should be noted that the weights for 0° AOA case are same for all locations (**Table 5.2**). Hence simple addition, in axial direction, would lead to pure axial force due to balance of force components in normal direction and their associated induced moments. Therefore, there is no explicit requirement or advantage of GA based computations for weight calculations in the phase of axial force recovery.

For 10° AOA case as well, there is no need to consider weights to obtain the pure axial force since weights for all the locations are same (**Table 5.2**). But weights have to be assigned for evaluation of pure normal force since the induced moments of forces do not cancel each other if at all the components in axial direction get balanced by reversing the direction of applied forces from leeward side. This fact is explicitly demonstrated in **Fig. 5.7b** which compares time history of recovered axial and normal forces with and without weights for 10° AOA case. Match for axial force recovery is inline with the unique value of weights for axial loads. But there is significant discrimination for normal force recovery due to unaccounted induced moments. Hence it is highly desirable to evaluate weights using GA and incorporate the same during ANFIS based training or recovery.

Similarly, the recovered axial and normal force for 10^0 AOA case along with the theoretically estimated steady state values of the forces are plotted in **Fig. 5. 7c** and **Fig. 5. 7d**. The calculated steady state values of the axial (F_{Axial}) and normal force (F_{Normal}) from the conventional force balance theory are 7.2 N and 2.4 N, respectively. Importantly, it is evident from the figure that the recovered axial and normal forces using multi point calibration method closely matches with the estimates obtained using balance theory. The time averaged axial force and normal force over the test duration from this recovery method is 7.25 N and 2.33 N, respectively. Therefore, the agreement of the aerodynamics coefficients (**Table 5. 3**) with the accelerometer balance theory is encouraging. Further, axial force shows minor deviations while the normal force suffers major under-prediction when ANFIS is trained using data for point 3. In this case, numerical value of the prediction is found to be 6.7 N for axial force and 1.78 N for the normal force. Significant discrepancy is observed in case of both axial and normal force predictions for ANFIS with training data set of ‘point-7’. Time averaged prediction is noted to be 1.35 N for axial force and 0.71 N for normal force. Deviation in the normal force in turn affects the value of lift and pitching moment coefficient for both the single point recovery procedures as depicted from **Table 5. 3**.

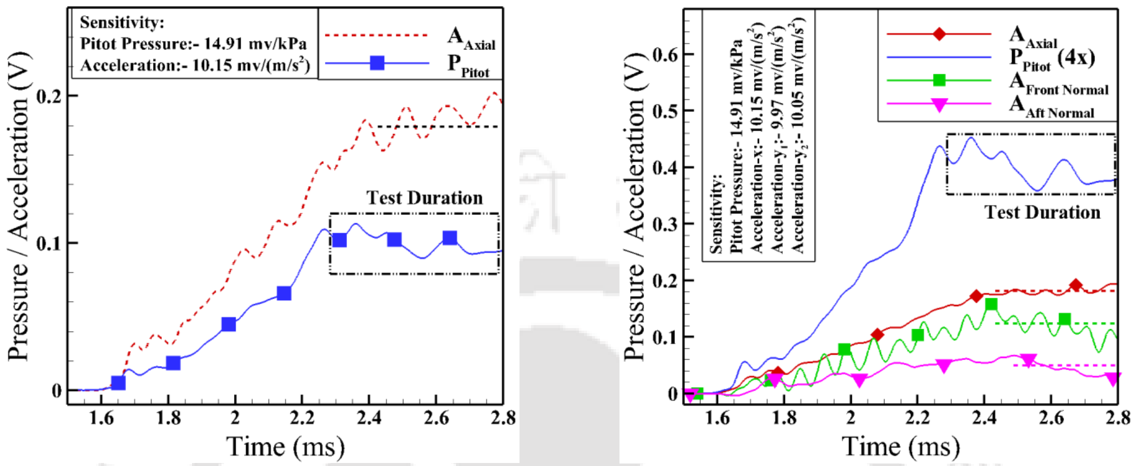

(a) **(b)**

Fig. 5. 6: Acceleration signals at (a) 0º AOA (b) 10º AOA.

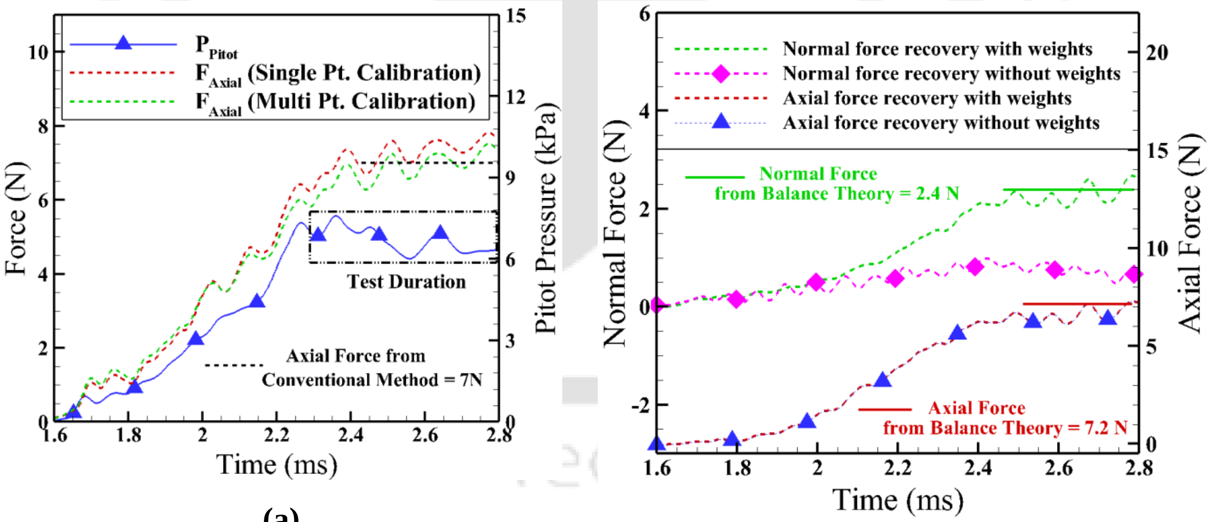

(a) **(b)**

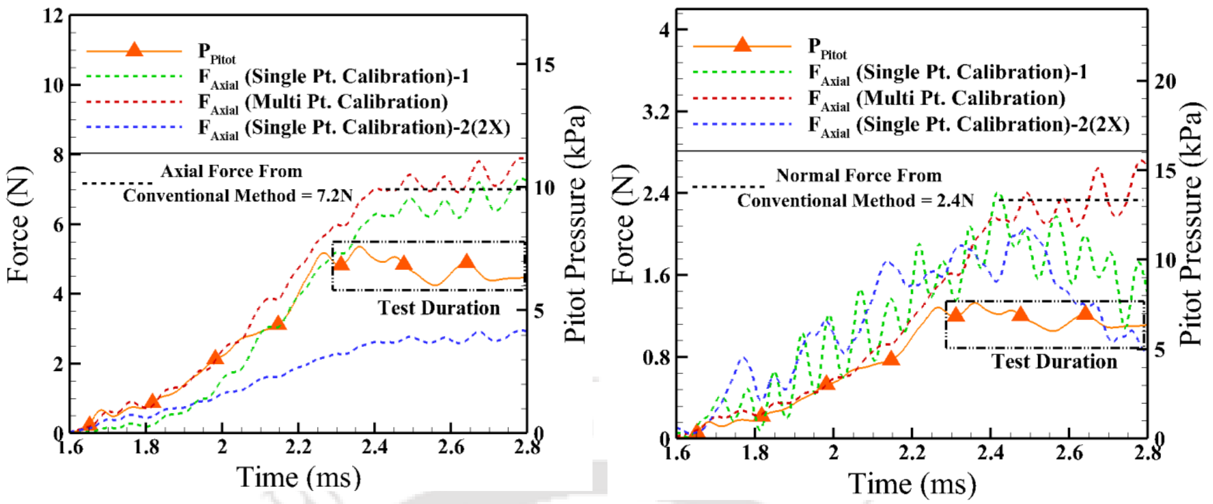

(c)

(d)

Fig. 5. 7: Recovery of (a) axial force at 0º AOA; (b) forces to demonstrate the effect of weight assignment (c & d) axial force and normal force at 10º AOA.

Table 5. 3: Recovered force and moment coefficients at different AOA.

AOA	**Technique**	**Coefficient of drag (C_d)**	**Coefficient of lift (C_l)**	**Coefficient of moment (C_m)**
0º	Force balance theory	0.503	-	-
	Single Point	0.515	-	-
	Multi Point	0.502	-	-
10º	Force balance theory	0.539	0.0793	0.124
	Single Point (Near C.P)	0.496	0.0423	0.0927
	Single Point (Away from C.P)	0.104	0.0334	0.037
	Multi Point	0.542	0.0741	0.121

This table clearly depicts that the percentage deviation is higher if ANFIS training employs datasets corresponding to point-7 than that of point-3. Major reason for this discrimination is the distance of loading point chosen for ANFIS training from the actual center of pressure location for the AOA test case. In case of 0º AOA experiments, recovery has been achieved from the single point force training only but that choice of point is nose of the blunt cone model. Further, nose of blunt cone or the stagnation point is the center of pressure for 0º AOA experiments; hence well match among single and multi-point force recovery techniques has been registered. But, as per the pressure distribution over the model for 10º AOA case, the axial location of center of pressure is at 8.04 mm from the nose of the model. However, it is known that ‘point-3’ and ‘point-7’ are located axially at 36mm and 81mm from the nose. Therefore, point-3 being closer to the center of pressure than point-7; recovery by accounting point-3 is comparatively better than that by accounting point-7. This demonstration clearly suggests that further improvement in recovery of aerodynamic coefficients would be possible if ANFIS architecture is trained with force applied at a point closer to the center of pressure corresponding to 10º AOA case. Thus, present studies clearly reveal that training of ANFIS using single point force and its responses is not advisable due to two reasons. Primary reason can be attributed to the fact that, accuracy depends upon distance between selected point and center of pressure for the experimental testing conditions. Secondly, the training becomes non-unique due to choice of point to be considered. Therefore, multipoint calibration or training technique and the presently adopted recovery procedure are seen to be effective in predicting time histories of the forces and predicting the steady state values of aerodynamic coefficients.

Summary

Shock tunnel experiments are successfully carried out on a blunt bi-conic model equipped with an internal three component accelerometer force balance system. In the phase of recovery of the aerodynamic coefficients for the shock tunnel tests at different angles of attack, a new methodology is devised for training the soft computing technique, ANFIS. This method accounts discretely applied multiple single point loads and corresponding acceleration responses. Genetic algorithm is used to obtain the weights of each point load applied during calibration, to arrive at the pure axial and pure normal components of an otherwise applied simultaneous multi-point load. Recovery of aerodynamic coefficients for the shock tunnel experiments is noticed to have encouraging match with the predictions of same from accelerometer balance theory if orthogonal inputs and their temporal acceleration responses are used to train the ANFIS architecture. This, multi-point force recovery method which integrates GA and ANFIS is found to be mathematically simpler than the methods available in the open literature. Further, consideration of only one point force and its response for ANFIS training is marked to be disadvantageous due to dependence on choice of point. Less deviation has been noticed in prediction of aerodynamic coefficients if the point of choice is nearer to the center of pressure. Present studies recommend the use of multi-point calibration or training because of higher accuracy irrespective of the locations of the loading points.

CHAPTER-6

Piezofilm, An Alternative Sensor for Force Measurement in Hypersonic Test Facilities

Overview

After successful development of multi point calibration method for implementation in accelerometer balance system, it is further planned to have a comparative assessment of piezofilm balance in regard to AFB system through experimentation in shock tunnel facility. A blunt double cone model, equipped with a three component piezofilm based force balance system, is tested in the IITB-Shock Tunnel at 0^0 and 10^0 angles of inclination. Same calibration methodology, implemented in the earlier chapter that involves GA and ANFIS, has also been used herein for training purpose. In order to arrive at the time varying forces, this balance is calibrated using impulse hammer tests at single or multiple points. Optimization technique is used to determine the weights of calibration loads to obtain the pure axial and normal forces and its associated responses. These weights, impulse hammer test signals and balance responses are considered for training the ANFIS network. Encouraging agreement has also been noted for the ANFIS based recovery of forces from piezofilm balance with AFB system as well as accelerometer force balance theory, in terms of both trend and steady state magnitude. Thus, present studies emphasize the strategy of implementation of previously evolved multi point calibration methodology to piezofilm balance for force measurement.

6.1 Introduction

Multi component stress wave force balance has been less explored due to complexity in developing prediction algorithms for deducing the forces and moments coefficients. However, as already seen, ANFIS can be considered as a better alternative. Also, to enhance the accuracy of the multi component balances, multi point calibration methodology is also developed in the previous chapter. In line with this, it has been planned to extend the multi-point calibration methodology towards force recovery in conjunction with implementation of three component piezofilm balance. Further, it is essential to compare the predictions from the piezofilm based SWFB with the established accelerometer force balance. Such verification would not only provide inter-balance comparison but also it is highly desirable to compare two measurement philosophies. Such efforts are reported in the literature but for single component or only drag measurement [Smith *et al.* (2018)]. Hence one of the objectives of the present studies is to compare the experimentally recorded output responses and then the final recovery using accelerometer and piezofilm based force balances. In view of this, details of the chosen blunt cone model, force balances, test facility and associated results are presented in the following sections.

6.2 Test Model and Force Balances

Present choice of test model is the same bi-conic blunt re-entry configuration, which has been earlierly tested in hypersonic shock tunnel. It has provision to equip internal force balance, which is in this case corresponds to piezofilm based stress wave force balance, as shown in **Fig. 6.1**. Three piezofilms are mounted to acquire the strain response (**Fig. 6. 1**). Two of those sensors are placed on two vertical bars while the third one is positioned on the horizontal bar. The piezofilm mounted on horizontal bar is termed here as axial strain sensor (S_{Axial}) while the one placed on vertical bar before C.G. is called as front lift strain sensor (S_{Front}) and the other on vertical stress bar after C.G. is aft strain sensor (S_{Aft}). This horizontal bar would be fastened at the test section mounting station for force measurement experiments. Current study makes usage of a PVDF (Polyvinylidene difluoride) type piezofilm sensor (Make: Measurement Specialties, LDT0-028K/L) having capacitance 0.5 nF. This piezofilm is actually has been tested for drag force measurement in shock tube, as elaborated in Chapter-4. The output of the sensor can be directly connected through the charge amplifier to the acquisition system. A charge amplifier having sensitivity 0.01 to 1000 mV/pC (in charge mode) is connected for signal conditioning. In the present experiments, a feedback capacitance of 10 nF, lower cut-off frequency of 0.1 Hz and higher cutoff frequency of 100 kHz are selected as the operational parameters for the amplifier. The response recorded, during the experiments, can be further related to the strain produced in the test model using **Eqn. 6.1** [Sirohi and Chopra (2000)]. Upon replacing all the parameters with their corresponding values of the PVDF sensor, the sensitivity factor is estimated to be around 12 mV/µ-strain. The balance design along with the major dimensions are illustrated in Fig. 6. 1.

$$\varepsilon = \frac{V_O}{K_P S_q^{*} A_F}$$

$$\text{Where} \qquad (6.1)$$

$$K_P = 1 - \nu \frac{d_{32}}{d_{31}} \qquad S_q^{*} = \frac{d_{31} Y_c l_c b_c}{C_F}$$

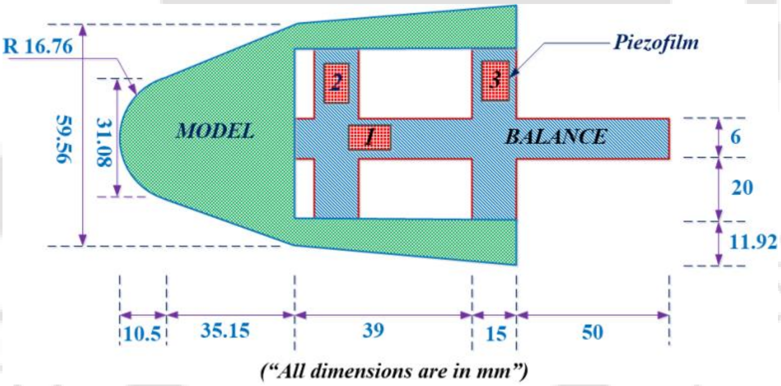

Fig. 6. 1: Schematic of the model integrated with piezofilm based stress wave force balance.

6.3. Force Balance Calibration Methodology

6.3.1 Calibration Experiments

Calibration experiments are highly essential before actual shock tunnel experiments. Objective of these experiments is to obtain the impulse response function of the test model force balance assembly or to establish the correlation between known impulse force and corresponding responses. As per the literature, convolution-deconvolution algorithms are preferred at this stage [Smith *et al.* (2001)]. But soft computing techniques like ANFIS are also used for the same objective but for acceleration responses only [Pallekonda *et al.* (2018)]. Hence, one of the major goals of present studies is to assess the applicability of soft computing technique, ANFIS, for training and inverse force prediction using strain response of the piezofilm. As in actual shock tunnel experiments, model experiences surface loading in the test duration; therefore, an attempt is made herein to improve calibration technique by accounting multiple impulses applied at different point on the test model as well as their respective strain responses. Therefore, this proposition is expected to be useful for any angle of attack testing of the model or for any test configuration. For these calibration experiments, the set up adopted is same as explained in earlier chapter for the case accelerometer balance. Schematic of this configuration and different force application locations are shown in **Fig. 6. 2**. All the impulse forces are applied in the local normal direction. Forces and corresponding strain responses are recorded in the acquisition system.

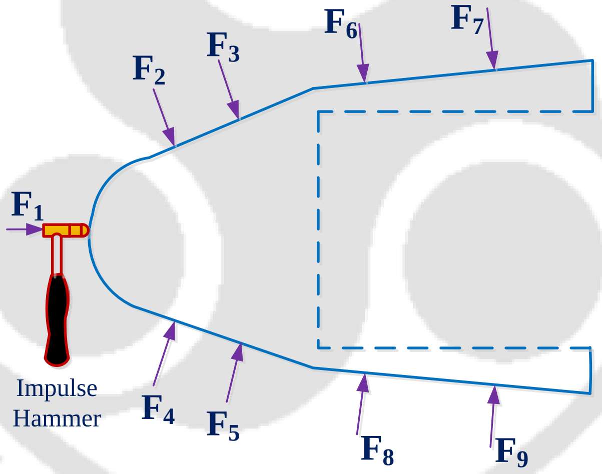

Fig. 6. 2: Locations of impulse hammer hits for dynamic calibration tests.

6.3.2 Force Prediction Methodology

Actual force measurement experiments in the shock tunnel should provide information about the axial and normal forces. Therefore, calibration tests are also expected to correlate between the axial and normal forces with their respective responses. But, the impulse forces applied as directed by **Fig. 6. 2** are in local normal direction. Therefore, it is essential to constitute overall axial and normal forces from applied impulses. As already explained in the earlier chapter, a new multi-point calibration methodology has been evolved, as a part of the improvement in force prediction. The same procedure has also been adopted for the case of piezofilm based force balance for estimation of the forces and its corresponding responses in mutually orthogonal directions, using the applied impulse forces and the recorded responses at the discrete locations as presented in **Fig. 6. 2.** Due to the nature of application of forces as illustrated in **Fig. 6. 2**, application of simple statics through vectorial superposition of all the loads will result in net pure axial load and zero resultant for normal load and moment about C.G. This analysis is found to be conclusive, as the optimization technique resulted in equal weights for different calibration location. Further, calculation of weights, intended for obtaining pure normal force, is attempted where central force, applied at Point '1', has not been taken into account, thereby assigning zero weightage to that location. Weights obtained in the previous chapter are used to achieve zero axial force and resultant moment thereby resulting pure normal loading condition. With usage of these weights, pure normal force and its corresponding responses are evaluated. Afterwards these orthogonal forces and their responses become the inputs for ANFIS architecture to evaluate the correlation among them.

Soft computing technique, ANFIS that has been used by many researchers for different applications has also been extensively incorporated for force prediction purpose. Based on present set of calibration experiments and earlier reported findings sigmoid (psig) type of input MF, constant type of output MF and hybrid training strategy with 500 epochs i.e. iterations have been selected as the optimum ANFIS architecture.

6.4 Experimental Facility

Present experimental studies are conducted in IITB shock tunnel [Trivedi and Menezes (2012)] using three component piezofilm based stress wave force balance. The schematic of this test facility is presented in **Chapter 2**. For the sake of comparative assessment with the accelerometer balance system, the model and the associated balance is mounted at the same location inside the test section. All the experiments have been carried out by considering nitrogen as driver gas and air as driven gas. Free stream flow conditions obtained in the test section is identical with the earlier values as mentioned in **Chapter 2**. Also repeated experiments have been conducted for ensuring the magnitude and trend of the acquired responses.

6.5 Results & Discussion

6.5.1 Calibration Methodology Validation

As explained earlier, initially, the strain signals at three locations are acquired for an impulsive loading at each location shown in **Fig. 6. 2**. These signals are then filtered using low-pass Butterworth filter at a frequency of 10 kHz. Signals of forces and their responses, recorded during calibration tests, are then used to estimate the effective axial and normal forces and their responses using the weights determined through GA. These orthogonal forces and corresponding strain responses are provided as input to the ANFIS algorithm of MATLAB for training. Here, input to the ANFIS network are the time histories of orthogonal forces and corresponding three strain signals. This training process is verified by recovering an impulsive force, applied at a point in one of the calibration tests. Hence, three responses of the applied impulse force are the inputs to the testing process of ANFIS. Recovery of such force from piezofilm based force balance and its comparison with the actual applied impulse are shown in **Fig. 6. 3.** Recovered forces have encouraging match with the actual ones in terms of both magnitude and trend. As an outcome of calibration experiments, it has been noted that the uncertainties in prediction of peak axial and normal forces are 1.56 % and 1.13 % for strain based measurements.

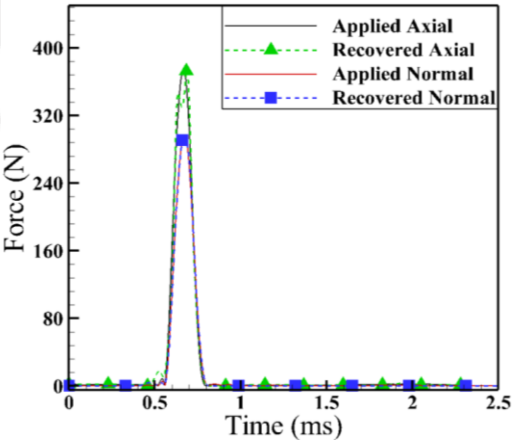

Fig. 6. 3: Comparison of applied and recovered force time histories of a typical calibration experiment using piezofilm force balance.

6.5.2 Prediction of Force and Moment Coefficients for Shock Tunnel Tests

Present set of objectives are achieved by conducting experiments for free stream conditions generated in IITB-shock tunnel. Strain signals are recorded, during these experiments for two AOA viz.0º and 10º. These strain responses and accelerometer responses are marked in **Fig. 6. 4** and **Fig. 6. 5**. Pitot pressure signal is also shown in these figures, purposely to display the experimental steady state or the test time. The steady state duration, given by this marker helps to note the steady state axial and normal accelerations for a given experiment.

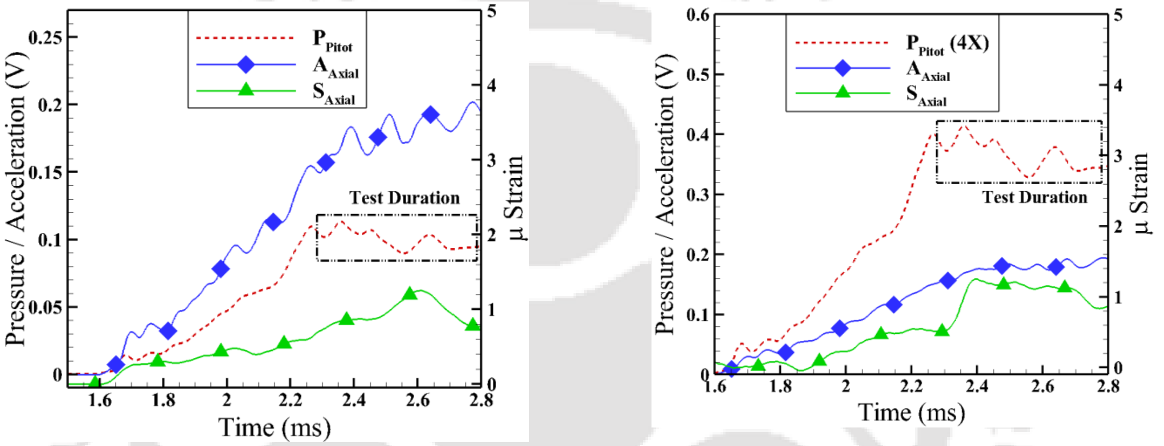

(a) **(b)**

Fig. 6. 4: Axial Responses at (a) 0º AOA (b) 10 º AOA.

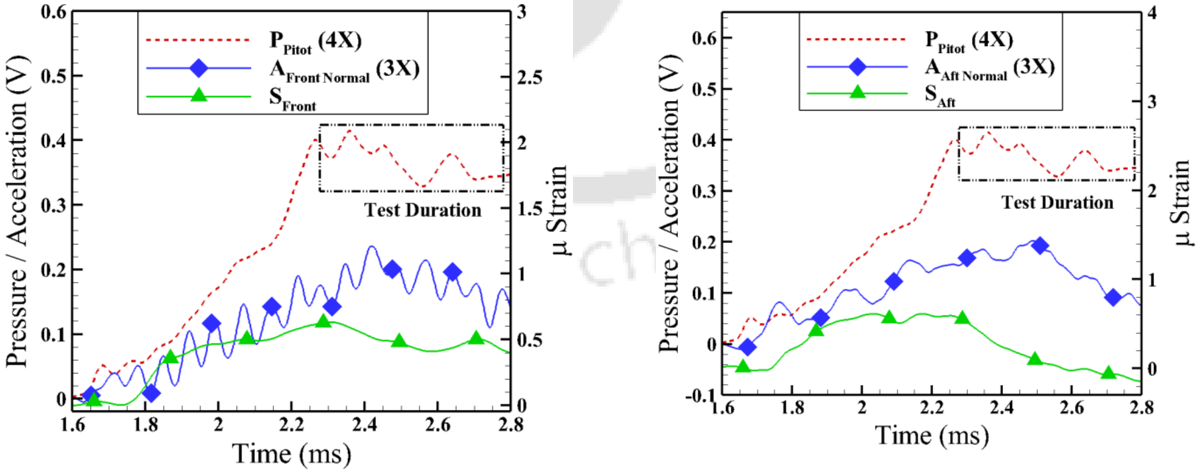

(a) **(b)**

Fig. 6. 5: (a) Front normal (b) Aft Normal responses at 10º AOA.

In line with one of the objectives, two separate ANFIS architecture trainings are considered for force recovery. Consideration of single and multi point trainings are essential to demonstrate the usefulness of multiple points for calibration in order to mimic the surface forces and also to cross verify, at least for piezofilm, since it has not been attained much given for force measurement in impulse facilities. In case of single point training, impulse force applied at point ‘1’ is considered for training and it resembles with practice followed in literature [Sahoo and Reddy (2010)]; while for multipoint training, all the impulse forces and their responses are accounted. After training, recovery of forces is obtained for 0^0 AOA. These recovered forces are shown in **Fig. 6. 6** for accelerometer and piezofilm balances respectively.

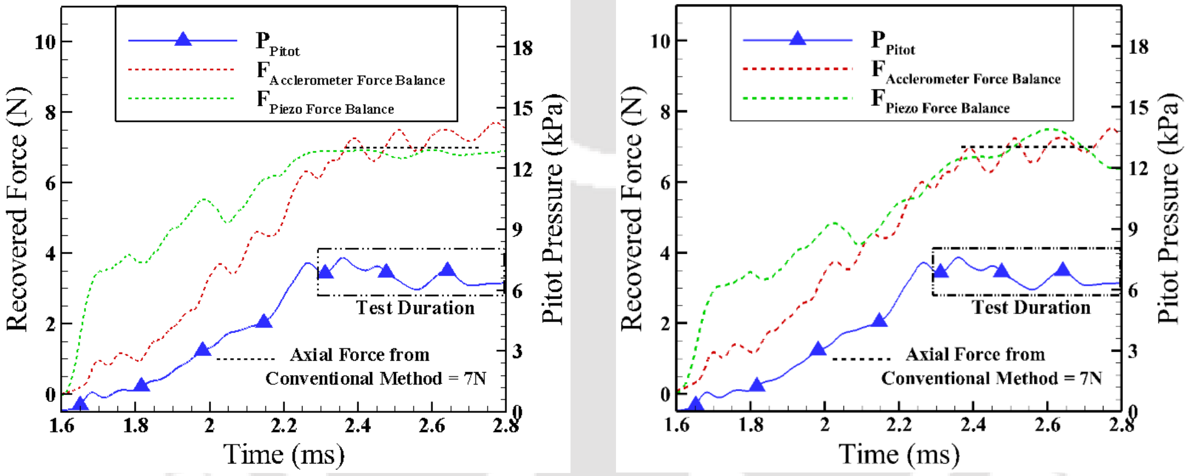

(a) **(b)**

Fig. 6. 6: Comparison of axial force recovery for accelerometer and piezofilm balance at 0º AOA: (a) single point calibration; (b) multi point calibration.

In both the figures, steady magnitude of the force, obtained from conventional accelerometer force balance theory, is highlighted using a horizontal line, which is noted to be at 7 N. Further, steady state value of the force from single point recovery using piezofilm responses is 6.9 N and the same from multi point recovery is 6.94 N. First obvious indication from these figures is the possibility of recovering force time histories from piezofilm signals with the help of ANFIS. Further, it provides both magnitude and trend of the force acted upon the model instead of its steady magnitude. However, prediction of drag force and hence the coefficient of drag (**Table 6. 1**) is same by single and multi-point techniques for 0º AOA case and even for both the force balances.

Likewise, axial and normal force time histories are also recovered using single and multi-point trained ANFIS architectures for 10º AOA case. Here, for single point training, the impulse force and corresponding response, are chosen. These predictions are shown in **Fig. 6. 7**. Here too the, accelerometer theory based force prediction is displayed. These values, for axial and normal forces, are 7.2 N and 2.4 N respectively. Advantage of multipoint calibration for stiffness (piezofilm) based force balances is evident from **Fig. 6. 8**. At one side, multi-point calibration portrays encouraging match for both (axial and normal) forces, while the single point calibration drastically fails to recover the normal force time histories for both the force balances. But, the time averaged axial force, for single and multi-point recoveries, with piezofilm based force balance are 6.6 N and 7.18 N respectively. Quite close match for axial force but large disagreement for normal force from the two force measurement techniques. Thus, single point training which was found to be suitable for 0º AOA was inadequate for 10º AOA. This deviation can be justified by the same philosophy of larger distance between the calibration location and center of pressure, as discussed in the previous chapter. Hence, the single point training would work for accelerometer as well as piezofilm based force balance if the loading point is closer to the center of pressure. However, since center of pressure varies with respect to AOA, calibration has to be performed separately for accurate execution of the single point methodology. In contrary, multi-point calibration is advisable for both inertia and stiffness based force balances irrespective of the experimental conditions. Further, it is worth to note that the magnitude of axial force and normal forces, predicted using multipoint calibration scheme, for piezofilm are having encouraging agreement with both the accelerometer based measurements and with the accelerometer balance theory based prediction. As a result, the deviation obtained in axial and normal force coefficients are in acceptable range with force balance theory. However, the trend of the normal force signals to achieve steady state values, obtained through both force measurement methodology seems to be different, which may be attributed to the sensing capability of both the sensors during the short test duration. Nevertheless, the piezofilm force balance in conjunction with ANFIS based multipoint prediction methodology is capable of successful prediction of the coefficients of forces and moments. Thus, present studies recommend the use of piezofilm sensors for force measurement in short duration impulse test facilities.

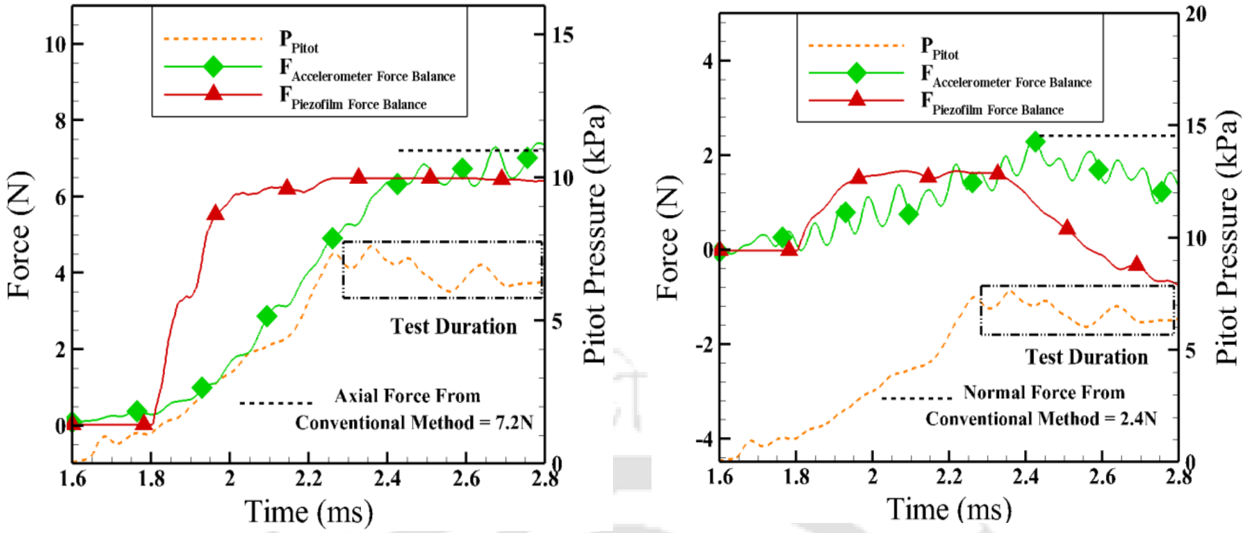

(a) (b)

Fig. 6. 7: Comparison of force recoveries at 10º AOA for accelerometer and piezofilm balance using single point calibration: (a) axial force; (b) normal force.

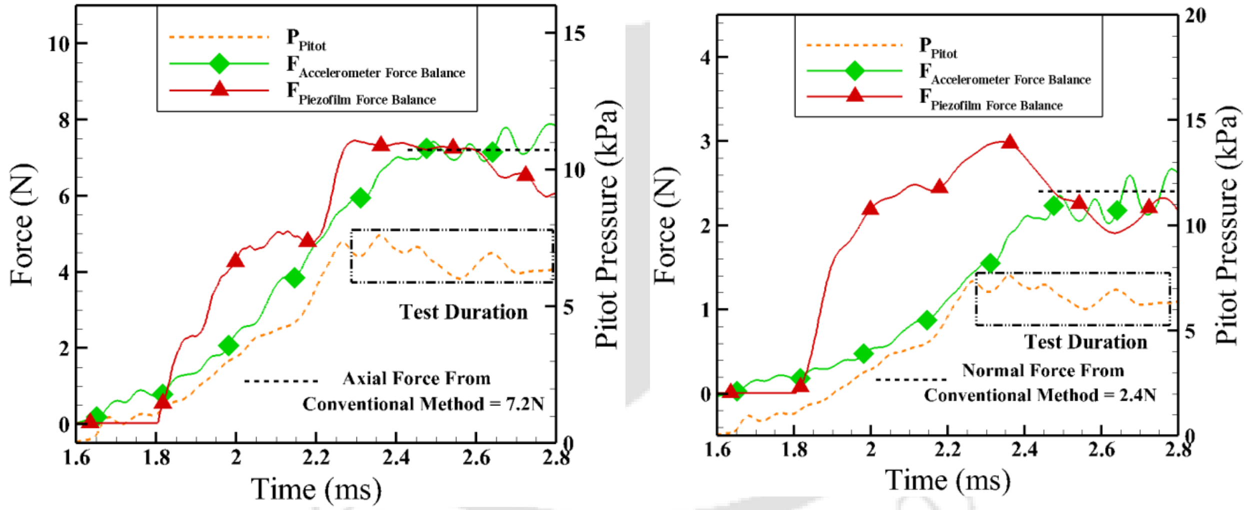

(a) (b)

Fig. 6. 8: Comparison of force recoveries at 10º AOA for accelerometer and piezofilm balance using multi point calibration: (a) axial force; (b) normal force.

Table 6. 1: Recovered force and moment coefficients at different AOA.

AOA	**Technique**	**Coefficient of drag (C_d)**	**Coefficient of lift (C_l)**	**Coefficient of moment (C_m)**

0º	Force balance theory	0.503	-	-
	AFB system	0.502	-	-
	SWFB system	0.498	-	-
10º	Force balance theory	0.539	0.0793	0.124
	AFB system	0.542	0.0741	0.121
	SWFB system	0.54	0.0835	0.127

Summary

Present studies are carried out to assess the usefulness of piezofilms for force measurement in impulse test facilities. A blunt double cone model is fabricated and tested in shock tunnel for force measurement using three component piezofilm based force balance and compared with that of the accelerometer balance. Before these shock tunnel tests, model integrated with the internal force balance is exposed to impulse hammer tests for dynamic calibration. These tests are verified using a force recovery method based on ANFIS and GA. Force measurement experiments in IITB-Shock Tunnel at 0º and 10º angles of inclination are successfully conducted for recording the piezofilm responses. Initially, force recovery from ANFIS training, with single point calibration test, is compared with the force recovery using multiple point force calibration tests. It has been observed that the dynamic calibration should have multiple hammer hits to mimic the actual surface loading for stiffness based force balances. Further, steady state magnitude of forces obtained from conventional accelerometer force balance theory are found to have reasonable match with the ANFIS based recoveries using both the force balances. This agreement in time varying forces among two force measurement philosophies has established that piezofilms are potential sensors for force measurement in short duration impulse test facilities.

CHAPTER-7

Sensitivity Analysis of Force Prediction Algorithms for Hypersonic Application

Overview

Piezofilm based balance is successfully employed for measuring forces and moment in the previous chapters, which provides an alternative method of force recovery for application in hypersonic facilities. As a new methodology, combination of multi point calibration and soft computing based prediction is employed. So, there is a necessity of in depth investigation of the capability of the force prediction algorithms. This will help in assessing the sensitiveness of the force recovery technique viz. ANFIS, in capturing small variation in force and moment coefficients. In this regard shock tunnel experiments have been conducted with two types of aerospike assemblies viz. hemispherical spike and sharp spike, incorporated on a bi-cone model. An internally mountable three-component accelerometer balance system has been employed for measuring the acceleration responses at various angles of attack. As a part of the assessment of the prediction technique, coefficients of forces and moment are recovered using ANFIS from the acceleration responses and are compared with the accelerometer force balance theory based prediction. Finally, CFD simulations have also been carried out to compliment the experimental results.

7.1 Introduction

Aerodynamic performance enhancement through active mode of drag reduction and thermal protection system (TPS) design has been a major concern of high speed aero-thermodynamics [Wang *et al.* (2016)]. Aerodynamic heating and high drag force, which is a consequence of lower bluntness of the nose portion of the hypersonic vehicles, in practice can increase the fuel requirement and thereby can affect the range in case of missiles. One of the foremost and modest techniques to address this issue is to introduce various spike configurations ahead of the nose of the vehicle. As a result of incorporation of spikes in the aerodynamic configurations, flow field near the stagnation region changes. The standoff distance of the strong shock generated ahead of the nose increases due to the presence of aerospike. Further, due to the adverse pressure gradient, flow separation occurs in the downstream of the aerospikes, resulting into low pressure and low temperature recirculation region near to the nose of the vehicle [Menezes *et al.* (2003)]. This, in turn lowers the magnitude of drag force and stagnation temperature up to a greater extent.

Several studies have been attempted through numerical and experimental approach to analyze the flow near the aerospikes and to quantify the decrement in coefficient of forces as well as stagnation point heat flux. Parameters like length and geometry of the spike plays a decisive role in altering the flow phenomena near to the stagnation zone [Zorea (1970), Hutt and Howe (1989)]. Crawford (1959) investigated the effect of Reynolds number on coefficient of drag with incorporation of a hemispherical spiked configuration. Various shapes viz. flat disk shape [Menezes *et al.* (2002), Motoyama *et al.* (2001)], sharp spike [Sahoo *et al.* (2016)], hemispherical spike [Deng *et al.* (2017)] and self-aligning spike [Wysocki *et al.* (2014)] have been explored for implementation in various experimental facilities. Further, to measure the force and moment coefficients for the spike mounted model in the experimental facilities, various active and passive techniques have been adopted. Active techniques like accelerometer balance [Menezes *et al.* (2002)] and strain gauge balance [Kalimuthu *et al.* (2010), Shang *et al.* (2001)] have been used. However, passive techniques like deduction of force coefficients from the distribution of pressure [Motoyama *et al.* (2001), Gnemmi *et al.* (2003)] have also been explored. Further, numerical simulation has been carried out for these aerospikes for obtaining the flow fields as well as to estimate the force and moment coefficients [Eghlima and Mansour (2017), Chinnappan *et al.* (2017)].

From the above studies, it has been perceived that most of the experimental studies rely on analytical relations to calculate the effect of aerospikes on drag coefficient [Menezes *et al.* (2002)]. Moreover, it is also observed that more attention has been focused towards quantification of force and moment values through surface pressure measurements which further helps in getting an estimate for the steady state magnitudes. Conversely, lesser attention has been given towards unsteady drag measurement over aerodynamic bodies in presence of spikes. To have the accurate estimates of the temporal variation of forces, dynamic calibration as already implemented for several blunt cone models [Kulkarni and Reddy (2010)], has to be conducted. These dynamic calibrations can be further utilized in conjunction with time domain [Prost and Goutte (1984)] or frequency domain based de-convolution technique [Mee (2003)] or soft computing based techniques viz. ANFIS [Ramesh *et al.* (2018)] to estimate the system response function or to develop relation between input and output calibration data. These parameters devised during training of the calibration data solely determines the accuracy of prediction of force and moment coefficients. However, extending de-convolution technique for multi component force prediction involves intense mathematical formulations, therefore is less explored by the researchers. Conversely, the soft computing based prediction don't require any mathematical expressions and solely rely on the response of the real systems and thereby avoid all types of assumptions that needs to be invoked in case of de-convolution technique. Nevertheless, the accuracy of force prediction using ANFIS needs to be enhanced which can be accomplished through appropriate selection of network parameters and through improvement in the calibration procedure.

In view of the limited applicability of accelerometer balance towards estimation in percentage decrement of force and moment values as well as requirement of improvising ANFIS based predictions for hypersonic applications, understated objectives have been defined for the current study. As a new method of force prediction involving ANFIS and GA is devised in previous chapters, the sensitiveness of this method to capture the small variation in forces needs an in-depth analysis. In previous situations this developed methodology is able to predict the force and moment coefficients for flow over blunt bodies, however to verify wider applicability of this method, it needs to be assessed through force and moment predictions in presence of spikes along with the aerodynamic model. In view of this, a biconic model equipped with sharp and hemispherical spike at various AOA is tested in shock tunnel facility where the modified method of force prediction is employed. To have a comparative analysis of these coefficients in steady state, force balance theory has been used. However, CFD computations have also been performed to complement and vindicate the experimental and analytical results.

7.2 Test Model and Spike Assemblies

For the current investigations a blunt bi-conic re-entry configuration equipped with internally mountable accelerometer balance has been chosen. Brief details related to the model and its associated balance system is described in **Chapter 5**. Spikes of different tip geometries are attached to the stagnation point of the model by means of threads. Usually these spikes act as a drag reduction device at lower AOA. The spikes used are solid stainless steel probes of 3 mm diameter. The current choice of tip geometries of the spikes include: 1) A hemispherical-faced aerodisc of 6 mm diameter and 2) A sharp/conical tip of 40º apex angle. Several types of spikes has been earlierly tested in various impulse facilities, however the above two aerodiscs usually results in less reduction in aerodynamic coefficients. Therefore, these two aerospikes has been chosen for the current study, as the sensitivity of the force balance as well as prediction algorithm can be only verified through accurate capturing of small change in aerodynamic coefficients. The hemispherical aerospike have been made-up of aluminum. The models equipped with different spike geometries are presented in **Fig. 7. 1** and **Fig. 7. 2**.

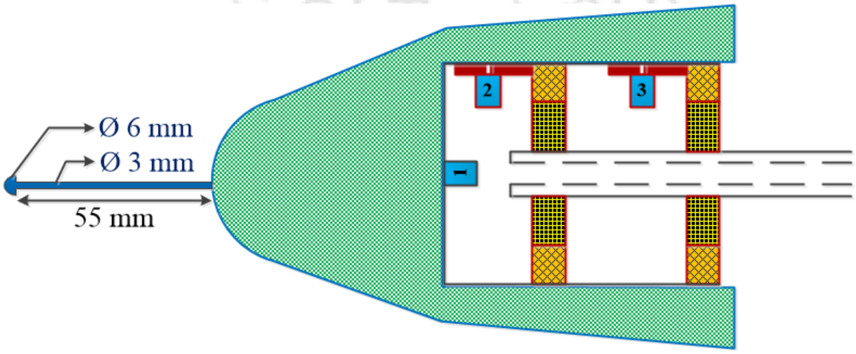

Fig. 7. 1: Bi-cone model with hemispherical spike.

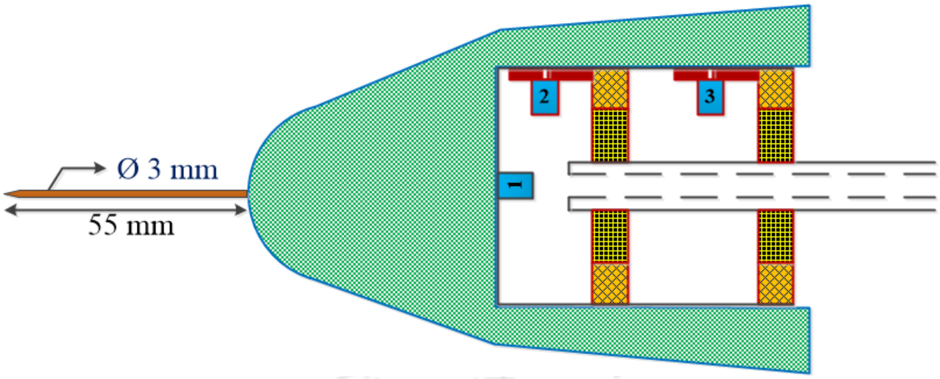

Fig. 7. 2: Bi-cone model with sharp spike.

7.3. Dynamic Calibration of Force Balance

7.3.1 Calibration Experiments

As the intention of the current study is focused towards unsteady force measurement for the spike mounted models, therefore execution of the dynamic calibration, before the actual shock tunnel experiments is essential. In this regard, the calibration set-up and methodology, that has been evolved in experiments without spike in **Chapter 5** is employed herein. As the new multi point calibration has an edge over the single point calibration, the same method is incorporated during the calibration of the model. The flow chart of the entire calibration and force prediction methodology as presented in **Chapter 5**, is also implemented for the current study.

7.4 Experimental Facility

Present experimental studies are conducted in IITB shock tunnel [Trivedi and Menezes (2012)] using three component accelerometer based force balance. Schematic of this test facility is presented in **Chapter 2**. Model equipped with hemispherical shaped aerodisk or sharp spike, is mounted in the test section of the shock tunnel. Experiments has been performed for these spikes incorporated model at 0° and 10° AOA, and acceleration responses for all the three accelerometers are recorded. Magnitude and trend of these responses is also ensured through repetitive experiments. For all the experiments, nitrogen is used as the driver gas and air as test gas. Experiments with the pitot sensor mounted in the test section are performed during one of the tests, to get an estimate of the steady state duration and also to calculate the free stream conditions prevailed in the test section.

7.5 Numerical Computation

Numerical inviscid simulations for the same slender bi-cone model without any spike and with hemispherical and sharp spike have been attempted with the commercial CFD solver ANSYS FLUENT 14.5. Experimental free stream conditions have been considered, so as to validate the results deduced using force recovery algorithms. During the simulation, the bicone model is placed within a cylindrical domain of length 0.26 m and radius 0.15 m. Similarly, for the simulation of model with spikes, the corresponding spike geometry along with the model has been generated. Numerical computations have also been carried out at different angles of inclination, for which experiments have been conducted. The geometry for the fluid simulation with the imposed boundary condition has been shown in **Fig. 7. 3**. Now, mesh is generated for the fluid domain having model with and without spike using ICEM CFD module of ANSYS. Element refinement has been done in the near wall region with an intention to capture the shock structure accurately. The maximum number of nodes and cells created for the simulations is 287090 and 274608 respectively for without spike case, whereas for model with hemispherical spike, 1008590 number of nodes and 976180 number of elements have been generated. Similarly, for the model with sharp spike, the mesh contains 1602567 number of nodes and 1564804 number of elements. The meshes along the mid plane of the domain, for the three configurations have been shown in **Fig. 7. 4** - **Fig. 7. 6**.

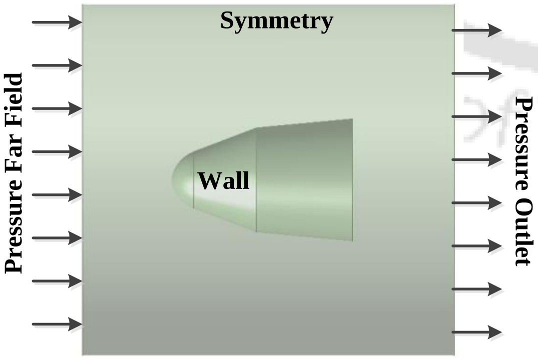

Fig. 7. 3: Geometry and boundary condition of the domain.

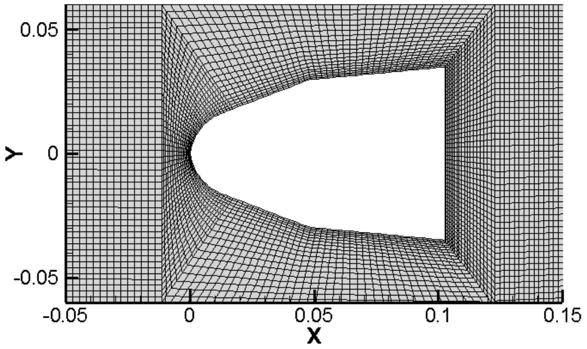

Fig. 7. 4: Mesh around the model without any spike.

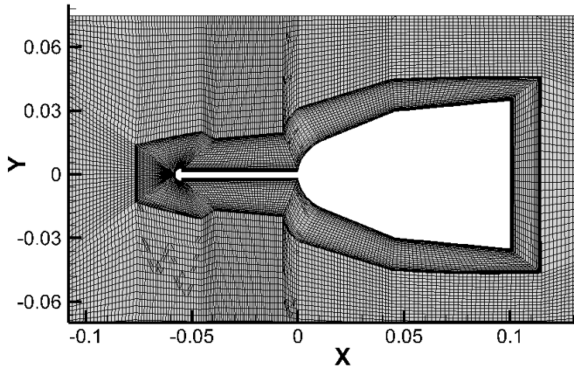

Fig. 7. 5: Mesh around the model with hemispherical spike.

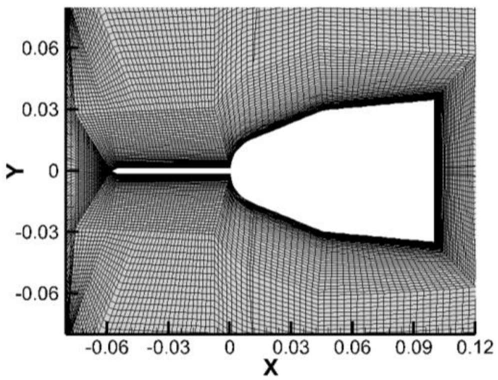

Fig. 7. 6: Mesh around the model with sharp spike.

For the CFD simulation working fluid has been chosen as air having constant specific heat of 1006.43 J/kg-K and molecular weight of 28.966 kJ/kg-mol. As in hypersonic flow regime, wave drag which originates mainly from high pressure on the windward side of the model in the presence of strong shock wave, is dominant over the other forces, therefore, inviscid simulation is carried out. Far field boundary condition with absolute pressure of 74.29 Pa, absolute temperature of 44.06 K and free stream Mach number of 8.36 has been considered for inlet whereas outlet boundary condition has been selected for flow exit. AUSM flux vector splitting scheme has been adopted to compute the inviscid flux vectors and implicit time scheme with higher order relaxation is performed using inbuilt ANSYS settings where Courant number is set between 0.5 and 1, to compute the temporal variation of the flow properties. Simulation is carried out for 1 ms having time step size of 4 μs and 20 iterations per time step to achieve temporally accurate solutions. This simulation duration is in line with the steady test duration as earlierly estimated from the pitot signal. The streamlines along with the pressure contours for each of the configurations at 0º and 10º AOA has been illustrated in **Fig. 7. 7**. To have a comparative analysis with the experimentally determined values, coefficient of drag, lift and pitching moments are noted down.

7.6 Results and Discussion

Before the actual recovery of force and moment coefficients for the shock tunnel experiments, the calibration process is initially validated. During this phase of calibration, the optimum network parameters for ANFIS and optimum weights for GA is determined. The same calibration data associated with the model without any spike (**Chapter 5**) has been employed herein for recovery purpose.

7.6.1 CFD Results

The flow features arising from the numerical simulation is explored in this section to ensure its correctness. From the contours of the model without any spike, presence of a strong bow shock wave at the fore-body of the model is evident. Due to these strong pressure gradient, model experiences by a large amount of aerodynamic drag. Similarly, the pressure contours for the model equipped with hemispherical spike signifies the presence of system of weaker oblique shock waves rather than a strong shock wave as seen in case of without spike. Also, a recirculation region is observed behind the aerospike and in front of the forebody, which in turn reduces the net pressure force acting on the model and hence experiences less drag force. Further, it is observed that due to the presence of spike, some part of the model remains under the aerodynamic shadow of it, thereby pushes the re-attachment point towards the edge of the model, which is beneficial from the prospective of drag reduction. The static pressure contour for the model with sharp spike at 0^0 and 10º AOA are analyzed which indicates nearly identical flow features for both the spike configurations. However due to the absence of any disc connected to the tip of the spike, the flow re-attachment point shifts inwards on the nose portion of the model, resulting in increase in pressure as compared to the hemispherical spike. Numerically obtained coefficients of force and moments for all the test cases are presented in **Table 7. 1**.

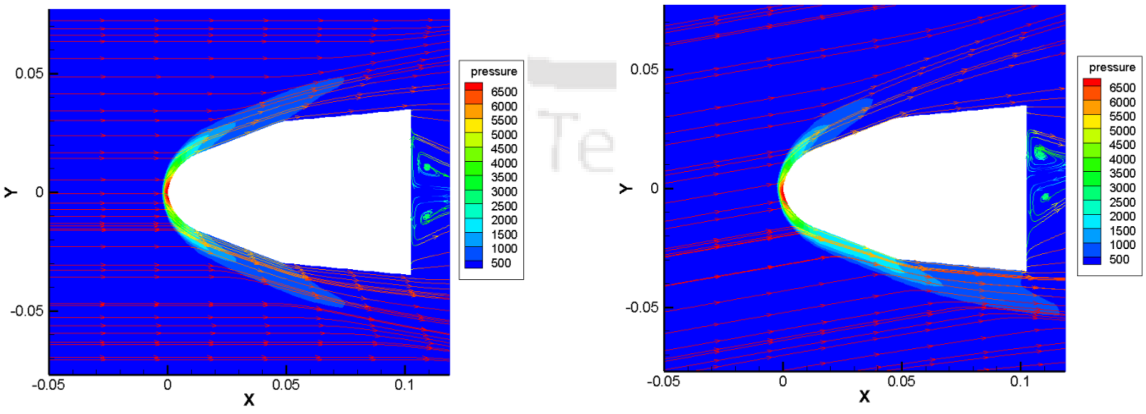

(a) **(b)**

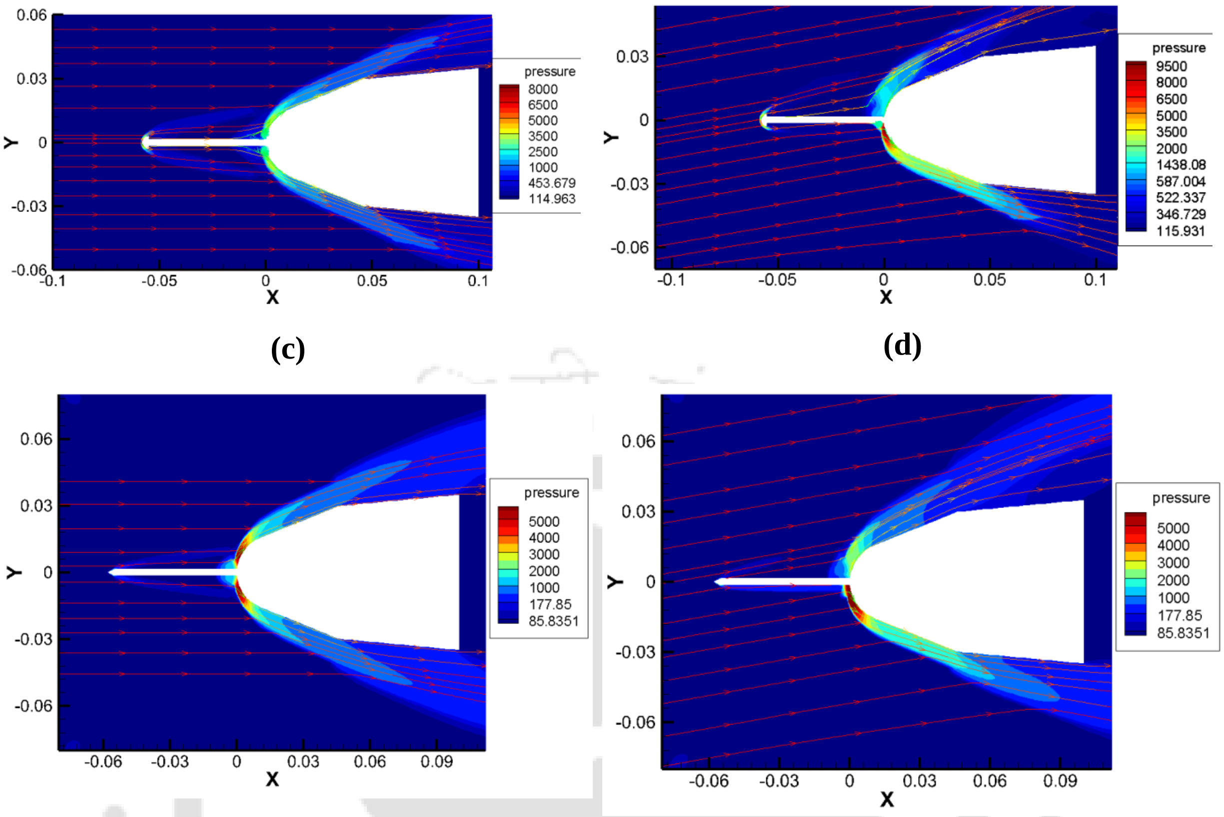

(c) (d)

(e) (f)

Fig. 7. 7: Pressure contours for (a, b) model without spike, (c, d) with hemispherical spike and (e, f) with sharp spike corresponding to AOA 0º and 10º.

Table 7. 1: Numerically estimated force and moment coefficients at different AOA.

AOA	Model Geometry	Coefficient of drag (C_d)	Coefficient of lift (C_l)	Coefficient of moment (C_m)
0º	Without spike	0.342	-	-
	Hemispherical Spike	0.29	-	-
	Sharp Spike	0.341	-	-
10º	Without spike	0.354	0.231	0.21
	Hemispherical Spike	0.335	0.264	0.231
	Sharp Spike	0.358	0.245	0.22

It can be observed that at 0º angle of incidence, hemispherical spike shows significant decrement in drag values. However due to the presence of the reattachment shock in the near wall region of the model, the sharp spike does not change the drag coefficient considerably. Similarly, at higher angle of attack viz. for 10º inclination, the hemispherical spike still acts as a drag reduction method but lift force and pitching moment is higher than the measured values for the model without spike. Further, the implementation of sharp spike at larger AOA leads to higher value of force and moment coefficients, which confirms the nonsuitability of aerospike as a drag mitigation technique which is also evident from earlier investigations [Menezes *et al.* (2002)].

7.6.2 Experimental Force Recovery

The force and moment measurement experiments on the model with and without spike are conducted in IITB-shock tunnel for free stream Mach number of 8.36. Acceleration signals are acquired during experiments for two angles of incidence viz. 0º and 10º. The acceleration responses corresponding to all the accelerometers, for model without any spike and model equipped with spike at 0^0 and 10^0 AOA are illustrated in **Fig. 7. 8** and **Fig. 7. 9**. Pitot pressure signal is also presented in these figures, to indicate the experimental steady test time.

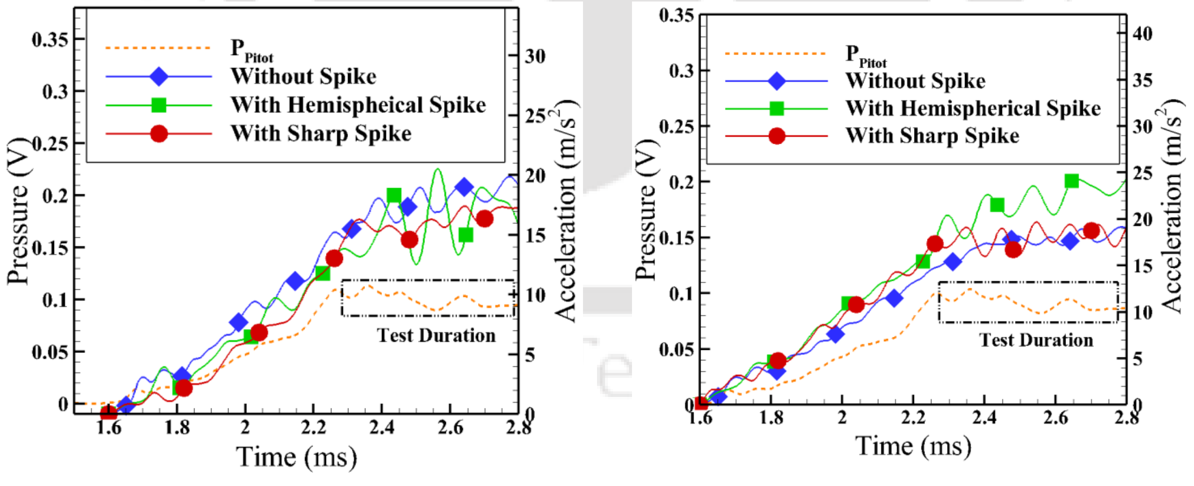

(a) **(b)**

Fig. 7. 8: Axial acceleration responses from AFB at (a) 0º AOA (b) 10º AOA.

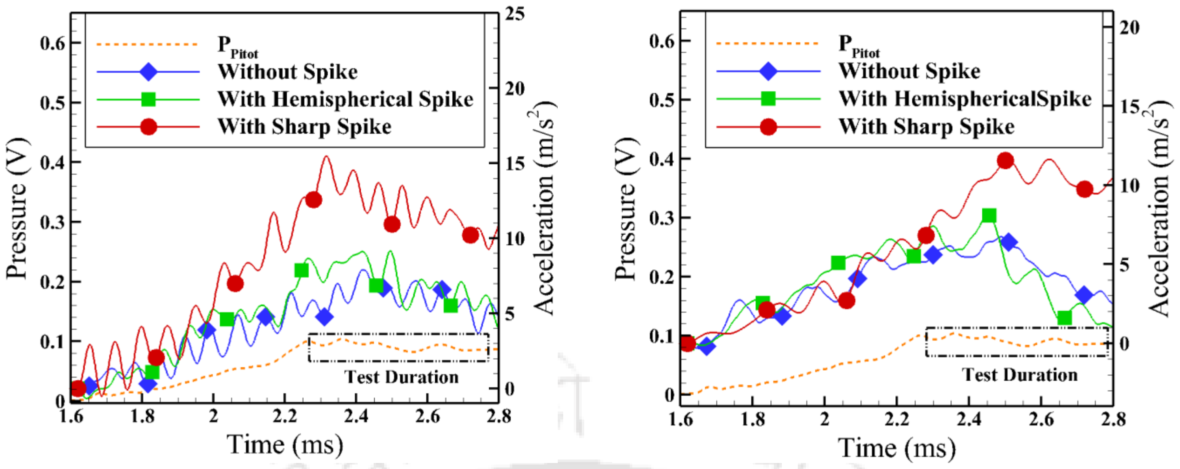

(a) **(b)**

Fig. 7. 9 : Acceleration responses from AFB at 10° AOA (a) Front normal (b) Aft Normal.

It is evident from these figures that, for all the test cases, the designed accelerometer balance is able to capture the minor variation of forces through measurement of temporal accelerations. Further, during the steady test duration, average value of axial and normal accelerations for a given experiment is noted and with usage of these values, the coefficient of forces and moment is determined using accelerometer force balance theory. Experimental values of these coefficients obtained using the aforementioned theory is presented in **Table 7. 2**. The measured force and moment coefficients for 0° angle of incidence are in line with the available literature data [Deng *et al.* (2017)], which emphasizes the use of spikes as a drag reduction device at small AOA. It is also perceived from the **Table 7. 2** that at 10° Angle of inclination, the spikes do not contribute to drag reduction due to the inward shift of the flow re-attachment point which resembles the experimental observations listed by Menezes *et al.* (2003). Since, the model with its associated internally mountable three-component accelerometer balance is able to measure the force and moment coefficients effectively for different AOA, so the designed balance system seems to be sensitive to small alteration in flow conditions.

Afterwards, the sensitivity analysis of the prediction algorithm is evaluated through recovery of force and moment coefficients, incorporating the temporal acceleration signals obtained during shock tunnel experiments. The trained ANFIS architecture is fed with the experimental acceleration responses obtained for 0° AOA, which in turn predicts the axial force for the model with and without spike, as presented in **Fig. 7. 10(a)**. As the force distribution during experiments closely resemble to that of surface loading condition, therefore, multi-point calibration methodology, as developed in the earlier chapters, is implemented during this study. After obtaining the temporal variation of forces using ANFIS, steady state acceleration magnitude is calculated for the test duration as depicted from the pitot signal and further using these steady state values corresponding drag coefficients for 0º angle of incidence is estimated, as shown in **Table 7. 2**. It can be perceived that, the hemispherical as well as sharp spike is acting as one of the drag mitigation technique. Hence, the percentage of drag reduction/the reduced coefficient of drag, in case of both the spikes closely matches with the corresponding values obtained using accelerometer balance theory. However, the reduction in drag obtained using numerical method is lower than the drag reduction predicted by the experimental results and also the drag coefficients are severely underpredicted in numerical computations. Use of Euler solver of ANSYS and choice of only first order numerical scheme are expected to be the possible reasons for this discrimination.

Likewise, axial and normal force for the model equipped with aerospike and without any spike, is recovered using the same procedure, as adopted earlier. Temporal variation of axial, front normal and aft normal acceleration responses corresponding to 10º AOA has been provided as input to the ANFIS for this purpose. The predicted axial and normal forces have been illustrated in **Fig. 7. 10(b)** and **Fig. 7. 10(c)**, respectively. From the figures, it is apparent that, incorporation of both the spikes at higher angle of incidence results in larger value of axial force in comparison to the model without any spike, which is also evident from the accelerometer balance theory. Inward shift of the flow re-attachment point on the fore body of the model enhances the axial force which gives rise to higher value of coefficient of drag (**Table 7. 2**). It confirms that the spike can not be used for drag reduction at higher angles of attack. It can be also observed that, in case of numerical computations the rise in drag coefficient for sharp spike is not significant as compared to the experimentally obtained values. In a similar manner, comparative assessment between numerical computation, accelerometer balance theory and ANFIS prediction for the normal forces acting on the model is attempted. This shows an increasing trend for both the spike geometry in regard to the model without any aerospike. Further, quantitatively a good agreement is observed between the predicted values through ANFIS and balance theory (**Table 7. 2).** Also, as the present choice of model is lifting in nature, so providing an AOA to the model leads to significant increase in lift coefficient and further enhancement can be achieved with usage of sharp spike to the model, as evident from **Table 7. 2**.

Having information related to the predicted axial force, normal force and numerically obtained location of center of pressure, coefficient of pitching moment is calculated which is also having a good agreement with the balance theory. Since, all the coefficients of forces and moment predicted using ANFIS have a good match with the results obtained from the accelerometer balance theory, it can be stated that the currently employed prediction algorithm is capable of capturing the minute alteration in forces acting on the model. Further, this fact is more strengthened, as the technique is able to predict these coefficients successfully in presence of the spikes at various angles of incidence.

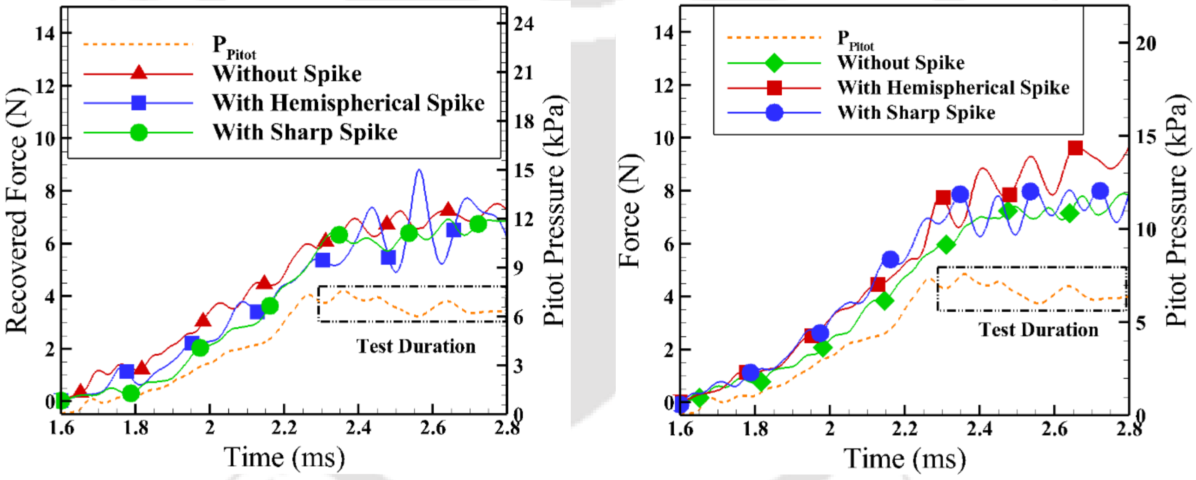

(a)

(b)

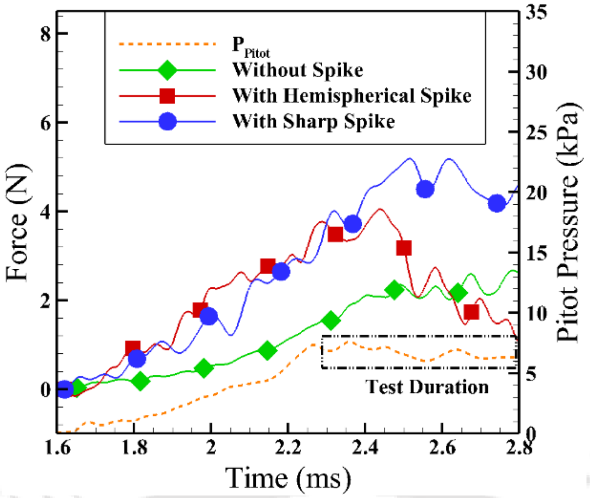

(c)

Fig. 7. 10 : Recovery of aerodynamic forces using ANFIS: (a) axial force at 0º AOA (b & c) axial and normal force at 10º AOA.

Table 7. 2: Recovered force and moment coefficients at different AOA using ANFIS.

AOA	**Model Geometry**		**Coefficient of drag (C_d)**	**Coefficient of lift (C_l)**	**Coefficient of moment (C_m)**
0º	Force Balance Theory	Without spike	0.503	-	-
		Hemispherical Spike	0.467	-	-
		Sharp Spike	0.457	-	-
	ANFIS Prediction	Without spike	0.502	-	-
		Hemispherical Spike	0.47	-	-
		Sharp Spike	0.456	-	-
	Force Balance	Without spike	0.539	0.0793	0.124
		Hemispherical Spike	0.637	0.0845	0.153

10º		Sharp Spike	0.571	0.251	0.247
	ANFIS Prediction	Without spike	0.542	0.0741	0.121
		Hemispherical Spike	0.63	0.0844	0.14
		Sharp Spike	0.571	0.239	0.243

Summary

An attempt has been made to investigate the sensitiveness of the accelerometer force balance system as well as the prediction methodology viz. ANFIS in hypersonic flow regime. Experiments have been conducted on the earlier considered model equipped with hemispherical and sharp spikes which serve as drag mitigation device at lower AOA. The acceleration responses for spike equipped model at 0º AOA indicate about 5-10% reduction in drag. However it is observed that at higher AOA, the spikes do not reduces the drag due to the inward shift of the flow re-attachment point. This observation is validated from the accelerometer force balance theory as well from prediction through ANFIS. Since both the balance theory and the prediction algorithm are able to capture the coefficients of the forces and moment accurately. It exhibits enough sensitivity to take in account any minute alteration in flow features. CFD simulation have also been carried out to estimate forces and moment for all the test cases, which serve as a supporting proof for some of the experimental measurements and also provide detailed information of the flow around the spikes.

CHAPTER-8

Conclusions and Scope of Future Work

8.1 Conclusion

Recent trend in unsteady aerodynamics poses various challenges that need to be eventually catered through flow diagnostics based measurement methodologies that incorporate fast responsive sensors. In line with the aforementioned fact, current study is focused towards delicately handling the complicacies associated with force measurement in transient environments. Mainly, present investigation encompasses design, fabrication and calibration of various force balances to be used in impulse facilities having reasonably small steady test duration. During this study, capability of different force prediction methodologies is also assessed through recovery of the coefficients of forces and moments from the experimental responses. Following inferences have been deduced during the course of current analysis.

- The initial stage of experimentation has been focused towards acquisition of transient strain history in supersonic flow condition, specifically with usage of the shock tube facility present at IITG. In view of this, a hemispherical model along with its stress bar is fabricated and FEM simulation has been performed to arrive at an appropriate location for strain measurement which is found to be 5 mm from the rear end of the test model.
- During the dynamic calibration, different circuit configurations associated with strain gauge have been incorporated and results have been analyzed in time as well as frequency domain to have an in-depth exploration of the effect of circuits on strain measurement. Comparative assessment is carried out through recovering force time histories using frequency based de-convolution technique which depict half bridge circuit as the most suitable for application in impulsive loading condition.
- Afterwards, experiments have been conducted in shock tube using model mounted with strain gauges and stress bar, to capture the strain response. Drag force on the hemispherical model is predicted through de-convolution technique and is estimated to be 330 N which is having a deviation of ± 8.1% as compared to numerical results.

- Encouraging match between numerical prediction and recovered force from piezofilm (± 5.98%) and strain gauge (± 8.4%) using both the techniques is observed. Henceforth, present investigation emphasizes the use of piezofilm as an alternative to the strain gauge for stress wave force balance to measure aerodynamic forces and moments in short duration test facilities.
- A new multi-point calibration methodology in association with the soft computing technique for more accurate measurement of drag, lift and pitching moment coefficients is developed.
- A bluff bi-cone shaped model integrated with a three-component internally mountable accelerometer balance system is dynamically calibrated using the new multi-point calibration method. The responses are superposed using weights assigned to them to calculate the responses due to forces in orthogonal directions. The assigned weights have been estimated through optimization technique and the modified responses are fed to the ANFIS algorithm for training purpose.
- The new calibration methodology is employed to recover the forces and moments from the acceleration responses acquired during tests conducted in shock tunnel at Mach 8. Encouraging match has been observed between force balance theory and ANFIS with the proposed calibration methodology at lower as well as higher angle of attack.
- Also, results have been compared with the conventional single point calibration methodology where the significance of calibration location is assessed. Lesser deviation has been noticed in prediction of aerodynamic coefficients if the point of choice is nearer to the center of pressure.
- The same philosophy of multi point calibration is also extended for the force prediction in case of an internally mountable piezofilm balance. It has been observed that piezofilm balance is also effective in predicting time histories of the forces at different angle of attack and recovering the steady state magnitude of aerodynamic coefficients.
- Lastly, attention is focused towards investigating the sensitiveness of the accelerometer balance system as well as the prediction methodology viz. ANFIS in hypersonic flow regime. To get an insight on the same, experiments have been

conducted on the earlier considered model equipped with hemispherical and sharp spike which serves as drag reduction device at lower angle of attack.

- The acceleration responses at 0° angle of attack indicates about 5-10% reduction in drag on the model with spikes. The same is also confirmed from the recovery of forces using ANFIS as prediction algorithm. However, some discrepancy with the magnitude of drag force obtained from the numerical simulations.
- It has been also noted that, at higher angle of incidence, the spikes do not reduce the drag due to the inward shift of the flow re-attachment point. This observation is validated from the accelerometer force balance theory as well from the force prediction through ANFIS for model equipped with sharp spike. Henceforth, integration of spike in the model helps in demonstrating the capability of the prediction methodology and force balance to capture the minute alteration in forces acting on the model.

8.2 Future Work

Current investigation encompasses design and development of various force balances as well as prediction methodologies for application in supersonic and hypersonic flow environments. However, there is still scope for future improvements and some suggestions for further studies are discussed below:

- Present study incorporates only PVDF piezofilm for short duration force measurement; however, implementations of various other types of available piezofilm on response acquisition in impulse facilities need attention.
- Piezofilm based stress wave balance for thee component system has been a part of the current study. However, due to the instrumentation complicacies associated with strain gauge based balances, it has not be explored. Therefore, analysis of the multi component strain gauge balance can be carried out in conjunction with accelerometer / piezofilm balance system for quantitative assessment.
- Development of piezofilm based force balance in association with multi point calibration methodology, involving six component of forces and moments can be attempted.

- ANFIS can be extended as the prediction algorithm for recovering the forces and moments from six component force balance systems.
- Exploring de-convolution technique for application to multi component systems still needs attention. Force prediction using this method is mathematically intensive; nevertheless, it will provide an alternative method of force recovery.

References

Abdel-Jawad MM, Mee DJ and Morgan RG (2007), New calibration technique for multiple-component stress wave force balances, *Review of scientific instruments*, 78(6), 065-101.

Agarwal S and Sahoo N (2018), An experimental investigation towards calibration of a shock tube and stagnation heat flux determination, *International Journal of Aerodynamics*, *6*(1), 18-40.

Agarwal S, Sahoo N, Irimpan KJ, Menezes V and Desai S (2017), Comparative performance assessments of surface junction probes for stagnation heat flux estimation in a hypersonic shock tunnel, *International Journal of Heat and Mass Transfer*, *114*, 748-757.

Ahmed DI, Yusoff MZ, Amir AF and Kasolang S (2012), High speed flow characteristics in gun tunnel, In *AIP Conference Proceedings*,1440 (1), 330-340.

Anderson JD Jr (2004), Modern Compressible flow with historical perspective, *3rd edition (New York: McGraw-Hill)*.

Anderson M, Puranik B, Oakley J and Bonazza R (2000), Shock tube investigation of hydrodynamic issues related to inertial confinement fusion, *Shock Waves*, 10, 377-387.

Anjana J, Jayanth Kumar S, Mahapatra DR and Rathod VT (2013), Development of P (VDF-TrFE) films and its quasi-static and dynamic strain response, *International Journal of Engineering Research and Technology*, 2(12), 2598-2605.

Ardasheva MM, Nevskii LB and Pervushin GE (1985), Measurement of pressure distribution by means of indicator coatings, *Journal of Applied Mechanics and Technical Physics*, 26(4), 469-474.

Aune V, Fagerholt E, Langseth M and Børvik T (2016), A shock tube facility to generate blast loading on structures, *International Journal of Protective Structures*,*7*(3), 340-366.

Bernstein L and Pankhurst RC (1975), Force measurements in short-duration hypersonic facilities, *Advisory Group for Aerospace Research and Development Neuilly-sur-seine (France)*, Report No. AGARD-OGRAPH-214.

Chinnappan AK, Malaikannan G and Kumar R (2017), Insights into flow and heat transfer aspects of hypersonic rarefied flow over a blunt body with aerospike using direct simulation Monte-Carlo approach. *Aerospace Science and Technology*, 66, 119-128.

Cimbala, JM (2011) Stress, strain and strain gauges. USA: Penn State University

Cook MV *(*2012*)* Flight dynamics principles*,* a linear systems approach to aircraft stability and control, *Butterworth- Heinemann*.

Crawford DH (1959), Investigation of the flow over a spiked-nose hemisphere-cylinder, *NASA*, Report No. TN-D-118.

Davidson DF and Hanson RK (2009), Recent advances in shock tube/laser diagnostic methods for improved chemical kinetics measurements, *Shock Waves*, *19*(4), 271-283.

Davidson DF, Shao J, Parise T and Hanson RK (2017), Shock tube measurements of jet and rocket fuel ignition delay times, In *55th AIAA Aerospace Sciences Meeting*.

Deng F, Jiao Z, Liang B, Xie F and Qin N (2017), Spike effects on drag deduction for hypersonic lifting body, *Journal of Spacecraft and Rockets*, *54*(6), 1185-1195.

Desai S, Kulkarni V and Gadgil H (2016), Delusive influence of nondimensional numbers in canonical hypersonic nonequilibrium flows, *Journal of Aerospace Engineering*, 29(5), 04016030.

Desai S, Kulkarni V, Gadgil H and John B (2017), Aerothermodynamic considerations for energy deposition based drag reduction technique, *Applied Thermal Engineering*, 122, 451-460.

Dieulesaint E and Royer D (1980), Elastic waves in solids: applications to signal processing, *John Wiley & Sons.*

Dufrene A, MacLean M and Holden M (2012), High enthalpy studies of capsule heating in an expansion tunnel facility, In *43rd AIAA Thermophysics Conference*, 2998.

Dufrene A, MacLean M, Parker R, Wadhams T and Holden M (2010), Characterization of the new LENS expansion tunnel facility, In *48th AIAA Aerospace Sciences Meeting Including the New Horizons Forum and Aerospace Exposition*, 1564.

Dunn MG and Kang SW (1973), Theoretical and experimental studies of reentry plasmas, *NASA CR*, Report No.2232.

Duryea GR and Martin JF (1968), An improved piezoelectric balance for aerodynamic force, *IEEE Transactions on Aerospace and Electronic Systems*, (3), 351-359.

Edney BE (1967), Temperature measurements in a hypersonic gun tunnel using heat-transfer methods, *Journal of Fluid Mechanics*, 27(3), 503-512.

Eghlima Z and Mansour K (2017), Drag reduction for the combination of spike and counterflow jet on blunt body at high Mach number flow, *Acta Astronautica*, 133, 103-110.

Gnemmi P, Srulijes J, Roussel K and Runne K (2003), Flowfield around spike-tipped bodies for high attack angles at Mach 4.5, *Journal of Spacecraft and Rockets*, 40(5), 622-631.

Gordon S and McBride BJ (1994), Computer program for calculation of complex chemical equilibrium composition and applications, *NASA*, Report No.1331.

Hillier R (2015), Gun tunnel studies of shock-wave/boundary-layer interactions; laminar, transitional and turbulent, In *20th AIAA International Space Planes and Hypersonic Systems and Technologies Conference*, 3512.

Hills R (1961) A Review of measurements on AGARD calibration models, *Advisory Group for Aerospace Research and Development Paris (france),* Report No. AGARD-OGRAPH-64.

Hoffmann K (1989), An introduction to measurements using strain gages, *Hottinger Baldwin Messtechnik GmbH*, 126-134.

Holden M (2004), Experimental studies in the LENS shock tunnel and expansion tunnel to examine real-gas effects in hypervelocity flows, In *42nd AIAA Aerospace Sciences Meeting and Exhibit*, 916.

Hutt GR and Howe AJ (1989), Forward facing spike effects on bodies of different cross section in supersonic flow, *The Aeronautical Journal*, 93(926), 229-234.

Igra O and K Takayama (1993), Shock tube study of the drag coefficient of a sphere in a non-stationary flow, *Proceedings of the Royal Society, London A,* 442, 231-247.

Ilich Z, Grossir G, Paris S and Chazot O (2017), Experimental investigation of the VKI longshot gun tunnel compression process, *7th European Conference for Aeronautics and Aerospace Sciences.*

Itoh K, Ueda S, Tanno H, Komuro T and Sato K (2002), Hypersonic aerothermodynamic and scramjet research using high enthalpy shock tunnel, *Shock Waves*, *12*(2), 93-98.

Jessen C and Grönig H (1989), A new principle for a short-duration six component balance, *Experiments in fluids*, 8(3-4), 231-233.

Jiao X, Chang J, Wang Z and Yu D (2017), Numerical study on hypersonic nozzle-inlet starting characteristics in a shock tunnel, *Acta Astronautica*, *130*, 167-179.

Joarder R and Jagadeesh G (2003) A new free floating accelerometer balance system for force measurements in shock tunnels, *Shock Waves*, 13(5), 409-412.

Joshi MV, Reddy NM (1986), Aerodynamic force measurements over missile configurations in IISc shock tunnel at $M_\infty = 5.5$, *Experiments in fluids*, 4(6),338-40.

Kalimuthu R, Mehta RC and Rathakrishnan E (2010), Drag reduction for spike attached to blunt-nosed body at Mach 6, *Journal of Spacecraft and Rockets*, *47*(1), 219-222.

Kobayashi H, Maru Y and Fukiba K (2017), Experimental study on aerodynamic characteristics of telescopic aerospikes with multiple disks, *Journal of Spacecraft and Rockets*, 44(1), 33-41.

kulkarni V and Reddy KPJ (2010), Accelerometer-based force balance for high enthalpy facilities, *Journal of Aerospace Engineering*, *23*(4), 276-280.

Laurence SJ and Karl S (2010), An improved visualization-based force-measurement technique for short-duration hypersonic facilities, *Experiments in Fluids*, *48*(6), 949-965.

Lewis H and East R (1995), Measurement of free-flight dynamic stability derivatives of cones in a hypersonic gun tunnel, In *International Aerospace Planes and Hypersonics Technologies*, 6082.

Marineau E, MacLean M, Mundy E and Holden M (2012), Force measurements in hypervelocity flows with an acceleration compensated strain gage balance, *Journal of spacecraft and rockets*, 49(3), 474-482.

Marineau EC (2011), Force measurements in hypervelocity flows with an acceleration compensated piezoelectric balance, *Journal of Spacecraft and Rockets*, 48(4), 697-700.

Matsumoto E, Biwa S, Katsumi K, Omoto Y, Iguchi K and Shibata T (2004), Surface strain sensing with polymer piezoelectric film, *Ndt & E International*, 37(1), 57-64.

Mee DJ (2003), Dynamic calibration of force balances for impulse hypersonic facilities, *Shock Waves*, 12(6), 443-455.

Mee DJ, Daniel WJ and Simmons JM (1996), Three-component force balance for flows of millisecond duration, *AIAA journal*, 34(3), 590-595.

Menezes V, Saravanan S and Reddy KPJ (2002), Shock tunnel study of spiked aerodynamic bodies flying at hypersonic Mach numbers, *Shock Waves*, 12(3), 197-204.

Menezes V, Saravanan S, Jagadeesh G and Reddy KPJ (2003), Experimental investigations of hypersonic flow over highly blunted cones with aerospikes, *AIAA journal*, 41(10), 1955-1966.

Menezes V, Trivedi S and Kumar A (2011), An accelerometer balance for the measurement of roll, lift and drag on a lifting model in a shock tunnel, *Measurement Science and Technology*, 22(6), 067003.

Motoyama N, Mihara K, Miyajima R, Watanuki T and Kubota H (2001), Thermal protection and drag reduction with use of spike in hypersonic flow, *In 10th AIAA/NAL-NASDA-ISAS International Space Planes and Hypersonic Systems and Technologies Conference*, 1828.

Nanda SR, Agarwal S, Kulkarni V and Sahoo N (2017) Shock Tube as an Impulsive Application Device, *International Journal of Aerospace Engineering*, 2010476.

Naumann KW, Ende H and Mathieu G (1991), Technique for aerodynamic force measurement within milliseconds in shock tunnel, *Shock Waves*, 1(3), 223-232.

Naumann KW, Ende H, Mathieu G and George A (1993), Millisecond aerodynamic force measurement with side-jet model in the ISL shock tunnel, *AIAA journal*, 31(6), 1068-1074.

Nayak KC, Tripathy RK, Panda SR and Sahoo SN (2014), Prediction of cutting and feed forces for conventional milling process using adaptive neuro fuzzy inference system (ANFIS), *IAES International Journal of Artificial Intelligence*, 3(1), 24-35.

Nesline FW, Wells BH and Zarchan P (1981), Combined optimal/classical approach to robust missile autopilot design, *Journal of Guidance, Control, and Dynamics*, 4(3), 316-322.

Pallekonda RB, Nanda SR, Dwivedy SK, Kulkarni V and Menezes V (2018), Soft computing based force recovery technique for hypersonic shock tunnel tests, *International Journal of Structural Stability and Dynamics*, 18(5), 1871004.

Paull A, Stalker RJ and Mee DJ (1995), Scramjet thrust measurement in a shock tunnel, *The Aeronautical Journal*, 99(984), 161-163.

Persico G, Gaetani P and Guardone A (2005), Dynamic calibration of fast-response probes in low-pressure shock tubes, *Measurement Science and Technology*, 16(9), 1751.

Porat H, Morgan RG and McIntyre TJ (2017), Radiative heat flux measurements for titan atmospheric entry condition in a superorbital expansion tunnel, In *30th International Symposium on Shock Waves*, 139-143.

Prost R and Goutte R (1984), Discrete constrained iterative deconvolution algorithms with optimized rate of convergence, *Signal Processing*, 7(3), 209-230.

Ramesh P, Nanda SR, Kulkarni V and Dwivedy SK (2018), Application of neural-networks and neuro-fuzzy systems for the prediction of short-duration forces acting on the blunt bodies, *Soft Computing*, 1-14.

Ramesh P, Bommana D, Kulkarni V, Sahoo N and Dwivedy SK (2014), Experimental assessment of noncontact type laser-based force measurement technique for impulsive loading, *International Journal of Structural Stability and Dynamics*, 14(04).

Reis MLCC, Castro RM and Mello OAF (2013), Calibration uncertainty estimation of a strain-gage external balance, *Measurement*, 46(1), 24-33.

Robinson MJ, Mee DJ, Tsai CY and Bakos RJ (2004), Three-component force measurements on a large scramjet in a shock tunnel, *Journal of Spacecraft and Rockets*, 41(3), 416–425.

Robinson MJ, Schramm JM and Hannemann K (2011), Design and implementation of an internal stress wave force balance in a shock tunnel, *CEAS Space Journal*, 1(1-4), 45-57.

Rushton GH and Stetson KF (1967), Shock tunnel investigation of boundary-layer transition at M equals 5.5, A*IAA Journal*, *5*(5), 899-906.

Sahoo D, Das S, Kumar P and Prasad JK (2016), Effect of spike on steady and unsteady flow over a blunt body at supersonic speed, *Acta Astronautica*, *128*, 521-533.

Sahoo N and Reddy KPJ (2010), Force measurement techniques for hypersonic flows in shock tunnels, *International Journal of Hypersonics*, 1(1), 31-58.

Sahoo N, Mahapatra D R, Jagadeesh G, Gopalakrishnan S and Reddy KPJ (2003), An accelerometer balance system for measurement of aerodynamic force coefficients over blunt bodies in a hypersonic shock tunnel, *Measurement Science and Technology*, 14(3), 260.

Sahoo N, Mahapatra DR, Jagadeesh G, Gopalakrishnan S and Reddy KPJ (2007) Design and analysis of a flat accelerometer-based force balance system for shock tunnel testing, *Measurement*, 40(1), 93-106.

Sahoo N, Suryavamshi K, Reddy KPJ and Mee DJ (2005), Dynamic force balances for short-duration hypersonic testing facilities, *Experiments in Fluids*, 38(5), 606-614.

Sanderson SR, Simmons JM (1991), Drag balance for hypervelocity impulse facilities, AIAA *Journal*, 29(12), 2185-2191.

Santos M, Mattos B and Girardi R (2008), Aerodynamic coefficient prediction of airfoils using neural networks, *In 46th AIAA Aerospace Sciences Meeting and Exhibit*, 887.

Saravanan S, Jagadeesh G and Reddy KPJ (2009), Aerodynamic force measurement using 3-component accelerometer force balance system in a hypersonic shock tunnel, *Shock Waves*, 18(6), 425-435.

Shang JS, Hayes J, Wurtzler K and Strang W (2001), Jet-Spike bifurcation in high speed flows, *AIAA Journal*, 39(6), 1159-1165.

Simmons JM (1995), Measurement techniques in high-enthalpy hypersonic facilities, *Experimental thermal and fluid science*, 10(4), 454-469.

Simmons JM and Sanderson SR (1991), Drag balance for hypervelocity impulse facilities, *AIAA Journal*, 29(12), 2185-2191.

Sirohi J and Chopra I (2000), Fundamental understanding of piezoelectric strain sensors, *Journal of Intelligent Material Systems and Structures*, 11(4), 246-257.

Smith AL, Mee DJ, Daniel WJT and Shimoda T (2001), Design, modelling and analysis of a six component force balance for hypervelocity wind tunnel testing, *Computers & Structures*, 79(11), 1077-1088.

Smith DR, Gildfind DE, James CM, McIntyre T and Wheatley V (2018), Magnetohydrodynamic drag force measurements in an expansion tube, *In Flow Control Conference*, 3755.

Stalker RJ (1967), A study of the free-piston shock tunnel, *AIAA Journal*, 5(12), 2160-2165.

Takayama K, Reddy KPJ and Kumar CS (2014), Shock waves made simple, *Wiley India Pvt. Ltd. India*.

Tanno H, Itoh K, Saito T, Abe A and Takayama K (2003), Interaction of a shock with a sphere suspended in a vertical shock tube, *Shock Waves*, *13*(3), 191-200.

Tanno H, Komuro T, Sato K, Fujita K and Laurence SJ (2014), Free-flight measurement technique in the free-piston high-enthalpy shock tunnel, *Review of Scientific Instruments*, 85(4), 045-112.

Trivedi S and Menezes V (2012), Measurement of yaw, pitch and side-force on a lifting model in a hypersonic shock tunnel, *Measurement*, 45(7), 1755-1764.

Truitt RW (1959) Hypersonic Aerodynamics, *Ronald Press, New York*.

Tuttle SL, Mee DJ and Simmons JM (1995), Drag measurements at Mach 5 using a stress wave force balance, *Experiments in Fluids*, 19(5), 336-341.

Vadassery P, Joshi DD, Rolim TC and Lu FK (2013), Design and testing of an external drag balance for a hypersonic shock tunnel, *Measurement*, 46(7), 2110-2117.

Venukumar B, Jagadeesh G and Reddy KPJ (2006), Counterflow drag reduction by supersonic jet for a blunt body in hypersonic flow, *Physics of Fluids*, 18(11), 118104.

Vidal RJ (1956), Model instrumentation techniques for heat transfer and force measurements in a hypersonic shock tunnel, *Cornell Aeronautics Laboratory (CAL) Report*, No. AD-917-A-1.

Wang Y, Liu Y, Luo C and Jiang Z (2016), Force measurement using strain-gauge balance in a shock tunnel with long test duration, *Review of Scientific Instruments*, 87(5), 055-108.

Wang Y, Liu Y, Yuan C, Jiang Z and Zhao W (2015), Force measurement using a pulse-type strain-gaged balance in hypersonic shock tunnel, In *The proceedings of the 8th European Symposium on Aerothermodynamics for Space Vehicles, Lisbon, Portugal*.

Whitcomb RT (1976), A design approach and selected wind tunnel results at high subsonic speeds for wing-tip mounted winglets, *NASA*, Report No. TN-D-8260.

White D (1958), Influence of diaphragm opening time on shock-tube flows, *Journal of Fluid Mechanics*, *4*(6), 585-599.

Wysocki O, Schülein E and Schnepf C (2014), Experimental study on wave drag reduction at slender bodies by a self-aligning aerospike, In *New Results in Numerical and Experimental Fluid Mechanics IX*, 583-590.

Zhiguo L, Guojun L, Rongjuan Z, Hua J, Jichun L, Jun H and Shiran L (2017), The direct measurement of skin friction in shock tunnel, In *30th International Symposium on Shock Waves*, 149-154.

Zorea C and Rom J (1970), Effect of a spike on the drag and on the aerodynamic stability of blunt bodies in supersonic flow, *Journal of Spacecraft and Rockets*, 7(8), 1017-1019.

Appendix-A

Design of ANFIS Methodology for Six Component Force Balance

A.1 Numerical Modelling

A blunt cone model having 60º apex angle and 15º flare with internally mountable accelerometer based balance is shown in **Fig. A. 1**. The model is fabricated out of aluminum whereas the balance system is made up of stainless steel rings with circular cross-section, (40 mm outer diameter and 30 mm internal diameter) which is mounted inside the test model. The balance also comprises of two annular neoprene rubber bushes (30 mm outer diameter and 12 mm internal diameter) having 4 mm thickness, which is bonded with inner surface of the steel rings as well as with a sting.

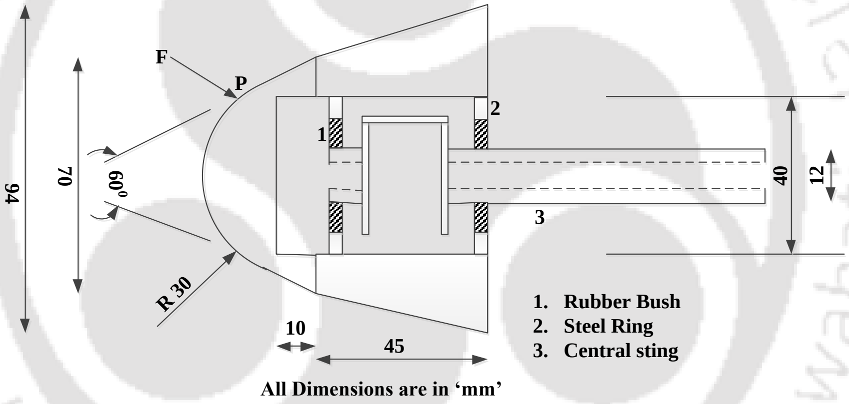

Fig. A. 1: Schematic diagram of the model.

Transient finite element analysis has been carried out for the above model using ANSYS 14.5 for a simulation time of 2 milliseconds which corresponds to the range of experimental test time. The model is meshed with 10-noded tetrahedral elements (Solid 187). After detailed mesh independence studies, the number of nodes obtained is 58985. The material properties assigned to different parts of the model during simulation is given in **Table A. 1**. During this simulation, boundary condition is provided such that it should exhibit free flying motion. In this regard, inner surface of the rubber has been kept fixed viz. zero displacement in all directions. The detailed mesh of the model is shown in **Fig. A. 2**.

Table A. 1: Material properties assigned during simulation.

Material	**Young's modulus (E) in GPa**	**Density (ρ) in kg/m^3**	**Poisson's Ratio (υ)**
Aluminum	70	2700	0.32
Steel	193	7850	0.27
Rubber	0.003	960	0.49

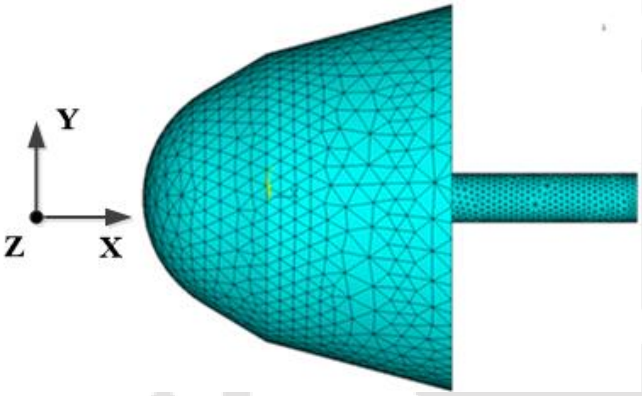

Fig. A. 2: Meshed model during FE analysis.

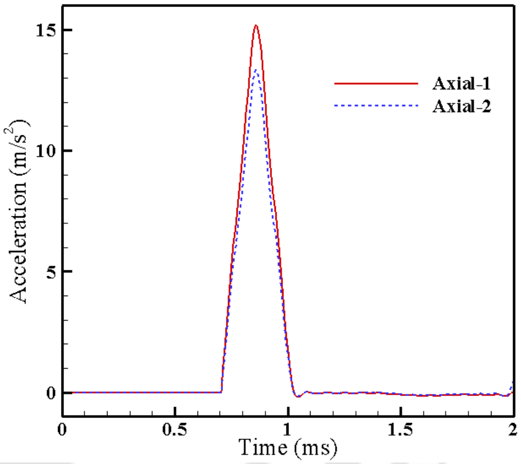

Fig. A. 3: Axial acceleration responses.

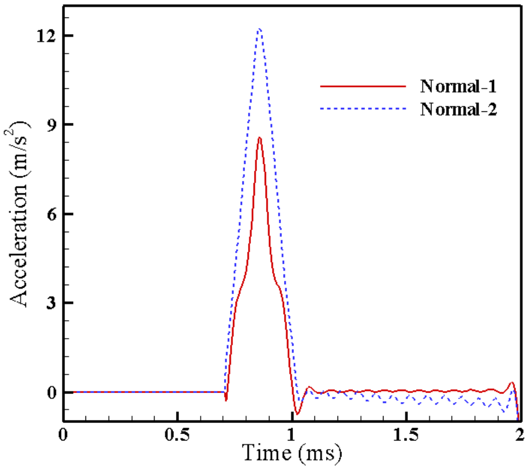

Fig. A. 4: Normal acceleration responses.

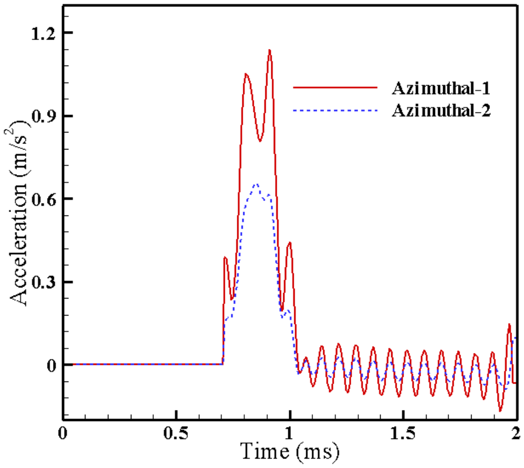

Fig. A. 5: Side acceleration responses.

During simulation different trend, orientation and magnitude of forces are applied at point 'P' on the model as shown in **Fig. A. 1**. Acceleration signals corresponding to the forces are obtained at six discrete points viz. two accelerations in each spatial direction. As, the actual design of six component accelerometer balance comprises of six accelerometers mounted in the balance assembly, six discrete locations have been chosen to obtain the acceleration responses during FE simulation. Thus obtained acceleration signals corresponding to 10N and 50N are employed for training of the ANFIS network whereas the signals corresponding to 20N and 30N are used for prediction purpose. Here, the line of force is along the Z-axis, while the plane containing the force vector makes an angle 10^{o} with XZ and YZ planes. Sample filtered acceleration signals are shown in **Fig. A. 3 - Fig. A. 5**.

A.2 ANFIS Implementation for Force Prediction

Present investigation deals with implementation of previously incorporated force prediction algorithm viz. ANFIS for short duration transient force and moment prediction for a six component force balance system. For the above analysis, transient accelerations obtained from FE simulation at six discrete locations are considered as input whereas forces and moments corresponding to resultant forces having magnitudes of 10 N and 50 N have been fed as the output to the network. However transient accelerations, forces and moments corresponding to resultant forces with magnitudes of 20 N and 30 N have been taken into account as the testing data for the optimized ANFIS network.

The present investigation emphasizes on prediction of impulse, ramp and hat force from the training data set of impulse forces employing the pre-obtained ANFIS structure. A universal training data sets comprising of two transient accelerations obtained at two discrete points along each axis can be considered irrespective of the force and moment to be recovered; however considering computational cost and accuracy of prediction, a modified training data set selection strategy has been adopted. For accurate prediction of forces, a training method is employed which uses transient accelerations corresponding to the spatial direction along which force has to be recovered. This technique has been devised keeping in view of the accelerometer balance theory which uses respective accelerations for which force magnitude estimation is desired. However, training of moment about any of the axis employs a method where single transient acceleration from each spatial direction is fed as input to the network. With this training data set, an attempt has been made to recover three forces and moments corresponding to impulse forces of resultant magnitudes of 20N and 30N as shown in **Fig. A. 6**.

Further as ANFIS has universal approximation capability and impulse force is usually considered as a universal function, so an attempt of validating the universality is made by incorporating the transient acceleration data sets corresponding to hat and ramp forces as input to the network. Keeping the training data sets same; forces and moments corresponding to resultant hat and ramp forces of 20N and 30N are recovered which are shown in **Fig. A. 7** and **Fig. A. 8**. The actual and predicted values of the forces and moments for impulse, ramp and hat excitations along each axis have been presented in **Table A. 2**.

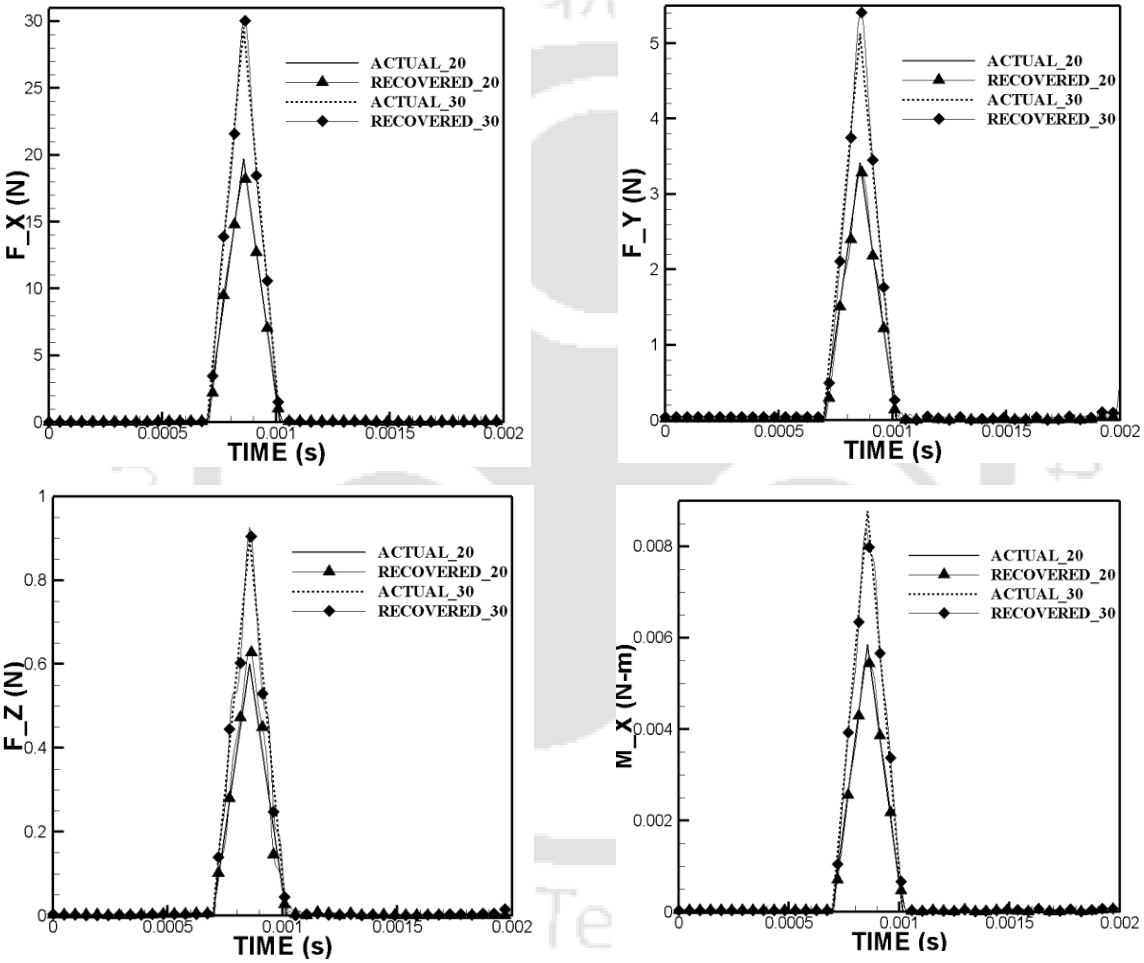

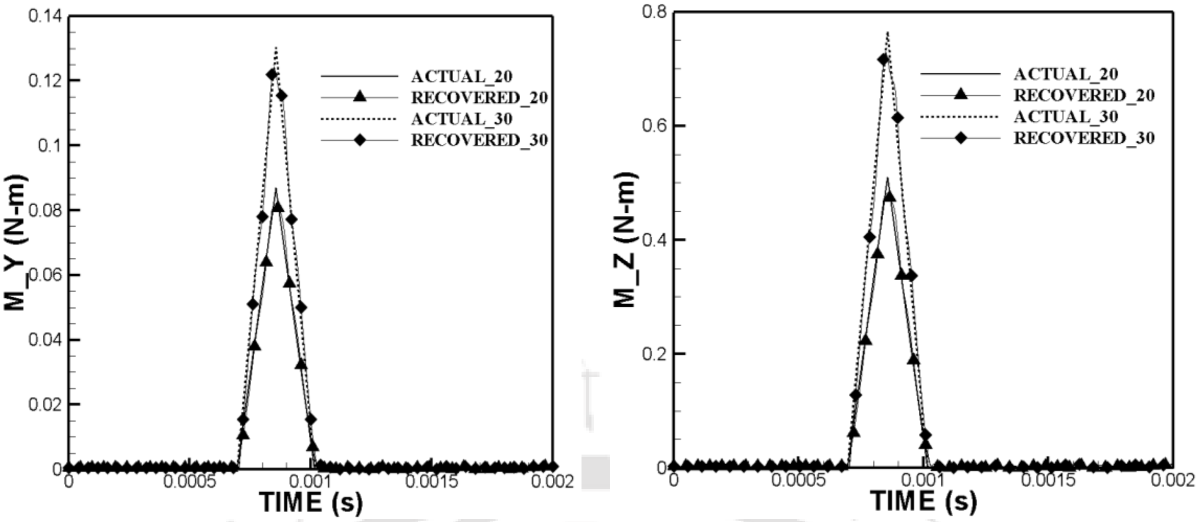

Fig. A. 6: Prediction of forces and moments for various impulse loads.

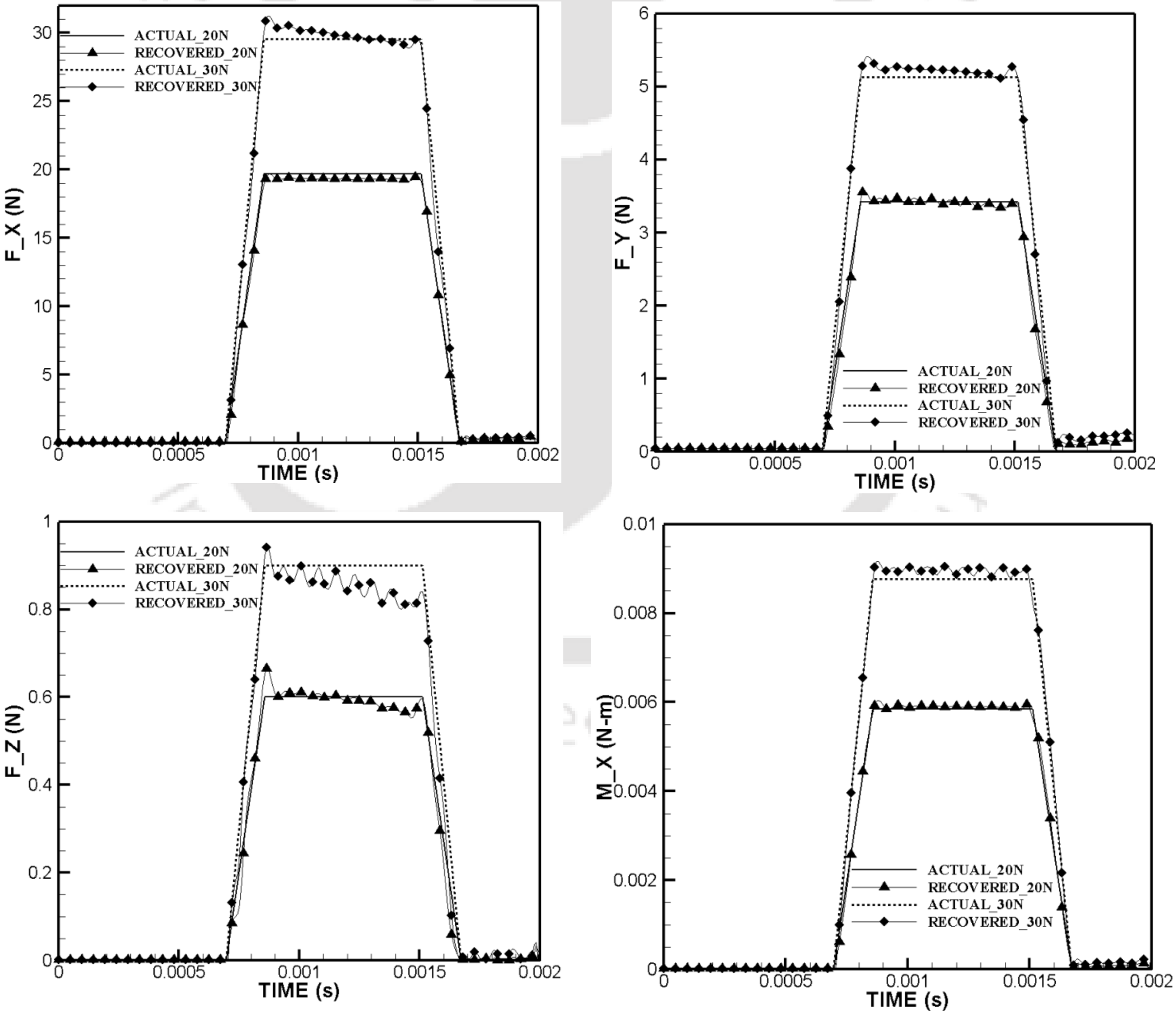

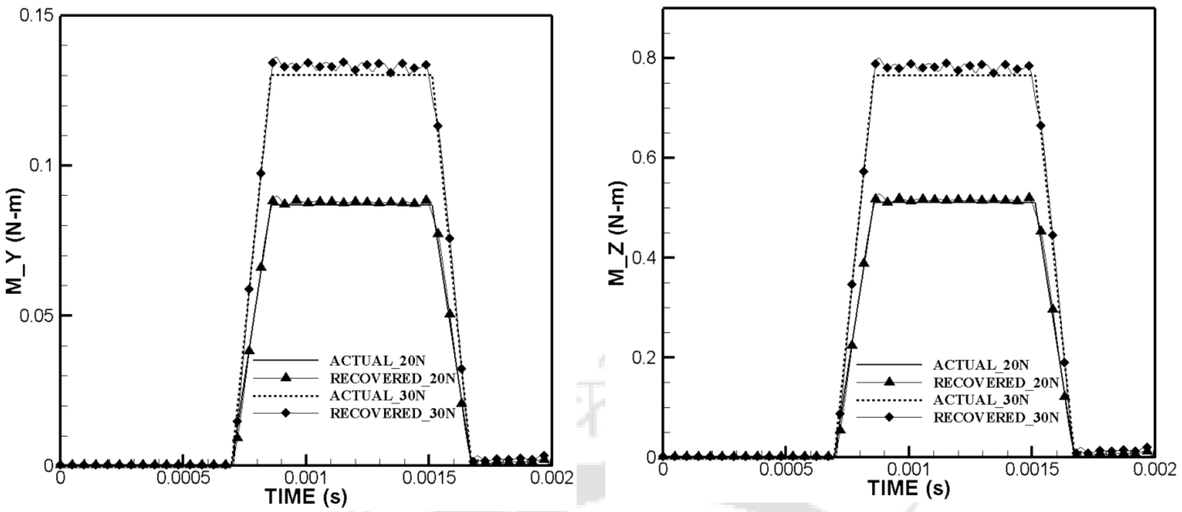

Fig. A. 7: Prediction of forces and moments for two excitations with hat distribution.

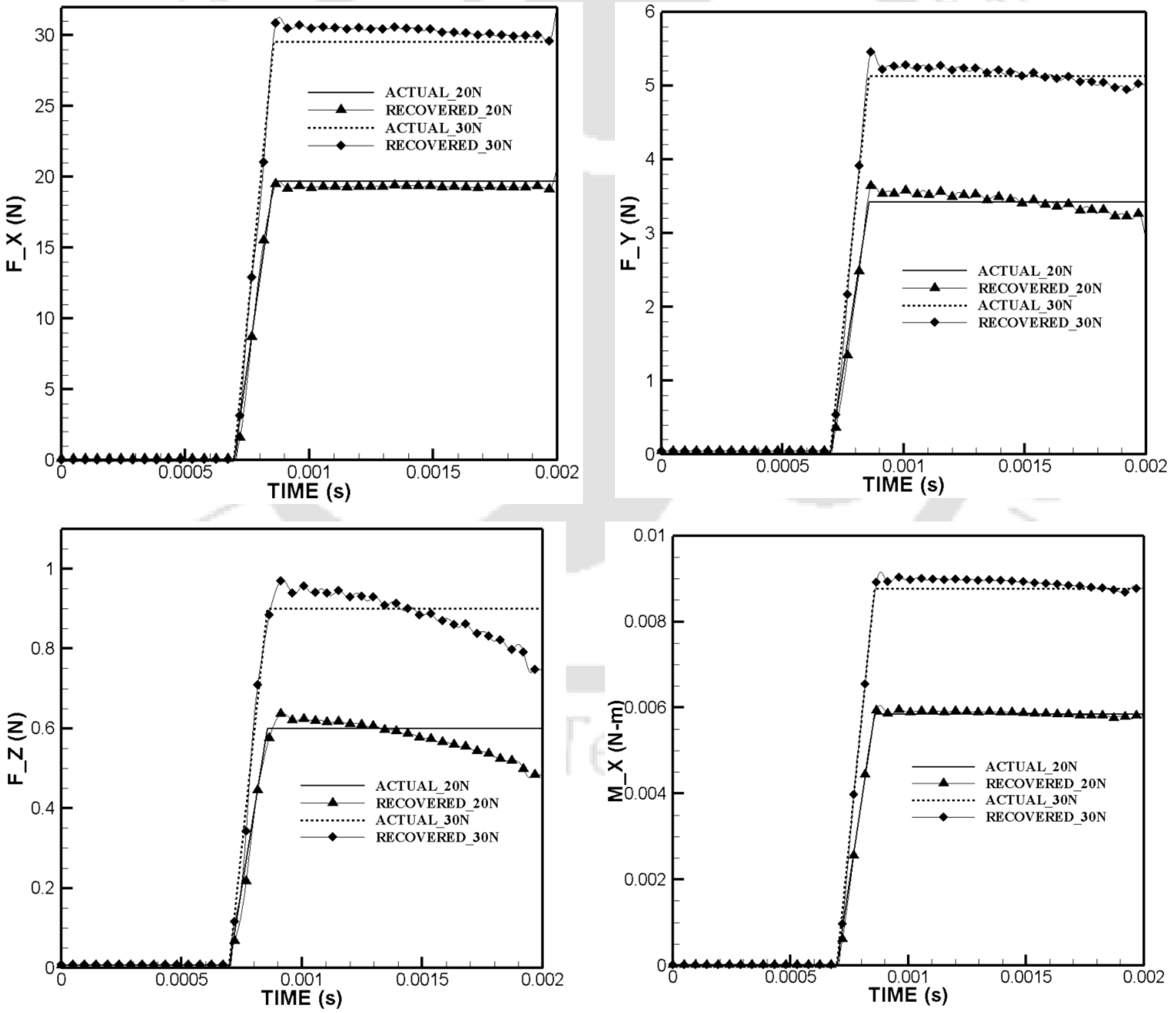

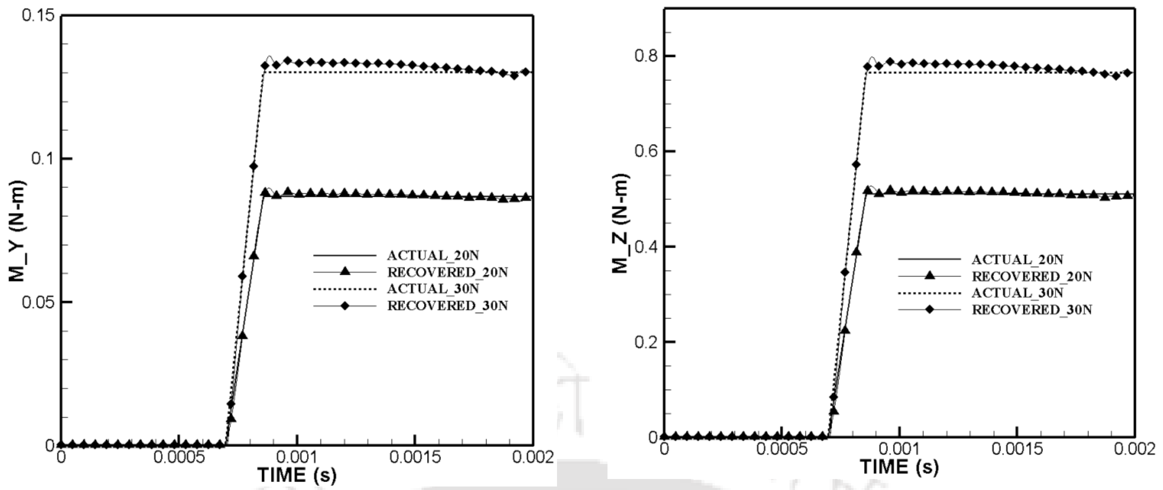

Fig. A. 8: Prediction of forces and moments for two ramp excitations.

Table A. 2: Actual and predicted values for impulse, Hat and Ramp forces of various magnitudes.

Nature	**Impulse**		**Hat**		**Ramp**	
	Actual	**Predicted**	**Actual**	**Predicted**	**Actual**	**Predicted**
F_X (N)	19.696	18.277	19.696	19.33762	19.696	19.324
	29.544	30.162	29.544	29.8652	29.544	30.352
F_Y (N)	3.42	3.301	3.42	3.418	3.42	3.4268
	5.13	5.42	5.13	5.226	5.13	5.1587
F_Z (N)	0.6	0.635	0.6	0.5955	0.6	0.5763
	0.9	0.927	0.9	0.857	0.9	0.885
M_X (N-m)	0.005849	0.005518	0.005849	0.005897	0.005849	0.00587
	0.008774	0.008374	0.008774	0.008948	0.008774	0.0089
M_Y (N-m)	0.086874	0.081983	0.086874	0.087641	0.086874	0.08722
	0.130311	0.124412	0.130311	0.132894	0.130311	0.13226
M_Z (N-m)	0.51026	0.481532	0.51026	0.514766	0.51026	0.512267
	0.76539	0.730742	0.76539	0.780563	0.76539	0.7768

Above figures and table clearly show that the adopted ANFIS architecture recovers the forces and moments with an accuracy of 7%. Hence, the architecture is reasonably accurate for measuring forces and moments on a supersonic/hypersonic test model.